THESIS

This is to certify that the

dissertation entitled

Surface Raman Spectra of t-1,2-bis(4-pyridyl) ethylene and Amino Acids at a Polycrystalline Silver Electrode

presented by

John J. McMahon

has been accepted towards fulfillment of the requirements for

Ph.D. degree in Chemistry

Gerald T. Babcock
Major professor

Date 12/11/81.

SURFACE RAMAN SPECTRA OF T-1,2-BIS(4-PYRIDYL)ETHYLENE AND AMINO ACIDS AT A POLYCRYSTALLINE SILVER ELECTRODE

By

John J. McMahon

A DISSERTATION

Submitted to

Michigan State University
in partial fulfillment of the requirements
for the degree of

DOCTOR OF PHILOSOPHY

Department of Chemistry

1981

ABSTRACT

SURFACE RAMAN SPECTRA OF T-1,2-BIS(4-PYRIDYL)ETHYLENE AND AMINO ACIDS AT A POLYCRYSTALLINE SILVER ELECTRODE

By

John J. McMahon

The Raman spectrum of t-1,2-bis(4-pyridyl)ethylene (t-BPE) adsorbed at a polycrystalline silver electrode is reported. Assignments of vibrational modes were based mainly on comparisons with the normal Raman spectra of t-BPE, its dihydrochloride and its dideuterochloride (also reported). The infrared spectrum of t-BPE and the vibrational spectra of trans stilbene and substituted pyridines were also utilized in the assigment of t-BPE surface Raman lines. A short history of surface-enhanced Raman scattering including examination of several of the proposed enhancement mechanisms is presented. Spectroscopic evidence for surface complex formation between t-BPE and the silver electrode is examined. The possibility of a resonance Raman enhancement mechanism resulting from perturbation of the electronic energy state distribution upon complexation is discussed. The influence of the metal conduction electron image field on the symmetry of the scattering system is theoretically scrutinized. Molecular reorientation of t-BPE molecules is observed in the surface Raman spectrum under certain conditions.

John J. McMahon

The conditions for molecular reorientation at the electrode surface are examined and a mechanism for the rearrangement is proposed. The excitation profile of t-BPE on silver is reported and demonstrates structure in the red region and at other wavelengths. Perturbation in the electronic state distribution of t-BPE upon complexation to the silver surface is invoked to account for the detailed structure in the excitation profile. Spectroscopic features, characteristic of the monoprotonated bipyridine, are observed in the surface Raman spectrum of t-BPE at pH 5.6. Photodegradation of multilayers of t-BPE on silver is also observed. Surface enhanced Raman scattering from L-glycine and L-leucine is reported and suggestions of molecular orientation are made.

TO CAITLIN

ACKNOWLEDGEMENTS

I wish to extend particularly grateful appreciation to Professor Gerald T. Babcock. Professor Babcock permitted experiments on surface Raman scattering to proceed utilizing his spectroscopic equipment, though the studies had little direct connection to his own research. Professor Babcock also provided considerable guidance in both theory and experiment without which completion of this thesis would have been impossible.

The assistance of Kendall L. Guyer in the construction of a suitable electrochemical cell, in the choice of t-BPE (the ideal adsorbate), and in general electrochemical discussions is gratefully acknowledged.

The efforts of Beverly Adams and Margaret Lynch in the preparation of this thesis are greatly appreciated.

Scientific discussions with Professors Katharine C. Hunt, George E. Leroi and Michael J. Weaver often stimulated my research and are acknowledged.

Special thanks to Rosemary and Caitlin for their unwavering support.

TABLE OF CONTENTS

LIST OF TABLES

Table Page

LIST OF FIGURES

LIST OF ABBREVIATIONS

ABBREVIATIONS

FWHH:	full width at half height
C_e:	ethylenic carbon
IP:	in plane
R:	alkyl substituent
sym. str:	symmetric stretch
HOMO:	highest occupied molecular orbital
ρ:	depolarization ratio
p:	polarized mode
dp:	depolarized mode

CHAPTER I

Introduction

Over the past three to four years there has been an explosion of experimental and theoretical studies of Raman scattering from metal surface adsorbates. Most of the experimental efforts have concentrated on the observation of enhanced Raman signals from pyridine at a silver electrode. The emphasis of these studies has been on the unmasking of the enhancement mechanisms which are apparently unique to the surface Raman studies.

Many fundamental questions continue to elude adequate explanation. For example, it is well understood that the long mean free path metal conduction electrons arrange to form an image dipole of a vibrating molecule which is adsorbed at the metal surface. However, the influence of this image field on the enhancement mechanism and on the Raman scattering selection rules for surface molecules has not been convincingly decided. Similarly, the question of whether a surface complex between metal and adsorbate is formed in the adsorption process remains unresolved. Many efforts to observe metal-ligand bond stretches in the surface Raman spectrum have failed.

sur

fie

the

kno

mer

tho

the

sig

dyn

met

kno

des

ox

Ra

syn

ele

wi

un

pr

cr

vi

ul

ti

co

These points are fundamental to an understanding of surface Raman intensities since the presence of an image field or a surface complex or both may significantly alter the symmetry of the light scattering species. Without knowledge of the symmetry of the scattering system, assignment of surface Raman spectra and interpretations based on those assignments become meaningless.

However, if accurate conclusions could be drawn about the symmetry of the adsorbates at a metal surface then significant far-reaching advances into the orientation, dynamics, and electrodynamics of molecules adsorbed at metal electrode surfaces would be forthcoming. For example, knowledge of adsorbate orientation can lead to more atomic descriptions of the double layer region. The structure of oxidation and reduction products observed in the surface Raman spectrum would also be discernable. The effect of symmetry distortions on the nature and wavelength of electronic transitions in the adsorbate could be concluded with the assistance of excitation profiles.

Raman studies of electrode-electrolyte interfaces are unique to surface spectroscopies in that the surface can be probed through solution owing to the small light scattering cross section of water. Electronic methods such as ultraviolet photoelectron spectroscopy, LEED, and Auger require ultrahigh vacuum conditions. In solution, electrode potentials may be maintained providing a new, researcher-controlled parameter. The ability to vary electrode

potential continuously while monitoring structure-dependent Raman spectra should lead to new insights into the effect of electron transfer on molecular structure.

Continued investigations are certainly warranted and in this thesis some of the above mentioned points are addressed and experimentally examined. The influence of the image field on the "molecular" symmetry probed in the surface Raman experiment is scrutinized theoretically. Electronic and symmetry perturbations experienced upon complexation are discussed. Evidence of complexation from Raman frequencies in regions well above the low frequency metal-ligand stretching region are presented.

The system studied most extensively in this thesis is that of trans-1,2-bis(4-pyridyl)ethylene (t-BPE) adsorbed at a polycrystalline silver electrode. In order to obtain an understanding of the surface spectra the normal Raman spectra of polycrystalline and dissolved t-BPE were recorded. The Raman spectrum of the dipyridine has not been previously reported in the literature although the infrared spectra of the cis and trans isomers were obtained by Katsumoto.[1] The dihydrochloride and dideuterochloride were prepared and the normal Raman spectra recorded to assist in the assignment of vibrational modes.

Trans-1,2-bis(4-pyridyl)ethylene is a good choice of adsorbate for several reasons. The extensive conjugation of the bipyridyl ethylene produces a large normal Raman

scattering cross section facilitating experimental observation. The ligand offers an ethylene π system and two nitrogens through which binding to the silver surface may occur. The molecular symmetry is C_{2h} which requires mutual exclusion of Raman and infrared activities. Reductions in symmetry upon complexation to the metal surface should be recognizable with the appearance of infrared modes in the surface Raman spectrum. The hydrophobicity of t-BPE is demonstrated by its minimal solubility in aqueous solution; saturation is reached at approximately 3 millimolar concentrations. It is likely that this hydrophobicity assists in the adsorption of t-BPE to the silver electrode surface. Intense surface Raman scattering can be observed from molecules adsorbed from 250 nanomolar concentrations. t-BPE also has two protonation sites and is electroactive, undergoing a two electron reduction at -1.1 V versus SCE (at neutral pH). Both of these capabilities can be exploited in an accurate determination of surface coverage.

Finally, it is hoped that information received from studies of the enhancement mechanism and surface orientation can be extrapolated to the investigation of other molecules at the electrode surface. Raman scattering from small amino acids adsorbed on silver are recorded here. Amino acid surface studies were undertaken so that results may be applied to the study of large, biologically important molecules at metal surfaces. The enhanced light scattering from the amino acid residues of a protein molecule which

lie cl

of seq

Observ

by ads

fluore

metal

radiat

Raman

the pr

the ex

lie closest to the metal surface may lead to conclusions of sequence and primary, secondary, and tertiary structure. Observation of light scattering from proteins is facilitated by adsorption to a metal surface owing to the lack of fluorescent background. Through energy transfer to the metal surface, the biological molecule gains a non-radiative excited state decay pathway. Current resonance Raman studies of proteins probe only the chromophore since the protein substructures do not directly contribute to the excited state in resonance.

a si

al.[2]

thes

subj

betw

elec

silv

from

Inte

whic

the

suff

elec

allo

the

Ther

inte

elec

CHAPTER II

History of Surface Enhanced Raman Scattering (SERS)

Intense light scattering from pyridine adsorbed at a silver electrode was first reported by Fleischmann et al.[2] in 1974, and in 1975 at copper electrodes.[3,4] In these experiments a polycrystalline silver electrode was subjected to a series of cyclic linear potential sweeps between +200 and +300 mV relative to the saturated calomel electrode for about 15 minutes. Oxidation of silver to silver chloride and redeposition of silver metal resulted from this process and produced an exceedingly rough surface. Intensity enhancement in the light scattering experiment which followed was not recognized since the increase in the electrode surface area was large and considered sufficient to support large numbers of adsorbed molecules.

In 1977 van Duyne and Jeanmaire[5] repeated the silver electrode experiments under stricter potentiostatic control allowing a much smaller amount of charge to pass during the oxidation-reduction cycle (typically 25 or 50 mC/cm^2). Therefore, van Duyne was the first to recognize incredible intensity enhancement from pyridine adsorbed at a metal electrode surface. An enhancement factor based on estimates

of surface coverage was projected to be 4 to 6 orders of magnitude above normal Raman scattering intensity from the same number of molecules. Molecues which exhibit resonance Raman scattering in solution were also examined (e.g. methyl orange, and crystal violet) and found to yield even higher enhancement factors up to 10 orders of magnitude.[5,6] A wavelength dependence study of the pyridine on silver experiment over the 4600 Å to 6300 Å region was reported to follow the fourth power wavelength dependence of normal Raman scattering presumably eliminating a resonance Raman enhancement mechanism.

However, subsequent studies by other researchers[7-12] on excitation profiles of pyridine at metal surfaces revealed an increased enhancement in the red after normalizing for the ω^4 dependence. Pettinger et al.[8] were the first to suggest resonance Raman enhancement of vibrational mode intensities in a surface complex of silver and pyridine. This conclusion was reached by showing that the differential reflectance spectrum of a silver electrode, electrochemically cycled in an aqueous pyridine solution, fit the excitation profile exhibiting increased enhancement in the red. In typical resonance Raman studies the excitation profile of Raman intensities is compared with the visible absorption spectrum. Absorption spectroscopy is a transmittance experiment and is therefore inapplicable to surface probes (except for very thin metal films, i.e., less than 500 Å silver). Differential reflectance is

therefore the supportive method of choice. A drop in the metallic reflectivity is assumed to be accompanied by absorption at the surface. The application of this single model to SERS was complicated by Mie scattering from a rough surface which may interfere with reflectivity measurements.[13] Moskovits[10,11] however, maintained that both the dip in the reflectance spectrum and the excitation profile could be fit by modeling the rough surface as a layer of metal spheres lying on a flat substrate with adsorbate and medium filling the gaps. This model allowed for resulting dispersion in the metal dielectric constant which could be fit to the data.

It rapidly became evident that several theories could account for surface enhanced light scattering. King, van Duyne and Schatz[14,15] originally proposed an image field enhancement mechanism which they later showed accounted for the excitation profile of pyridine on copper.[16] Subsequently, a University of California, Santa Barbara, group headed by Horia Metiu extensively studied the image dipole theory in a semi-classical theoretical treatment. In a series of papers Metiu et al.[17-23] set up a Green's function approach to describe the field experienced by an adsorbate at a certain distance from the metal surfaces. Included in the terms of the field equation were the following: a) the field E_p, produced by the incoming light beam in the absence of the molecule but in the presence of the surface (contains the Fresnel reflectivity coefficients),

and b)

a dista

of the

of the

where

dielec

resona

Thus,

condit

distan

course

the im

of the

gained

These

polar

Philp

plasm

gener

tions

which

and b) the field, E_s, emanating from the induced dipole at a distance Z_m from the surface and including reflection of the radiation from the induced dipole off the surface of the metal. The induced dipole was derived to be

$$\mu = \frac{\alpha E_p}{1-\alpha(2\pi\varepsilon_0)^{-1}(2Z_m)^{-3}} \qquad (1)$$

where α is the molecular polarizability and ε_0 is the dielectric constant of the medium. The distance dependent resonance condition was therefore

$$\alpha = (2\pi\varepsilon_0)(2Z_m)^3 \ . \qquad (2)$$

Thus, for typical molecular polarizabilities the resonance condition could only be met at very short metal-adsorbate distance, on the order of 1 Å. Classical treatments, of course, breakdown in modeling such atomic dimensions and the image field theory remained an inadequate description of the enhancement process.

Another theory of surface enhanced Raman scattering gained prominence with a series of elegant experiments. These were coupling of electromagnetic radiation to surface polaritons at the electrode-electrolyte interface. M.R. Philpott[24] first predicted the effect of coupling surface plasmons to electronic transitions in molecules in 1975. In general, surface plasmons are solutions to Maxwell's equations for the system, metal in contact with a dielectric, which are non-radiative. That is, the phase velocity,

V_{pha}
in
the
pla
hav
pla
in
rat
pla

fou
di
as
gr
by
pa
co
of
by
th
ma
ph
re
ar
e
t
(

V_{phase}, of the surface waves is less than the speed of light in the medium, C/n_d, where n_d is the refractive index of the dielectric. In order to couple effectively to surface plasmons they must become radiative. Currently, two methods have been proven successful in the excitation of surface plasma waves. They are 1) excitation by evanescent waves in the attenuated or frustrated total reflection configuration and 2) coupling of light to non-radiative surface plasmons utilizing surface roughness.[25]

Verification of roughness induced coupling has been found experimentally by several researchers[26-30] and discussed by Raether.[29] Uniform roughness can be considered as a regular array of step functions such as a diffraction grating. The Fourier transform of this array is described by a superposition of sine functions characterized by a particular wave vector $\vec{k}_r = 2\pi d^{-1}$, where d is the grating constant. A rough surface may be viewed as a superposition of such gratings. Since the momentum of the wave is given by $h(\vec{k})$, where $\vec{k} = \vec{k}_x + \vec{k}_r$, (where $\vec{k}_x$ is the wavevector of the incoming light), the phase velocity of the surface wave may exceed C/n_d if $\vec{k}_r$ is large enough (conversely, the phase velocity of the incoming photon $W(\vec{k}_r + \vec{k}_x)$ becomes reduced). Thus, the surface plasmon becomes radiative and may couple to molecular electronic transitions. Philpott et al.[31,32] demonstrated enhanced Raman intensities from thin organic films adsorbed onto holographic metal gratings (prepared by application of two interfering laser beams

i.e. 4

of sil

E

metho

in 19

call

of re

sandw

(n_p)

is kn

magne

ϕ (ac

at th

wave

virt

evan

laye

low

a ra

face

coup

spac

have

and

sca

pla

i.e. 4579 Å to photoresist followed by vacuum deposition of silver).

Excitation of surface plasma waves in silver by the method of attenuated total reflection (ATR) was described in 1968 by Otto.[33] The attenuated total reflection studies call for a system in which the dielectric medium (index of refraction n_d) containing the molecules of interest is sandwiched between the metal and a high refractive index (n_p) material (prism) such that $n_p > n_d$. This arrangement is known as the Kretschmann[34] configuration. When electromagnetic radiation traverses the prism at the correct angle ϕ (according to Snell's laws) it undergoes total reflection at the interface with the dielectric medium. An evanescent wave is generated at the prism-dielectric interface by virtue of conservation of momentum constraints. The evanescent wave propagates through the dielectric spacer layer with a phase velocity C/n_p. Since n_p is large the low phase velocity of the evanescent wave converts it into a radiative surface plasmon at the metal-dielectric interface (for low k values). The radiative plasmon may then couple to electronic transitions in the molecules of the spacer layer. Several reviews of surface plasmon coupling have appeared in the literature (e.g. see references (25) and (35)). Experimental verifications of enhanced Raman scattering from adsorbates through ATR coupling of surface plasmons abound in recent publications.[36-44]

Though coupling to surface plasmons has been proven to enhance the Raman scattering intensities, the enhancement factors observed fall far short of the 10^4-10^6 reported by van Duyne. Indeed, even exactly on resonance surface plasmon coupling can only account for a factor of 10 to 100.[38] Ultimately, the giant Raman intensities observed may be accounted for by several cooperative mechanisms.

Other theories to explain the anomalous surface Raman intensities have been proposed which have not enjoyed the widespread acceptance of either the image field theory or surface plasmon coupling. These include resonance Raman from surface transients or radicals,[45,46] normal Raman scattering from molecules intercalated in a dense carbon matrix at the electrode surface,[47-49] resonance Raman scattering from slightly perturbed surface and molecular states,[50] and radiative excitation and recombination of particle-hole pairs.[51,52] Of these, Cooney's work on the role of surface carbon helped researchers recognize the important influence of surface impurities and correctly cautioned coverage interpretations. Regis and Corset[46] have observed enhanced surface Raman scattering from bipyridines on silver. Their assignments were particularly useful in the assignment of the Raman spectrum of t-1,2-bis(4-pyridyl)ethylene on silver in this report.

Studies of adsorbates deposited under ultrahigh vacuum conditions have provided considerable information on coverage dependencies of intensities,[53,54] orientation of

molecules at the surface,[55] energy transfer between adsorbates and metal,[56-58] influences of impurities,[47] roughness phenomena,[59] and luminescent background identification.[60-61] Demuth et al.[55] examined an interesting coverage dependent phase transition on silver. When the coverage was increased the Raman spectrum was interpreted to indicate a transition from flat molecules to end-on configured pyridines. Conflicting reports from Bell Laboratories leave the question of distance for maximum intensity enhancement from the metal surface unresolved. Smardzewski et al.[53] initially reported that molecules closest to the surface exhibited the largest intensity enhancement. This conclusion was reached by observation of Raman spectra from a monolayer of deuterated pyridine followed by increasing coverages of undeuterated pyridine. The deuterated pyridine closest to the surface exhibited the most intense Raman scattering. Rowe et al.[58] measured the enhancement as a function of molecule-surface separation reaching the opposite conclusion i.e. molecules beyond those immediately adjacent to the metal surface also exhibited Raman intensity enhancement. The controversy is representative of the overall conflict currently in the SERS field. That is, is the enhancement effect a chemical one, requiring the formation of a chemical bond to the surface and enhancing only those molecules attached to metal atoms? Or, is the enhancement factor a result of electromagnetic phenomena, in which the field at the molecular position is enlarged due to the

presen

in the

contro

direct

CN^-, a

other

Pyraz

contr

surfa

pyrid

rule

are

whic

resu

impo

demo

of

of

exc

and

hea

sin

sca

spe

py

wa

presence of the surface, thus, allowing molecules simply in the vicinity of the metal to become enhanced? This controversy remains unresolved.

Although the greatest concentration of effort has been directed at the study of pyridine, pyridine derivatives and CN^-, applications of surface enhanced Raman scattering to other molecules have also appeared in the literature. Pyrazine,[62,63] for example, has provoked considerable controversy over the appearance of ungerade modes in the surface Raman spectrum. Similar to t-1,2-bis(4-pyridyl)ethylene, pyrazine has a center of symmetry and the rule of mutual exclusion is operative. Forbidden bands are also observed in the surface Raman spectrum of benzene which have been discussed in terms of symmetry lowering resulting from surface site symmetry.[64,65] Biologically important molecules have been observed on silver[66-68] and demonstrate advantages of surface studies. Some benefits of surface studies of biological molecules are the absence of flourescent background owing to the non-radiative excited state decay pathway provided by the metal substrate, and general absence of decomposition problems from over-heating in the beam with the metal surface acting as a heat sink. Moskovits and DiLella[69] observed surface Raman scattering from ethylene and propylene on silver. These spectra were helpful in the assignment of t-1,2-bis(4-pyridyl)ethylene SERS. Several other molecules including water,[70] CO,[71,72] and EDTA[73] have also been observed on

silver substrates.

Several of these enhancement mechanisms and surface techniques have been reviewed in the literature.[74,75] In this thesis only the mechanism of resonance Raman enhancement by surface complexes is addressed.

CHAPTER III

THEORY OF RESONANCE RAMAN SCATTERING FROM SURFACE COMPLEXES.

One mechanism which has recently advanced to the forefront of surface Raman discussions is resonance Raman scattering from surface complexes. The formation of a medium strength chemical bond between cyanide and the silver surface has been demonstrated.[76,77] However, similar efforts to observe a silver-pyridine stretching vibration have generally failed. In this chapter the implications of surface complex formation on the intensities of Raman signals from adsorbates is discussed.

Complex formation at the metal surface requires localization of metal electron densities. Such localization was examined by Goddard and McGill[78] in a review of quantum chemical methods applied to surfaces. The model found suitable for surface electron localization was intermediate between a lone metal atom and the delocalized metallic matrix, i.e. a cluster of metal atoms. With the orbital localization suggested by cluster formation a connection is made between the roughness requirements of surface enhanced Raman scattering,[79-81] the adatom hypotheses,[82-84] and a surface complex induced resonance Raman enhancement

mechanism.[85,86] That is, clusters of metal atoms formed in surface preparation procedures (e.g. oxidation-reduction cycle) result in orbital localization which may be utilized in overlaps of adsorbate electron densities.

Metal-adsorbate electron density overlaps may significantly alter the distribution of electronic states. Thus the possibility of coming into resonance with a low lying excited state of the complex even with red excitation becomes very real. Therefore, mechanisms of resonance Raman scattering warrant further study. According to Rousseau et al.[87] the total scattering cross section is

$$\sigma = \frac{8\pi\omega_s^4}{9c^4\hbar} \sum_{e,v} \frac{1}{\hbar} \left| \frac{\langle gj|r_\rho|ev\rangle\langle ev|r_\kappa|gi\rangle}{(\omega_{g,e}-\omega_L-i\Gamma_I)} + ar \right|^2 \qquad (1)$$

where the bracket represents the $\rho\kappa$th component of the molecular polarizability, $\alpha_{\rho\kappa}$; ω_L is the laser excitation frequency; ω_s is the scattering frequency. gi (electronic state g and vibrational state i), ev and gj represent respectively ground, intermediate and final vibronic states in the scattering event. r_e and r_κ are electronic position operators, with ρ and κ representing incident and scattered polarizations respectively. Γ_I is the linewidth of the intermediate state and ar represents antiresonance sums. The sum runs over all vibrational-electronic states except initial and final states, i.e., $|gj\rangle + |gi\rangle$. When the frequency of the incident photon matches the frequency

of the electronic transition (resonance condition) the scattering cross section becomes large and intensities increase. Most of the adsorbates examined in SERS experiments exhibit no resonance Raman scattering in solution owing to the lack of low lying (visible) electronic states. Therefore complex formation must be presumed if the enhancement mechanism of resonance Raman scattering is invoked. The metals which have demonstrated surface enhanced Raman scattering (Cu, Ag, Au, Hg) are all d^{10} metals. This wealth of electrons may be used to occupy normally unoccupied adsorbate molecular orbitals upon complex formation as observed for the $Ru(NH_3)_5$(t-1,2-bis(4-pyridyl)ethylene) complex[88] (see Figure 1) in which π^* states in the bipyridine ligand are occupied. In the pentaminebispyridylethylene ruthenium II complex the complex symmetry is C_s removing degeneracies occurring in the C_{2v} pentamine ruthenium substrate. The attachment of t-1,2-bis(4-pyridyl)ethylene to the silver surface should similarly reduce the symmetry of the molecule probed in the Raman experiment. Perturbation of the potential energy of the normal modes in the adsorbate upon complexation may also be invoked to account for minor shifts of vibrational frequencies observed in the surface scattering experiments.

When considering the electronic distributions of states in a surface complex in more detail some important conclusions can be made. Excluding for the moment the influence of the image dipole, formed by rearrangement

Figure 1: Energy State Perturbation in t-1,2-bis(4-pyridyl)ethylene upon Complexation to $Ru^{II}(NH_3)_5$. The point groups for the ligand, complex and $Ru(NH_3)_5$ are given. Ru(II) has a d^6 electron configuration and thus the lowest three levels in the energy level diagram for the complex are occupied.

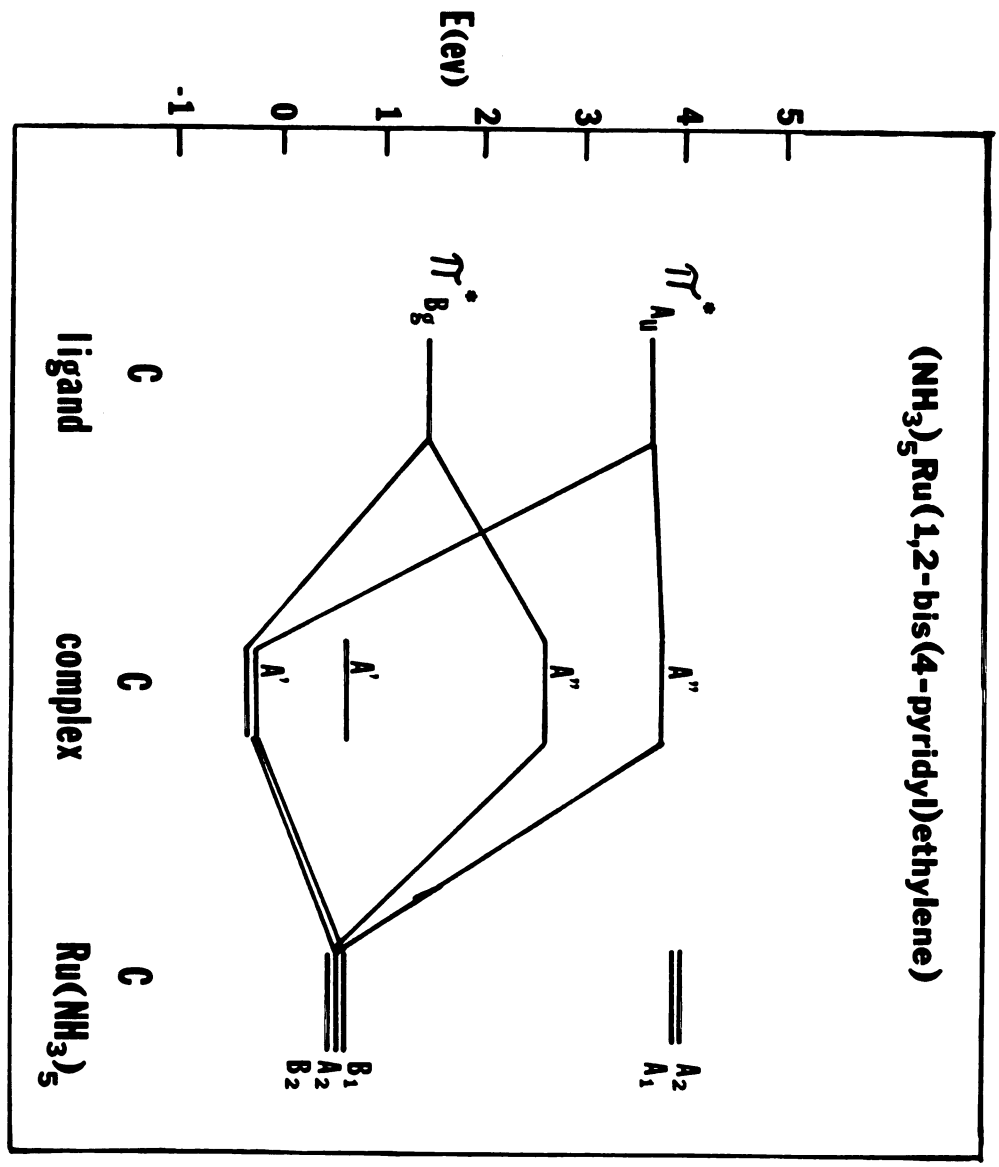
(NH3)5Ru(1,2-bis(4-pyridyl)ethylene)
E(ev)
5
4
3
2
1
0
-1
π* Au
π* Bg
A"
A'
A'
A"
A2
A1
B1
A2
B2
C
ligand
C
complex
C
Ru(NH3)5

of conduction electrons in the metal in response to the adsorbate electron distribution, the complex would have one-sided symmetry. Thus, all D group and higher symmetries would be eliminated owing to the absence of multiple rotation axes. The low symmetry would then be expected to lift most d electron degeneracies in the metal increasing the electronic density of states as observed in some low symmetry metal complexes.[89] With a high density of states, between which most transitions would be allowed, excitations in the red may result in resonance Raman intensity enhancement. Therefore, increased enhancement in the red, which is experimentally observed in all SERS studies and must be accounted for by any enhancement theory, is explained by the concept of a low symmetry surface complex.

Returning now to the influence of the image field on the symmetry of such a surface complex some previous misunderstandings are discovered. Pearce and Sheppard[90] suggested the influence of a "surface selection rule" operating on the IR spectra of molecules adsorbed at a highly polarizable metal surface. In this model, the system which interacts with an external electromagnetic field is not the original charge distribution (a molecule) but the system "molecule + image". As depicted in Figure 2, Pearce and Sheppard visualized a vibrating dipole at a metal surface producing dipole charge in the "perfect" metal. For an oscillating dipole oriented parallel to the surface the image would oscillate in the opposite direction

Figure 2: Surface Selection Rule Formalism. R is the operation connecting the adsorbate dipole with its conduction electron image. Γ is an irreducible representation.

in plane

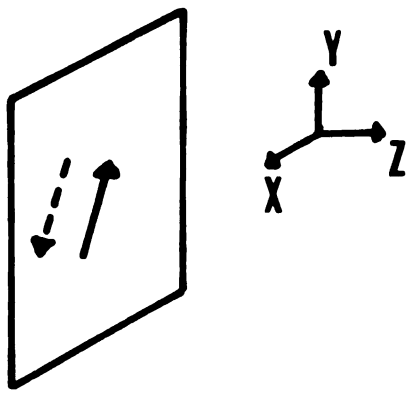

out of plane

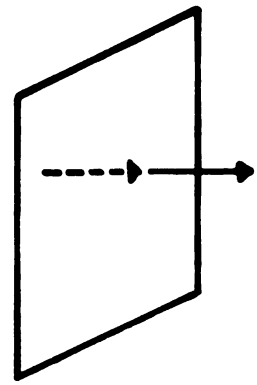

$$R\begin{pmatrix} x \\ y \\ z \end{pmatrix} = \begin{pmatrix} -x \\ -y \\ z \end{pmatrix} \qquad R = \begin{pmatrix} -1 & 0 & 0 \\ 0 & -1 & 0 \\ 0 & 0 & 1 \end{pmatrix}$$

$\{E + R\}$ is isomorphous with a C_2 axis.

$$\Gamma_{z^2} = \Gamma_{y^2} = \Gamma_{x^2} = \Gamma_{xy} = A$$
$$\Gamma_{xz} = \Gamma_{yz} = B$$

For C_{2h}:

$z \parallel Z$ (end-on)	$z \parallel X$ (flat)
$A_g(x^2, y^2, z^2, xy)$	$A_g(x^2, y^2, z^2)$
	$B_g(yz)$

cancelling out that motion in the adsorbate. Alternately, a dipole oscillating along the normal to the surface would be reinforced by the oscillating image dipole.

Hexter and Albrecht[91] considered in more detail the symmetry effects of the "surface selection rule" on both infrared and Raman activities. It is found that a new symmetry operation, that of reflection in the plane (σ_h) and charge conjugation C, is added to the total symmetry of the molecule + image system. The new point group generated by the new operation is $M = G \times \{\overrightarrow{E + R}\}$ where G is the molecular point group and $R = \sigma_h C$. The operation $\{\overrightarrow{E + R}\}$ is similar to a crystallographic screw axis, i.e. it is isomorphous to a C_2 axis. The effect of R on a cartesian column vector is demonstrated in Figure 2 and the R matrix developed with the normal to the surface designated z. Therefore in the infrared spectrum only motions polarized along z will be active i.e. $\Gamma_z = A$; $\Gamma_x = \Gamma_y = B$; and only A representations are active. In the Raman spectrum, in which components of the polarizability tensor transform as the direct product of the cartesian vectors, only symmetric direct products will be active, i.e. $\Gamma_{z2} = \Gamma_{x2} = \Gamma_{y2} = \Gamma_{xy} = A$; $\Gamma_{xz} = \Gamma_{yz} = B$. The expected Raman activities for two different orientations of a C_{2h} molecule, of which t-1,2-bis(4-pyridyl)ethylene is an example, on a metal surface are derived in Figure 2.

The effect of the image dipole would therefore be to increase the symmetry of the system (molecule + image). Increasing the symmetry can generally be expected to decrease the number of Raman active modes. In many surface studies the number of vibrations observed has increased over that observed in solution suggesting "surface selection rule" breakdown. The validity of the "surface selection rule" lies in the degree to which the image dipole charge distribution exactly mimics the adsorbate oscillations on the metal surface. It must be understood that the oscillations on the surface are those of nuclei. The charge distributions in the metal are made up of electrons alone and respond only to fluctuations in charge distributions in the adsorbate. The response of the conduction electron image to the adsorbate nuclear vibration therefore depends entirely upon the variation of the electronic wavefunction with normal coordinate (Q_k). The magnitude of that response decides the contribution to the Raman scattered light intensity by the image dipole. A sufficient but necessary requirement for "surface selection rule" breakdown is that the image field show a different nuclear coordinate dependence of the electronic wavefunctions. Different electronic response functions on either side of the silver surface will result in a lower symmetry system as probed by the Raman experiment. The "surface selection rule" requires an increase in symmetry, and thus would breakdown. The specific electronic dependence on

nuclear coordinate in the Raman scattering tensor has been reviewed by Clark and Stewart,[94] and their treatment is applied here to the adsorbate at a metal surface system.

The normal coordinate dependence of the electronic wavefunction can be examined more closely by considering the solutions to the Schrödinger equation for the system. By introducing a zeroth-order Born-Oppenheimer approximation the wavefunction for the Raman scatterer in Eqn. (1) becomes

$$\Psi_{gj} = \Theta_g(\xi,Q)\phi_j^g(Q) \tag{2}$$

where $\Theta_g(\xi,Q)$ is the electronic wavefunction for state g and $\phi_j^g(Q)$ is the jth vibrational state function of the ground electronic state. ξ and Q represent electronic and nuclear coordinates respectively. The integration over electronic coordinates in Equation (1) leads to a transition moment

$$(\vec{M}_e)_{gi,ev} = \langle\phi_v^e|(\vec{m}_\rho(Q))_{g,e}|\phi_i^g\rangle \tag{3}$$

and the corresponding moment of κ polarization in (3). $(m_\rho(Q))_{g,e}$ is the pure electronic transition moment

$$(\vec{m}_\rho(Q))_{g,e} = \langle\Theta_e|\vec{r}_\rho|\Theta_g\rangle \tag{4}$$

at nuclear configuration Q. In order to integrate Equation (3) over nuclear coordinates the explicit form of the Q dependence in $(\vec{m}_\rho(Q))_{g,e}$ is required. Following

Albr

seri

Subst

into

a_p

In a

the e

Equat

theor

Eqn.

Rayle

conta

in Ra

depen

exper

to th

Raman

on the

neglec

Albrecht[92] and Rousseau[87] $(m_\rho(Q))_{g,e}$ is expanded in Taylor series about the nuclear coordinates

$$(m_\rho(Q))_{g,e} = (m_\rho(Q_0))_{g,e} + \left(\frac{\partial m_\rho}{\partial Q_k}\right)_{0,g,e} Q_\kappa \qquad (5)$$

Substituting the result into the transition moment and into Equation (1), the molecular polarizability becomes

$$\alpha_{\rho\kappa} = \sum_e (m_\rho(Q_0))_{g,e}(m_\kappa(Q_0))_{g,e} \frac{1}{\hbar} \sum_v \frac{\langle j|v\rangle\langle v|i\rangle}{(\omega_{g,e}-\omega_L-\Gamma_e)}$$

$$+ \sum_e \left(\frac{\partial m_e}{\partial Q_\kappa}\right)_0 \left(\frac{\partial m_\kappa}{\partial Q_\kappa}\right)_0 \frac{1}{\hbar} \sum_\kappa \sum \frac{\langle j|v\rangle\langle v|Q_\kappa|i\rangle + \langle j|Q_\kappa|v\rangle\langle v|i\rangle}{(\omega_{g,e}-\omega_L-i\Gamma_e)} \qquad (6)$$

In a normal Raman experiment in which the v-dependence of the energy denominators is negligible the integrals in Equation (6) may be evaluated by invoking the closure theorem (i.e. $\sum_v |v\rangle\langle v| = 1$). Thus, the first term in Eqn. (6), Albrecht's A term, will be responsible only for Rayleigh scattering (i.e. j = 1) and the second term which contains the explicit nuclear coordinate dependence results in Raman scattering. The absence of nuclear coordinate dependence in the first term of Eqn. (6) in a normal Raman experiment requires that the image field will not contribute to the intensity of the Rayleigh scattering. In a resonance Raman experiment the dependence of the energy denominators on the excited-state vibrational quantum numbers cannot be neglected and closure cannot be applied. The vibronic

expansion of the energy denominator, according to Tang and Albrecht[93] is given by

$$(\omega_{e,v} - \omega_{g,i} - \omega_L)^{-1} = \sum_{N=0}^{\infty} (-1)^N \frac{(\omega_{e,v}-\omega_e{}^0)^N}{(\omega_e{}^0-\omega_{gi}-\omega_L)^{N+1}} * \tag{7}$$

where $\omega_e{}^0$ is the vertical transition frequency evaluated at the equilibrium nuclear configuration of the ground state. The N = 0 term is the normal Raman case. Keeping only the N = 1 term and recognizing that in the adiabatic approximation $\omega_{e,v}|v\rangle = \frac{1}{\hbar}\langle e|\mathcal{H}|e\rangle|v\rangle$ the first term in Equation (6) becomes

$$A' = \sum_{e\neq g} (m_\rho(Q_0))_{g,e}(m_\kappa(Q_0))_{g,e} \frac{1}{\hbar} \sum_v \frac{\langle j|\langle e|\mathcal{H}-\omega_e|e\rangle|v\rangle\langle v|i\rangle}{(\omega_e{}^0-\omega_{g,i}-\omega_L)^2} \tag{8}$$

The Hamiltonian in Equation (8) can be expanded about the equilibrium nuclear configuration following Clark and Stewart.[94]

$$\frac{1}{\hbar}\langle e|\mathcal{H}(Q) - \omega_e{}^0|e\rangle = \frac{1}{\hbar}\langle e|\mathcal{H}(0) + (\frac{\partial\mathcal{H}}{\partial Q})_0 Q + \ldots - \omega_e{}^0 e$$

$$= \frac{1}{\hbar}\langle e|\mathcal{H}(0)|e\rangle + \langle e|\frac{\partial\mathcal{H}}{\partial Q}|e\rangle_0 Q + \ldots - \omega_e{}^0$$

and

$$= \frac{1}{\hbar}\langle e|\frac{\partial\mathcal{H}}{\partial Q}|e\rangle_0 Q \tag{9}$$

---

*Note: the damping factor has been omitted since the expansion is strictly only valid far from resonance.

since $\frac{1}{\hbar}\langle e|\mathcal{H}(0)|e\rangle = \omega_e{}^0$. This leads to a revised A term which includes the resonance Raman case:

$$A' = \sum_{e\neq g} (m_\rho(Q_0))_{g,e}(m_\kappa(Q_0))_{g,e} \sum_v \frac{1}{\hbar} \frac{\langle j|Q|v\rangle\langle e|\frac{\partial\mathcal{H}}{\partial Q}|e\rangle_0\langle v|i\rangle}{(\omega_e{}^0-\omega_{gi}-\omega_L)^2} \tag{10}$$

Thus, if a force, given by the derivative of the potential part of the Hamiltonian* with nuclear coordinate ($F_e{}^0 = (\partial Ve/\partial Q)_0$), is experienced upon excitation into an excited state, then the first term in Equation (6) may contribute to observed Raman intensities. To experience a force in the excited state the equilibrium position in that state must be shifted relative to the ground state equilibrium position. The shift in equilibrium position will be only along totally symmetric normal coordinates since the matrix element $\langle e|\frac{\partial\mathcal{H}}{\partial Q}|e\rangle$ vanishes for non-totally symmetric coordinates. Thus, resonance Raman scattering by the A' term will result in enhancement of totally symmetric vibrations.

In the second term of Equation (6), Albrecht's B term, the dependence of the electronic wavefunction on nuclear coordinate is explicitly contained in the coefficients $(\partial m_\rho/\partial Q_k)_0$ and $(\partial m_\kappa/\partial Q_k)_0$. Following Albrecht[92] the

---

*Note: In the adiabatic Born-Oppenheimer approximation the potential energy of a nuclear vibration is equal to the total electronic energy therefore

$(\partial Ve/\partial Q)_0 = \langle e|\frac{\partial\mathcal{H}}{\partial Q}|e\rangle_0$.

coordinate dependence of the electronic moment may be treated as a Herzberg-Teller perturbation i.e.

$$\left(\frac{\partial m_\rho}{\partial Q_k}\right)_0^{g,e} = \sum_s m_\rho^{g,s}(Q_0) \quad \frac{1}{\hbar} \langle e | \partial \mathcal{H}/\partial Q_k | s \rangle \ . \qquad (11)$$

Therefore, it is evident that contributions to the Raman intensity from both the A term and the B term depend on the quantity $(\partial \mathcal{H}/\partial Q_k)$. In the A term $(\partial \mathcal{H}/\partial Q)$ produces vibronic mixing within one excited state and in the B term $(\partial \mathcal{H}/\partial Q_k)$ couples different electronic excited states. Since the overlap of energy bands in the electronic manifold of the valence and conduction electrons is extensive in the metal and limited in the adsorbate the magnitudes of $(\partial \mathcal{H}/\partial Q_k)$ in the adsorbate and image dipole are likely to be quite different. Since $(\partial \mathcal{H}/\partial Q)$ is responsible for the intensity of the resonance Raman scattered light that intensity emanating from either side of the silver surface will not be the same. Therefore, contrary to the prediction of the "surface selection rule", the image field can only act to reduce the symmetry of the scattering system not increase that symmetry.

Thus, with the absence of any symmetry ordering influence by the conduction electron image, the system being probed in the Raman experiment returns to a one-sided attachment of an adsorbate to the surface. Symmetry reductions caused by the one-sided nature of the system,

the mismatch of the image field, and low site symmetry experienced by an adsorbate at the surface of a metallic matrix, result in expectations of extremely low symmetry scattering systems. The most common point group expected, even for highly symmetrical adsorbates, is C_1. Of course, in such low symmetry all modes will become Raman active and, in general, an increase in the number of observed Raman lines is expected. However, in a resonance Raman mechanism only those modes effective in coupling electronic excited states through electron density overlap are enhanced. Thus, all possible vibrations may still not be observed. For example, t-1,2-bis(4-pyridyl)ethylene adsorbed at a silver surface may actually be attached through either of the nitrogen atoms (but not both) in an "end-on" configuration or may lie flat on the surface. In the end on configuration only the nitrogen atom experiences electron density overlap with the metal. Thus, it might be expected that the surface Raman spectrum observed would not be much perturbed from the normal Raman spectrum. In the flat configuration, in contrast, the entire molecule experiences some overlap of electron density with the metal and all vibrations (both infrared and Raman active) are expected to be observed.

Conclusions drawn in this chapter are extrapolated to the discussion of orientation and enhancement mechanism of t-1,2-bis(4-pyridyl)ethylene at a silver electrode surface. The experimental surface Raman spectra and discussions are presented in Chapter 6.

The surface complex enhancement mechanism has been slow to attain fruition. This has mainly been the result of a lack of success in observation of a metal-adsorbate stretch in the low frequency region. For all surface Raman studies a very complicated low frequency region is observed which has hindered assignments. The appearance of a strong, Ag-Cl stretching mode in electrolyte studies near 230 cm^{-1} also may cloud assignments in the region. Pettinger and Wetzel[85] recently applied reduced potential difference spectra (RPDS) to the low frequency Raman spectrum of pyridine on silver. In doing so the Bose-Einstein term $(e^{\omega/kT} - 1)^{-1}$ in the prefactor of the Raman cross section could be eliminated revealing hidden structure in the low frequency region. A silver-pyridine symmetric stretch was assigned to a 210 cm^{-1} line.

Efforts to find a metal-adsorbate stretch may be doomed at the outset. Such a mode can be expected to be considerably damped owing to one atom of the vibrating pair being associated in a large metal matrix (see, for example the treatment of free damped motion by Ross[95]). The low amplitude resulting from damping will result in low Raman intensity. Forces associated with the electric field at a metal electrode also may act to damp the oscillations of an adsorbate metal bond.

Experimental evidence of surface complex formation in the system t-1,2-bis(4-pyridyl)ethylene at a silver

electrode is presented in this thesis. Assignments are made without regard to the "surface selection rule".

CHAPTER IV

Experimental

Raman Spectrometer

All Raman spectra reported in this thesis were obtained with a Spex Industries model 1401 Ramalog system. Photon detection was accomplished with a cryostatted (-20°C) RCA model C31034 GaAs photomultiplier tube in photon counting mode. All spectra were recorded with a resolution better than 2 cm^{-1}.

Samples

Polycrystalline samples and aqueous solutions were sealed in 1.7 mm capillary tubes. High vapor pressure methylene chloride solutions were placed in a Raman cuvette. A translating Raman cuvette holder and brass cooling jacket were constructed for optimal sample management. Opaque polycrystalline samples were observed in a back scattering geometry. The incident laser beam was allowed to pass through a hole in a 45° mirror just prior to striking the capillaried sample. The back scattered radiation was thus reflected into the entrance slit of the double monochromator.

The first electrochemical cell utilized in surface Raman studies was constructed from a hollowed-out lucite cylinder. Raman spectra were observed through a quartz optical flat. Because of difficulties in maintaining the system free from impurities, the lucite cell was replaced with a glass cell which could be cleaned by immersion in concentrated nitric acid solutions. The working electrode was a polycrystalline silver disk fitted to a teflon sheath. The surface area of the silver disk in contact with electrolyte solution was measured to be 0.11 cm^2. The working electrode was generally placed very close to the observation window only after the oxidation-reduction cycle was complete. This was done to prevent non-uniform coverage of the electrode surface caused by concentration gradients which develop during the cycling procedure. Subsequent movement of the electrode surface close to the observation window permitted observation of maximum intensity from surface species and a minimum from the bulk solution.

The reference electrode was a silver-silver chloride electrode. This was prepared by electrolyzing a coating of silver chloride onto a silver coated platinum wire which was immersed in a saturated silver chloride solution (prepared by addition of a few drops of silver nitrate to a saturated KCl solution). The body of the reference electrode was ¼" glass tubing to which an ultrafine mesh porous plug was attached. Generally, the reference electrode was

attached to another ¼" glass tube containing the supporting electrolyte. This prevented potential drift accompanying minor leakage. The reference potential of the Ag/AgCl couple was 50 mV relative to the saturated calomel electrode. All electrode potentials reported in this thesis are referenced to the saturated calomel electrode (SCE). In supporting electrolytes containing $NaClO_4$ the reference electrode was prepared with saturated NaCl solution instead of KCl so as to prevent precipitation of $KClO_4$ which is minimally soluble in water. The counter electrode was a heavy gauge platinum wire. Nitrogen gas (Airco Inc., 99.99% pure) was bubbled into solutions prior to electrolysis and often during Raman observation to limit the formation of silver oxides. All surface spectra were recorded at an angle of incidence of 60° for maximum scattering intensity as observed by Pettinger et al.[97] This system is shown in Fig. 3.

The electrochemical cell was controlled with an Eco Control Inc. model 550 potentiostat and model 731 digital integrator. Generally, 50 mC/cm^2 (or 5.5 mC for this electrode) were allowed to pass during the oxidation-reduction cycle (i.e. the potential was maintained at +100 mV versus SCE until sufficient charge passed and then the potential was returned to -600 mV versus SCE). This cycling yielded a rough electrode surface. The reflectivity of the metal surface drops during the oxidation-reduction cycle producing a slightly yellow coating even

in the simple chloride blank. Varying amounts of residual charge remained after completion of the ORC depending on adsorbate and electrolyte. Potential drift was negligible ($\sim \pm 2$ mV) over the course of a typical Raman experiment. Potential cycling was carried out in the presence of adsorbates. For solutions of t-1,2-bis(4-pyridyl)ethylene at millimolar concentrations potential cycling produced a dark brownish-black coating at the electrode surface. However, similar Raman intensities were observed for 500 nM solutions of bis pyridyl ethylene which upon cycling yielded a yellow surface coating undistinguishable from that observed in the chloride blank.

The silver electrode surface was subjected to mechanical polishing before each experiment. This consisted of applications of Al_2O_3 powders (Buehler Ltd.) of diminishing size finishing with 3 micron powder. The electrode was then rinsed with methanol and water and transferred to the electrochemical cell with a drop of water attached to inhibit oxide formation.

Lasers

A Spectra Physics model 165-08 argon ion laser (4 watts all lines) with model 265 exciter was used for 5145 Å excitation and to pump a continuously tunable Spectra Physics model 365-09 dye laser with three-plate birefringent filter. A Classen filter was used to assume monochromaticity of dye laser emissions. Rhodamine 6G

Figure 3: Experimental arrangement in the SERS experiment. R = reference electrode (Ag/AgCl); W = working electrode (polycrystalline silver); C = counter electrode (platinum wire); FL = focusing lens; CL = collection lens; ϕ_{inc} = angle of incidence relative to the surface normal.

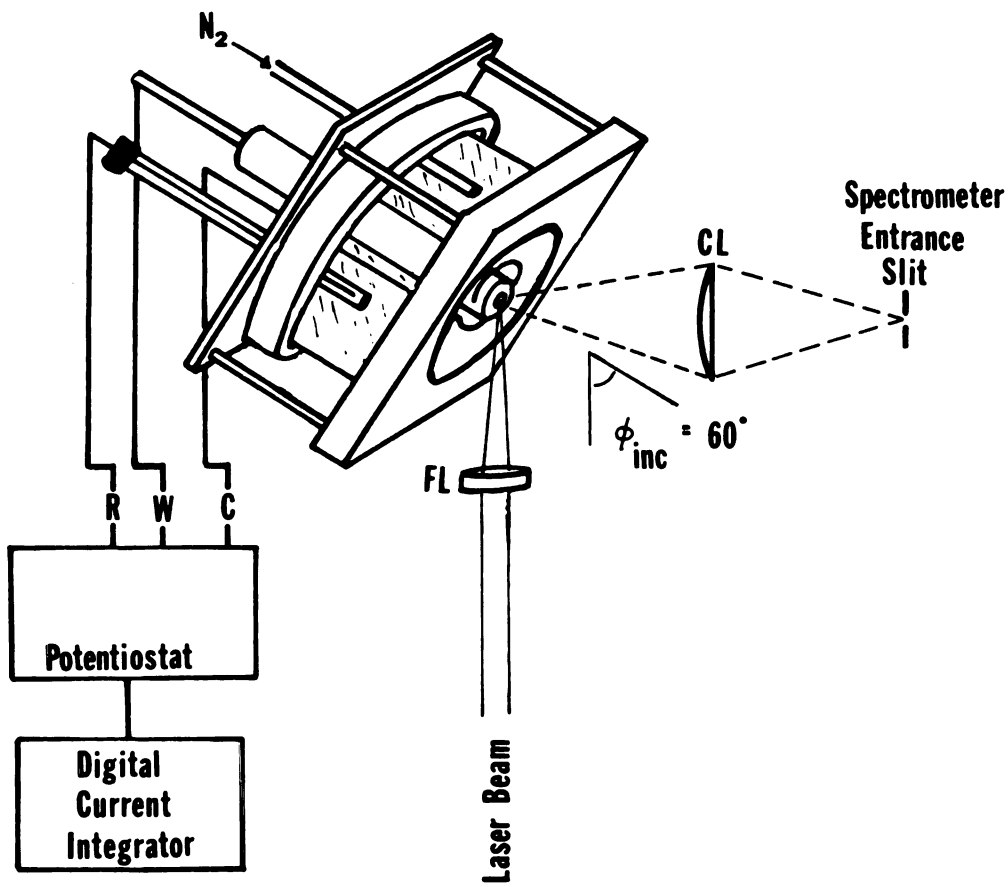
N_2
Spectrometer
Entrance
Slit
CL
ϕ_{inc} = 60°
FL
R
W
C
Potentiostat
Digital
Current
Integrator
Laser Beam

(Exciton Chem. Co.) was the dye used in obtaining excitation profiles of surface molecules covering the range 5600 Å to 6600 Å. For red excitation a Spectra Physics model 164-01 krypton ion laser was employed.

Excitation Profiles

Excitation profiles of species adsorbed to the silver electrode surface were obtained in order to examine the electronic manifold of states in the surface-molecule system. The 935 cm^{-1} line of sodium perchlorate (0.5 M) served as an internal standard. The intensity of the 935 cm^{-1} line could be varied by positioning the electrode surface at various depths in the electrolyte. Because of the potential dependence of the surface concentration of ClO_4^- a better choice of internal standard is necessary for comparison of potential-dependent excitation profiles. The teflon sheath fitted to the silver electrode serves this purpose well. Both the metal surface and the teflon could be illuminated simultaneously with the application of cylindrical focusing. The Raman spectrum of teflon is reported here and is generally uninterfering with the surface Raman spectrum of t-1,2-bis(4-pyridyl)ethylene (see Figure 4).

It became necessary in the course of carrying out excitation profile experiments on surface adsorbates to assure that the laser beam remained focused to the same point on the surface with each excitation wavelength.

Figure 4: Normal Raman spectrum of teflon and surface Raman spectrum of t-1,2-bis(4-pyridyl)ethylene on silver with teflon standard.

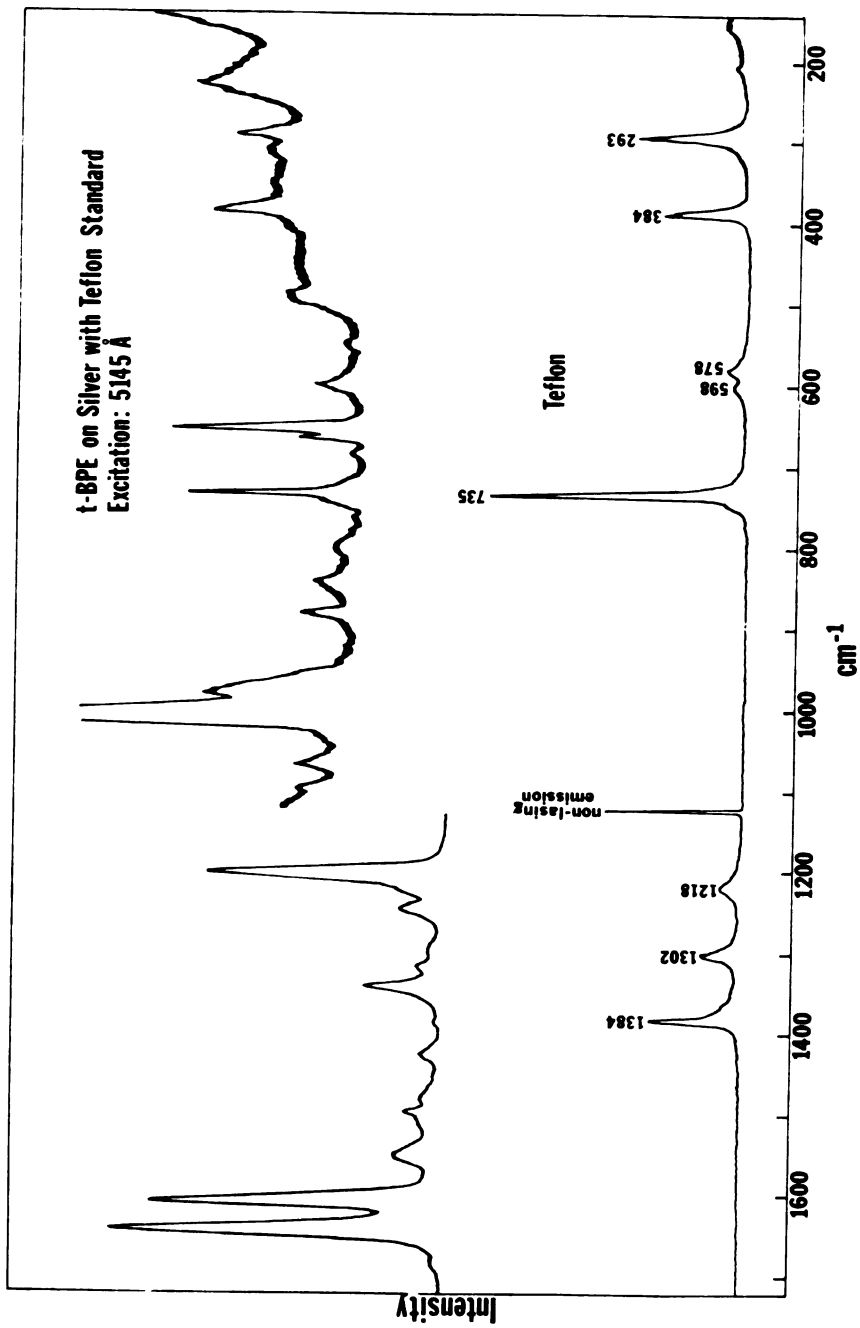
t-BPE on Silver with Teflon Standard
Excitation: 5145 Å
Teflon
non-lasing emission
1384
1302
1218
735
598
578
384
293
200
400
600
800
1000
1200
1400
1600
cm-1
Intensity

Since tuning the dye laser requires passage through a birefringent filter of refractive index greater than 1 each excitation frequency will traverse space with a different vector (similar bending occurs during passage through the Classen filter). Therefore an aperture was placed just prior to the sample and the laser direction adjusted to pass through the aperture and thus illuminate the same point on the surface regardless of excitation frequency. Spectra were recorded every 100 cm^{-1} during the excitation profile.

The excitation profiles reported in this thesis are corrected for the ν^{-4} dependence of the Raman scattered light intensity.[5] Spectroscopic intensities were normalized to the intensity of the 935 cm^{-1} line of the perchlorate, but not normalized relative to intensities at different excitation frequencies since doing so would effectively double the relative error in each profile data point. Therefore the most intense peaks in the profile belong to the most intense peaks in the spectrum itself. A program for ν^{-4} correction and normalization was written for a Hewlett-Packard 67/97 calculator and is available upon request.

Laser Power Measurement

Laser powers were measured with either a Photodyne model 44XL optical power meter or a Coherent Radiation model 210 power meter.

Visible Absorption Spectra

Absorption spectra of t-1,2-bis(4-pyridyl)ethylene, its dihydrochloride and a silver complex of t-BPE were obtained on a GCA/McPherson model Eu-700 series UV/Vis spectrometer.

Sample Preparation: t-1,2-bis(4-pyridyl)ethylene(t-BPE)

Trans-1,2-bis(4-pyridyl)ethylene (Aldrich Chem. Co.) was recrystallized from hot water; some orange color was removed in the process. Normal Raman spectra of polycrystalline t-BPE were recorded. Since t-BPE is only sparingly soluble in water, reaching saturation at about 3 mM concentrations, spectra were recorded in methylene chloride solutions. Solutions for surface studies ranged from 2.5 mM t-BPE (heavy coverage) to 250 nM t-BPE (light coverage). Supporting electrolytes were either 0.1 M KCl or 0.1 M NaCl and 0.5 M $NaClO_4$. For "light coverage" surface studies fresh polishing pads were used owing to the presence of residual t-BPE on used polishing pads, which could influence bulk concentrations and therefore coverage.

t-1,2-bis(4-pyridyl)ethylene dihydrochloride and dideuterochloride

Trans-1,2-bis(4-pyridyl)ethylene dihydrochloride was prepared by dissolving t-BPE in methanol and adding concentrated hydrochloric acid until no further crystallization was evident. The pinkish orange crystals were collected on

a 15 mesh buchner funnel and washed with methanol. The Raman spectra of polycrystalline and aqueous solutions of the dihydrochloride were obtained.

Trans-1,2-bis(4-pyridyl)ethylene dideuterochloride was prepared by bubbling DCl into a methanol solution of t-BPE. DCl was prepared[98] by slow addition of 5 ml D_2O to 30 ml benzoyl chloride and refluxing under light heating. Unreacted D_2O and benzoyl chloride were collected in an ice trap and DCl in a liquid nitrogen trap. DCl was bubbled through the t-BPE solution until no further crystallization was evident. The pinkish-orange crystals were collected and washed with methanol. A similar preparation was attempted by using chloroform as the solvent and a pink compound was obtained after considerable DCl was passed through solution. This compound was insoluble in water and was air oxidized overnight to a yellow crystalline compound. It is believed that this pink compound was the addition product of DCl across the ethylene double bond. However physical evidence of its structure is currently incomplete.

Silver Complex of t-1,2-bis(4-pyridyl)ethylene $(Ag_n(t\text{-}BPE)_m$

A silver complex of bis pyridyl ethylene was prepared by addition of an aqueous solution of silver nitrate to an ethanol solution of t-BPE until no further crystallization occurred. Crystallization appeared complete after addition of silver nitrate to 1:2 ($AgNO_3$/t-BPE) molar ratio with

t-BPE. Crystals were collected and washed with both ethanol and water. The complex was found to be soluble only in n-butyl amine and pyridine. The silver complex was found to be insoluble in water, ethanol, CCl_4, CH_3Cl, CH_2Cl, $CHCl_3$, dimethyl sulfoxide, tetrahydrofuran, ammonium hydroxide, methyl amine, n-propyl amine, CS_2, methanol, acetone, cyclohexane, n-hexane, diethyl amine, and benzene. The Raman spectrum of the polycrystalline silver complex was obtained and is reported here.

Amino Acid Solutions

Amino acid solutions were prepared to 0.05 M in 0.1 M KCl stock solution. Observation of Raman spectra of the amino acids on silver adsorbed from neutral solution was unsuccessful. However spectra were observed from solutions in which the pH was adjusted above the isoelectric point of the particular amino acids. Glycine and leucine surface spectra were recorded at a bulk solution pH of 11.0.

AgOH, Ag_2O

Raman spectra of polycrystalline silver hydroxide (AgOH) and silver oxide (Ag_2O) were obtained for comparison with surface spectra to examine the possible occurrence of surface oxide formation. Commercially available silver oxide (Fisher Chemical) was used without further purification. Silver hydroxide was prepared by addition of excess hydroxide (KOH) to an aqueous solution of silver nitrate until the solubility product of silver hydroxide

(1.52×10^{-8}; 20°C)[99] was exceeded. Both silver oxide and silver hydroxide are black polycrystalline substances and therefore a back scattering geometry was required to obtain the Raman spectrum. The specific geometry was described previously in this chapter.

CHAPTER V

Polycrystalline and Solution Raman Spectra of t-1,2-bis(4-pyridyl)ethylene, its dihydrochloride and its dideuterochloride

In order to understand the surface Raman spectrum of trans-1,2-bis(4-pyridyl)ethylene (t-BPE) more clearly the normal Raman spectrum was recorded. The Raman spectra of the dihydrochloride and dideuterochloride are also reported to assist in assignment of vibrational modes. The Raman spectra of these compounds have not previously been reported in the literature although the infrared spectra of both the trans[1,100] and cis[1] isomers have been reported. Both solution and polycrystalline spectra are reported. Solution depolarization ratios are also determined. The Raman spectra are shown in Figures 5 and 6 and the vibrational frequencies are listed in Table 1. The pyridine ring vibrations are assigned according to Wilson notation.[101] All normal Raman spectra reported here were obtained with 6471 Å excitation.

Symmetry Considerations

The molecular point group symmetry of t-1,2-bis(4-pyridyl)ethylene is C_{2h}. The center of symmetry in the molecule requires that infrared and Raman activities be

TABLE 1: Raman Spectra of t-1,2-bis(4-pyridyl)ethylene, t-1,2-bis(4-pyridyl)ethylene dihydrochloride and t-1,2-bis(4-pyridyl)ethylene dideuterochloride. Excitation: 6471 Å.

-Symmetry--			Assignment	-----t-BPE--------			---t-BPE H_2Cl_2--			t-BPE D_2Cl_2	
C_{2v}	C_{2h}	D_{2h}	(Wilson #)	CH_2Cl_2	ρ	Solid	H_2O	ρ	Solid	D_2O	Solid
						43			48		43
											54
			Lattice								58
			Modes								70
						81			80		83
									99		100
						121			134		141
			Skeletal			208					224
			Vibration	225		240	230		240	229	243
	A_g		2 × 121			242					
									296		304
						370			370		370
A_2	B_g		16a				401			402	399
B_1	B_g		16b			486			480		466
A_1	A_g		6a	650	.17p	641	643		643	640	645
B_2	A_g		6b	667	.64dp	671	653	.67dp	651	651	651
B_1	B_g		10a	880	.68dp	878	887	.70dp	879	882	879
A_2	B_g		10b			888			894	902	901
A_2	B_g		5	954		958					
B_1	B_g		17a	970		976	997		997	970	996
A_1	A_g		1	993	.11p	995	999	.21p	1008	996	1005
A_1	A_g		18a			1069			1062		1066
	A_g					1184					
	A_g	A_g	C - ϕ str.	1195	.21p	1198	1210	.28p	1203	1210	1206

Table 1 Continues.

Table 1 Continued.

-Symmetry--			Assignment	-----t-BPE--------			---t-BPE H_2Cl_2--			t-BPE D_2Cl_2	
C_{2v}	C_{2h}	D_{2h}	(Wilson #)	CH_2Cl_2	ρ	Solid	H_2O	ρ	Solid	D_2O	Solid
A_1	A_g		9a	1220	.13p	1225					1215
B_2	A_g		9b NH def.	1233	.32p	1234	1260	.50p	1254	1294	1260
B_2	A_g		3	1313	.19p	1319	1320		1333	1323	1335
A_1	A_g		2 × 6b			1342					
B_2	A_g		14	1338	.22p	1351	1341	.29p	1346	1346	1349
A_1	A_g		2 × 11				1378	.40p	1373		1374
A_1	A_g		4 + 11	1411	.38p	1411					
B_2	A_g		19b	1422	.53p	1419	1518	.36p	1512	1463	1514
A_1	A_g		19a	1492	.17p	1491	1508sh		1500sh	1502	1505sh
A_1	A_g		2 × 4			1541					
B_2	A_g		8b	1549	.24p	1549			1605	1567	1606
A_1	A_g		8a	1597	.40p	1597	1642	.36p	1635	1638	1635
A_1	A_g			1620		1611					
	A_g	A_g	C=C str.	1641	.27p	1638	1642	.36p	1644	1638	1643
B_2	A_g	A_g	2 ν_4 eth.	1671		1676	1672		1674	1671	1672
			N-D str.							2400br	
			(2 × 1200)							2510br	
		A_g	ν_1 C_e-H str.			3013					
						3024					3024
			CH			3038			3031		3039
			stretch	3060		3054			3050		
									3059		3068
							3109		3085	3102	3092
	A_g	A_g	(2 × C=C str.)				3270br		3266		
	A_g		N-H str.				3400br				

Figure 5: Normal Raman Spectra of polycrystalline t-1,2-bis(4-pyridyl)ethylene, its dihydrochloride and dideuterochloride.
EXCITATION WAVELENGTH: 6471 Å (Kr^+).

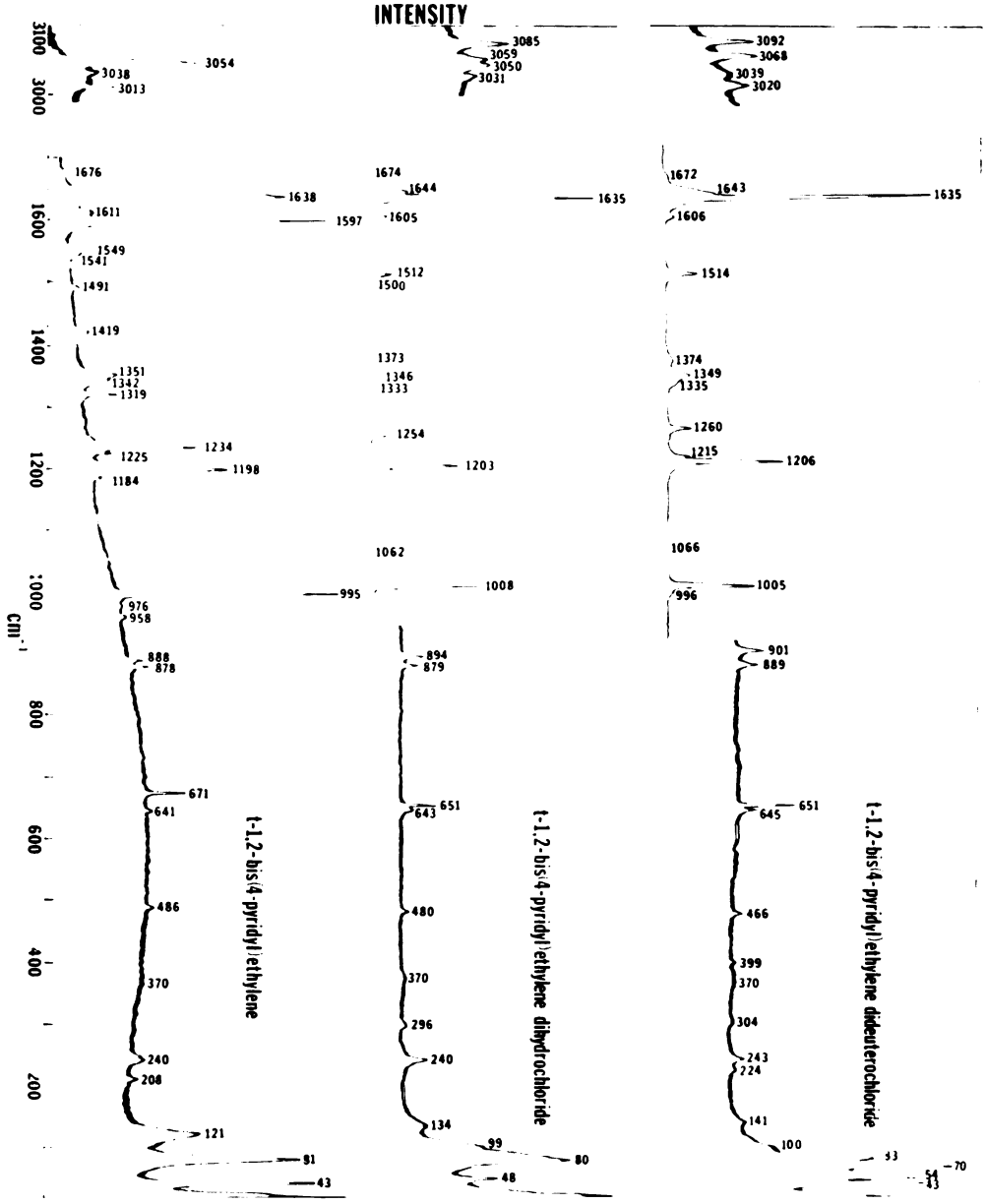
INTENSITY
cm⁻¹
3100
3000
1600
1400
1200
1000
800
600
400
200
3054
3038
3013
3085
3059
3050
3031
3092
3068
3039
3020
1676
1611
1549
1541
1491
1419
1351
1342
1319
1234
1225
1198
1184
1638
1597
1674
1644
1635
1605
1512
1500
1373
1346
1333
1254
1203
1062
995
1008
1672
1643
1635
1606
1514
1374
1349
1335
1260
1215
1206
1066
996
1005
976
958
888
878
671
641
486
370
240
208
121
91
43
894
879
651
643
480
370
296
240
134
99
80
48
901
889
651
645
466
399
370
304
243
224
141
100
93
70
54
43
t-1,2-bis(4-pyridyl)ethylene
t-1,2-bis(4-pyridyl)ethylene dihydrochloride
t-1,2-bis(4-pyridyl)ethylene dideuterochloride

Figure 6: Normal Raman Spectra of t-1,2-bis(4-pyridyl)ethylene in CH_2Cl_2, the aqueous solution of the dihydrochloride, and the dideuterochloride in D_2O.
EXCITATION WAVELENGTH: 6471 Å (Kr^+).

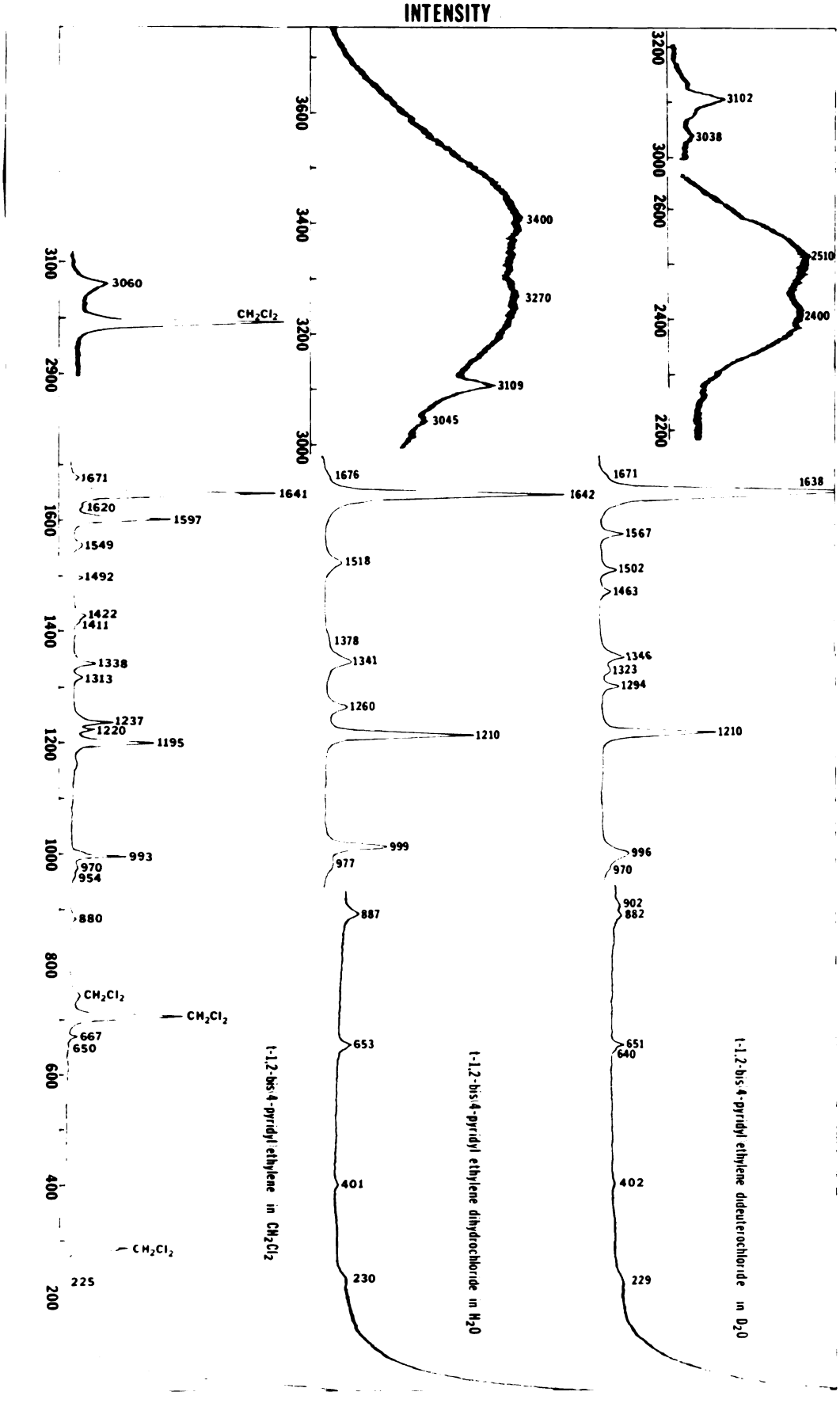
INTENSITY
3100
2900
3060
CH2Cl2
1671
1641
1620
1597
1549
1492
1422
1411
1338
1313
1237
1220
1195
993
970
954
880
CH2Cl2
CH2Cl2
667
650
CH2Cl2
225
t-1,2-bis(4-pyridyl ethylene in CH2Cl2
3600
3400
3200
3000
3400
3270
3109
3045
1676
1642
1518
1378
1341
1260
1210
999
977
887
653
401
230
t-1,2-bis(4-pyridyl ethylene dihydrochloride in H2O
3200
3000
2600
2400
2200
3102
3038
2510
2400
1671
1638
1567
1502
1463
1346
1323
1294
1210
996
970
902
882
651
640
402
229
t-1,2-bis-4-pyridyl ethylene dideuterochloride in D2O

mutually exclusive. Since the molecule is made up of two pyridine rings, vibrations in one ring may be in-phase or out-of-phase with the same vibrations in the other ring. In-phase vibrations will be of A symmetry (A_g, A_u) i.e. symmetric with respect to the C_2 axis. Out-of-phase motions will be antisymmetric with respect to the C_2 axis or of B symmetry (B_g, B_u). Analysis of the number of irreducible representations for t-BPE predicts the observation of 23 A_g, 10 B_u, 11 A_u, and 22 B_u modes in the vibration spectra. Only gerade modes will remain Raman active. Thus by correlating the symmetry representations of pyridine (C_{2v}) modes to the molecular symmetry (C_{2h}) as in Table 2 it becomes evident that each pyridine motion correlates to one Raman active mode and one infrared active mode. Combinations and overtones involving ungerade modes, whose direct products transform as gerade representations, can also be observed in the Raman spectrum of t-BPE. In Table 2 ethylene modes (D_{2h}) are also correlated to the molecular symmetry (C_{2h}). The vibrational modes associated with the symmetry species in the correlated symmetries (C_{2v},D_{2h}) are[102,103] included in Table 2. Further correlation to possible surface complex symmetries is also examined in Table 2. The choice of axes is consistent with pyridine assignments in reference (104). The crystallographic space group symmetry was not determined in this study. Therefore, correlation to crystal and site symmetries for polycrystalline Raman spectral assignment was impossible. Efforts

TABLE 2: Correlation of symmetries of the pyridine rings and ethylene to the molecular symmetry of t-1,2-bis(4 pyridyl)ethylene and further correlation to possible surface complex symmetries.

----------Modes-------- pyridine	Correlated -Symmetry- C_{2v}	Molecular -Symmetry- C_{2h}	Surface Complex ---Symmetries-- C_s
2, 13, 20a, 8a, 19a,	A_1	A	A'
9a, 18a, 12, 1, 6a			A"
17a, 10a, 16a	A_2	B	C_2
17b, 5, 10b, 4, 11, 16b	B_1	A	A
20b, 7b, 8b, 19b, 6b	B_2	B	B
14, 3, 15, 18b			C_1
			A

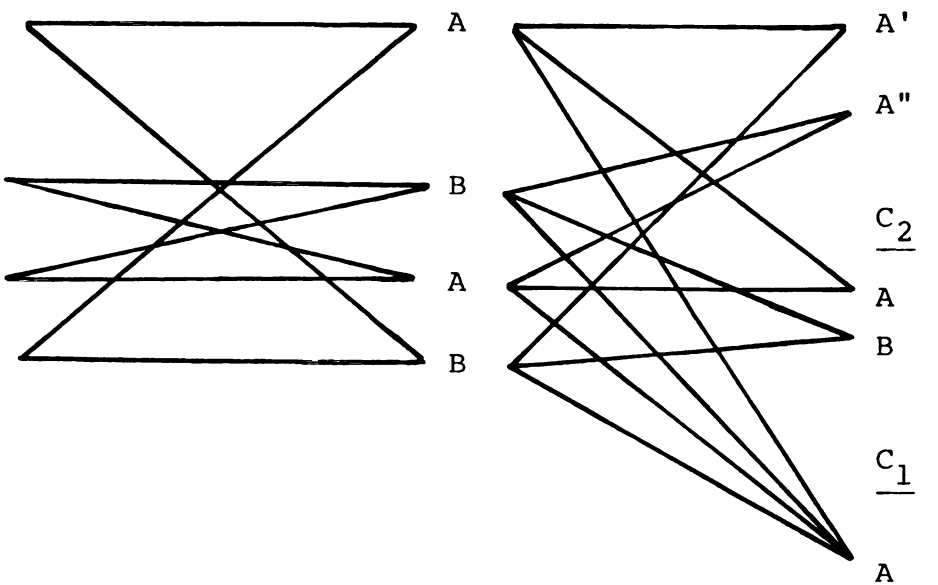

TABLE 2 CONTINUES.

TABLE 2 CONTINUED.

Modes ethylene*	Correlated -Symmetry- D_{2h}	Molecular -Symmetry- C_{2h}	Surface Complex ---Symmetries-- C_s
ν_3, ν_2, ν_1	A	A	A'
			A"
ν_5, ν_6	B_{1g}		
ν_8	B_{2g}	B	C_2
	B_{3g}		A
ν_4	A	A	B
ν_7	B_{1u}		
ν_{10}, 9	B_{2u}	B	C_1
ν_{12}, ν_{11}	B_{3u}		A

Choice of Axes:

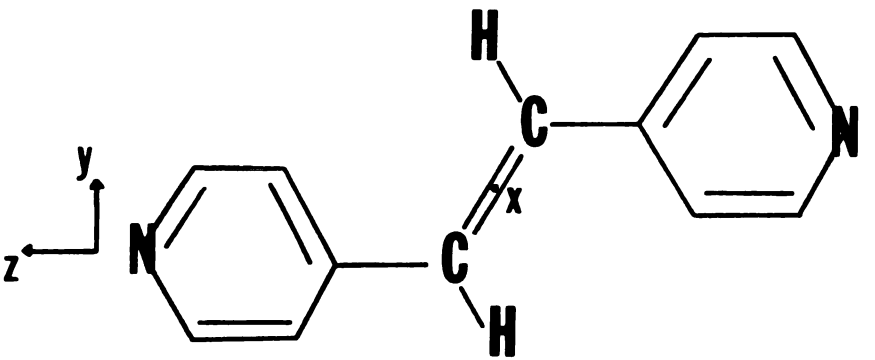

to grow adequate single crystals for X-ray examination are underway.

Frequency Region 0-600 cm^{-1}

Assignments in this region of the Raman spectrum of t-1,2-bis(4-pyridyl)ethylene are particularly difficult. Other than the lattice modes, most of the bands in this region are of very low intensity and quite broad. Lines at 486, and 400 cm^{-1} have been assigned to pyridine motions 16b and 16a respectively following Spinner.[104] The frequency at 225 cm^{-1} has been assigned to a skeletal vibration in accordance with a similar motion in trans-stilbene.[105] The X-ray crystal structure determination is required in order for assignment of modes in the lattice region of the polycrystalline Raman spectra to be made possible.

Vibrations 6a and 6b

The in-phase (A_g) components of orthogonal pyridine vibrations 6a and 6b appear at 641 cm^{-1} and 671 cm^{-1} respectively in the Raman spectrum of polycrystalline t-BPE. Assignment of these modes is fortified by comparison with the same motions in the dihydrochloride. In the Raman spectrum of polycrystalline t-1,2-bis(4-pyridyl)ethylene dihydrochloride the vibration 6b is observed shifted down to 651 cm^{-1} while vibration 6a appears slightly shifted up to 643 cm^{-1}. The downward shift of 6b frequency is exactly analogous to that observed in the Raman spectra

of 4-methyl pyridine and 4-methyl pyridine hydrochloride as reported by Spinner.[102] There, the frequency of the 6b motion in 4-methyl pyridine appears at 669 cm^{-1} and 651 cm^{-1} in the hydrochloride. In t-BPE, the behavior of vibration 6a upon formation of the hydrochloride follows that observed for pyridine and pyridinium chloride. In pyridine the 6a vibration appears at 605 cm^{-1}; it falls at 607 cm^{-1} in pyridinium chloride,[103] a similar shift to higher frequency upon salt formation. A further consideration in the assignment of vibrations 6a and 6b is the relatively weak intensity of 6a relative to 6b in the Raman spectrum of t-BPE and its hydrochloride. In some substituted pyridines and pyridine hydrochlorides the 6a vibration is too weak to be observed[102] or appears with very weak intensity. The intensity of 6b is also greater than that of 6a in the Raman spectrum of trans-stilbene (the analogous molecule to t-BPE with benzene rings instead of pyridine).[105] Regis and Corset[106] report a 6b/6a intensity ratio of 25/4 in the Raman spectrum of methyl viologen (N,N'dimethyl-4,4' bipyridine). In methylene chloride solution the 6a vibrational mode, appearing at 650 cm^{-1}, exhibits a depolarization ratio of 0.17 indicative of a polarized mode as expected for a mode of A_g symmetry. Vibrational mode 6b, however, appears depolarized with a depolarization ratio of 0.64 though the symmetry of this mode is also A_g. The difference in depolarization ratios arises because the vibrational mode 6b transforms as the α_{yz} component

of the polarizability tensor (in the coordinate frame designated in Table 2) while 6a transforms as α_{xx}, α_{yy}, and α_{zz}. Therefore, in the polarizability invariants for vibration 6b only the derivative of the yz component of the polarizability with respect to normal coordinate $(\partial\alpha_{yz}/\partial Q_k)$ will be non-zero. The α_{yz} component appears only in the anistropic polarizability invariant and the spherical invariant therefore vanishes, resulting in a predicted depolarization ratio of 3/4. Situations such as this where a totally symmetric vibration is expected to demonstrate a high degree of depolarization, are not common in group theory. In fact the only point groups in which off-diagonal polarizability tensor components transform as the totally symmetric representation are C_{2h} (the case examined here) and the very low symmetry point groups C_2, C_i, C_s, and C_1.

Vibration 6b cannot effectively couple to the N-H deformation in the dihydrochloride since the motion of the nitrogen atom and hydrogen atom are in the same direction (the form of the normal coordinates for pyridine vibrations are given in Appendix A).[107] Thus, no shift is observed upon deuteration of the dihydrochloride with vibration 6b appearing at 651 cm^{-1} in both salts. Assignments of vibrations 6a and 6b are particularly important to the understanding of the Raman spectroscopy of t-BPE adsorbed at a silver electrode (see Chapter 6). Comparison of Raman

frequencies for modes 6a and 6b in representative molecules is made in Table 2a.

Out-of-Plane Vibrations

All out-of-plane molecular vibrations appear in the Raman spectrum with a frequency below 1000 cm^{-1}. Only the out-of-phase components of such vibrations are observed in the Raman spectrum since the active symmetry is B_g for out-of-plane modes. A pair of lines appearing in the polycrystalline Raman spectrum of t-BPE at 878 cm^{-1} and 888 cm^{-1} have been assigned to pyridine ring vibrations 10a and 10b respectively. The form of the normal coordinate vibrations 10a and 10b as provided by Long and Thomas[107] demonstrates that vibration 10a has no component of motion involving the nitrogen atom while 10b involves nitrogen motion (see Appendix A). Therefore, protonation or deuteration of the ring is expected to have little effect on vibrational frequency of vibration 10a. In the Raman spectrum of both t-1,2-bis(4-pyridyl)ethylene dihydrochloride and dideuterochloride vibration 10a appears unshifted at 879 cm^{-1}. Vibration 10b, in contrast, appears at 894 cm^{-1} in the polycrystalline Raman spectrum of the dihydrochloride and at 901 cm^{-1} in the dideuterochloride spectrum.

Analogously, pyridine ring vibration 5 has a component of nitrogen motion and can therefore couple to the out-of-plane N-H deformation. In the Raman spectrum

TABLE 2a: Comparison of Raman frequencies of modes 6a and 6b in representative molecules. Vibrational frequencies are in wavenumbers (cm^{-1})*.

	6a	6b
t-BPE	641	671
pyridine	605	652
4-methylpyridine	a	669
t-BPE H_2Cl_2	643	651
pyridinium chloride	607	637
4-methylpyridine hydrochloride	a	651
t-BPE D_2Cl_2	645	651
pyridine deuterochloride	602	634
4-methylpyridine deuterochloride	b	b

a. Too weak to be observed.

b. No available data

*Frequencies reported were those observed with polycrystalline samples for all molecules except pyridine and pyridine deuterochloride. Liquid pyridine Raman frequencies are reported. Pyridine deuterochloride frequencies were observed in D_2O solution.

of polycrystalline t-BPE vibration 5 appears with a frequency of 958 cm^{-1} but cannot be found in the Raman spectra of the dihydrochloride and dideuterochloride. The form of normal coordinate 17a (Appendix A) exhibits zero amplitude at the nitrogen position as in vibration 10a. Therefore, 17a is not expected to couple effectively with the N-H out-of-plane deformation and its frequency should be shifted little in the Raman sepctrum of the dihydrochloride and dideuterochloride relative to its position in the t-BPE Raman spectrum. In the Raman spectrum of polycrystalline t-BPE 17a appears at 976 cm^{-1} and at 970 cm^{-1} in methylene chloride. In the dihydrochloride and dideuterochloride salts 17a appears at 997 and 996, respectively, demonstrating better than a 20 cm^{-1} shift. However, in the Raman spectra of the aqueous solutions 17a appears at 977 cm^{-1} and 970 cm^{-1} for the dihydrochloride and dideuterochloride, respectively, which is shifted only slightly from the motion in the solution t-BPE Raman spectrum. The out-of-phase components of some of the out-of-plane modes do not appear in the Raman spectrum of t-BPE though they transform as Raman active representations (B_g). Those vibrations absent are ν_4 and ν_{11}. Interestingly, these can be observed in the surface Raman spectrum of t-BPE.

Ring "Breathing" modes ν_1 and ν_{12}-

The totally symmetric ring "breathing" vibration ν_1 appears in the vicinity of 1000 cm^{-1} in all pyridines

substituted pyridines, and pyridine hydrochlorides. ν_1 is the most intense Raman line in the spectrum of pyridine and occurs with high intensity in the spectrum of t-BPE. In polycrystalline t-BPE ν_1 vibration appears at 995 cm^{-1}. In the Raman spectrum of the dihydrochloride ν_1 appears at 1008 cm^{-1}. The form of the normal coordinate vibration ν_1[107] (Appendix A) shows that the in-plane motion contains nitrogen motion which is directed among the N-H bond in the hydrochloride. Therefore ν_1 may couple to the N-H stretch and is expected to occur at a lower frequency upon deuteration. In the dideuterochloride of t-BPE ν_1 appears at 1005 cm^{-1}, which demonstrates the expected shift relative to the dihydrochloride.

In the Raman spectrum of pyridine another very intense line appears at 1030 cm^{-1} and has been assigned to the trigonal ring "breathing" vibration ν_{12}. This vibration is conspicuously absent from the Raman spectrum of t-BPE and its chloride salts. The symmetry of this in-plane deformation is A_1 symmetry in pyridine and thus the in-plane analogue of ν_{12} in t-BPE transforms as the totally symmetric representation and is expected to be observed in the Raman spectrum in the frequency region 1030-1040 cm^{-1}. The appearance of ν_{12} in the surface Raman spectrum of t-BPE and in the normal Raman spectrum of a polycrystalline silver complex with t-BPE is important evidence for the formation of a silver complex at the electrode surface (see Chapter 6).

Frequency Region 1050-1300 cm^{-1}

The in-phase component of in-plane ring deformation ν_{18a} is very weakly observed in the polycrystalline Raman spectrum of t-BPE at 1069 cm^{-1}. The orthogonal counterpart to vibration 18a, 18b is also expected in the frequency region 1050-1100 cm^{-1} but is not observed in the Raman spectrum of t-BPE.

At 1184 cm^{-1} in the polycrystalline t-BPE Raman spectrum a very weak line is observed on the tail of the very intense C_{eth} - ϕ stretch at 1198 cm^{-1}. This weak line is probably a combination or overtone which is in Fermi resonance with the very intense symmetric stretching vibration. If this is the case the symmetry of the combination of overtone must be Ag. All 2nd overtones will be totally symmetric since the result of the direct product of any representation with itself is the totally symmetric representation. However, the second overtone of a vibration of frequency 592 cm^{-1} is required and no such vibration is observed in either the infrared[100] or Raman spectrum of t-BPE. Interestingly, a very weak line near 600 cm^{-1} is observed in the surface Raman spectrum of t-BPE which may be the fundamental whose overtone comes into Fermi resonance with the C_{eth} - ϕ stretch. Assignment of this surface mode is incomplete (see Chapter 6).

As mentioned above, the totally symmetric stretch between the ethylenic carbons and the pyridine rings occurs with high intensity in the polycrystalline Raman spectrum

of t-BPE at 1198 cm^{-1}. Upon formation of the dihydrochloride and dideuterochloride this vibration shifts to higher frequencies appearing at 1203 cm^{-1} and 1206 cm^{-1} in the hydrogenated and deuterated analogues, respectively. The frequency and intensity of the C_{eth} - ϕ stretch are analogous to that observed in the Raman spectrum of trans-stilbene.

Vibrations 9a and 9b appear next in the Raman spectrum of t-BPE. 9a appears at 1225 cm^{-1} in the polycrystalline spectrum of t-BPE, shifts under the intense neighboring C_{eth} - ϕ stretch in the spectrum of the dihydrochloride and is barely visible at 1215 cm^{-1} in the Raman spectrum of the dideuterochloride. These observed shifts correspond to those observed in the Raman spectrum of 4-methylpyridine. As reported in reference (104), 9a appears in the range 1220-1210 in 4-substituted pyridines and shifts to 1205 cm^{-1} in 4-methylpyridine.[102] The shift to higher frequency upon deuteration of the dihydrochloride is also observed in the Raman spectrum of pyridinium chloride. In the hydrogenated salt 9a appears at 1198 cm^{-1} and at 1202 in the deuterated analogue.[108]

Vibration 9b is antisymmetric with respect to the C_2 axis, transforming as the B_2 representation in pyridine, and thus the component of nitrogen motion (Appendix A) is involved in $N\text{-}H^+$ in-plane deformation in the dihydrochloride and dideuterochloride. In the Raman spectrum of polycrystalline t-BPE 9b is assigned to the intense line at

1234 cm^{-1} which shifts to 1254 cm^{-1} in the dihydrochloride and drops sharply in intensity. Similar to vibration 6b, 9b exhibits a rather high depolarization ratio for a mode of A_g symmetry since the vibration transforms as the yz component of the polarizability tensor as discussed earlier. In the D_2O spectrum of the dideuterochloride 9b appears at 1294 cm^{-1}. The shift to higher frequency by 30 cm^{-1} in the solution (D_2O) spectrum is an indication of the extensive hydrogen bonding occurring in solution.

Frequency Region 1300-1400 cm^{-1}

In this region of the spectrum pyridine ring vibrations ν_3 and ν_{14} appear. The Raman line at 1319 cm^{-1} in the spectrum of polycrystalline t-BPE is assigned to the in-phase pyridine ring motion ν_3 in accordance with assignments in other pyridine molecules[104] and trans-stilbene.[105] Similar to vibration 9b, the frequency of ν_3 increases upon salt formation, appearing at 1333 cm^{-1} in the polycrystalline dihydrochloride.

In the Raman spectrum of polycrystalline t-BPE vibration 14 appears at 1351 cm^{-1} and at 1338 cm^{-1} in methylene chloride. Vibration 14 correlates to the B_2 representation in the pyridine molecular point group as do vibrations 3, 6b and 9b. As for vibrations 3 and 9b, ν_{14} demonstrates a frequency increasing in going to the dihydrochloride and dideuterochloride in the solution Raman spectra. Lines at 1346 cm^{-1} in the solution spectrum of the dihydrochloride and 1349 cm^{-1} in the solution spectrum of the

dideuterochloride are assigned to ν_{14}. On the low frequency side of ν_{14} in the Raman spectrum of polycrystalline t-BPE appears a vibration at 1342 cm^{-1}. This line is probably the overtone $2x6_b$ which is in Fermi resonance with the totally symmetric vibration 14. The weak line appearing in the Raman spectrum of t-BPE dihydrochloride and dideuterochloride near 1375 cm^{-1} is probably an overtone of vibration 11 which is of A_u symmetry and not observed in the Raman spectrum. In the surface spectrum of t-BPE, however, ν_{11} appears near 685 cm^{-1} as discussed in the next chapter.

Vibration Pair 19a and 19b

Pyridine ring vibrations involving non-hydrogen stretches and bends occur in the frequency region 1400-1650 cm^{-1}. Vibration 19b is assigned to a weak line observed at 1419 cm^{-1} in the Raman spectrum of polycrystalline t-BPE. Similar to vibrations 6b and 9b, vibration 19b demonstrates the characteristic high depolarization ratio, measured at 0.53. Vibration 3 (B_2) demonstrates a very low depolarization ratio (.19) which may be a result of accidental degeneracy with a combination, perhaps $2x6_a$. As with other vibrations which transform as the B_2 symmetry representation in the correlated pyridine symmetry (C_{2v}) 19b couples with $N\text{-}H^+$ deformation in the salts of t-BPE. Thus, the vibrational frequency of motion 19b shifts to 1512 cm^{-1} and 1514 cm^{-1} in the dihydrochloride and

dideuterochloride, respectively. (Further evidence of hydrogen bonding involving the nitrogen proton in solution is evidenced by the shift of the frequency of 19b in the dideuterochloride down to 1463 cm^{-1} upon dissolution in D_2O.) On the low frequency shoulder of the 1422 cm^{-1} line a line appears at 1411 cm^{-1} in the Raman spectrum of polycrystalline t-BPE. This is another example of Fermi resonance in the spectrum. This mode is probably the totally symmetric combination $\nu_4 + \nu_{11}$. As discussed earlier, neither ν_{11} nor ν_4 appear in the normal Raman spectrum of t-BPE. ν_4 is observed weakly at 740 cm^{-1} in the infrared spectrum of t-BPE.[109] ν_{11} is observed at 685 cm^{-1} in the surface Raman spectrum of t-BPE as mentioned above.

Pyridine vibration 19a is observed at 1491 cm^{-1} in the Raman spectrum of polycrystalline t-BPE. 19a has a component of nitrogen motion along the N-H bond and therefore is expected to be responsive to formation of the salts. In the polycrystalline dihydrochloride and dideuterochloride 19a appears as shoulders at 1500 and 1505 cm^{-1}, respectively.

Vibration Pair 8a and 8b

Still another example of Fermi resonance in the Raman spectrum of polycrystalline t-BPE appears at frequency 1541 cm^{-1} on the shoulder of fundamental 8b at 1549 cm^{-1}. The overtone is probably $2\nu_{11}$. The out-of-phase component

of vibration 4 is not observed in the Raman spectrum as discussed previously. However, the in-phase (Au) component appears in the infrared spectrum[100] at 740 cm^{-1} and in the surface spectrum of t-BPE (Chapter 6) two lines are observed at 720 cm^{-1} and 740 cm^{-1}. Thus the Bg out-of-phase component probably occurs at 720 cm^{-1} and the overtone is expected at 1540 cm^{-1}.

Typical of other b vibrations which may couple to N-H deformation vibration 8b, appearing at 1549 cm^{-1} in the Raman spectrum of polycrystalline t-BPE, shifts upon dissolution of the dideuterochloride salt in D_2O from 1606 cm^{-1} to 1567 cm^{-1}. An analogous shift is observed for vibration 19b. Vibration 8a appears as the most intense line in the Raman spectrum at 1597 cm^{-1} in polycrystalline t-BPE. Spinner[102] observed that 8a shifted by nearly 30 cm^{-1} to higher frequency upon formation of the hydrochloride in the Raman spectrum of 4-methylpryidine. A similar shift of vibration 8a is observed in the Raman spectrum of t-BPE with formation of the dihydrochloride.

Ethylenic C=C Stretch

The totally symmetric stretch of the central ethylene carbon atoms appears at 1638 cm^{-1} in the Raman spectrum of polycrystalline t-BPE. Upon formation of the dihydrochloride and dideuterochloride salts the carbon-carbon stretch probably overlaps the intense 8a vibration. The weak high frequency shoulder of vibration 8a in the

polycrystalline Raman spectra of the salts has been assigned to the C=C symmetric stretch although the low intensity is not completely understood.

C-H, N-H(D), Stretching Motions

The C-H stretching frequencies appear in the Raman spectrum of t-BPE between 3000 cm^{-1} and 3100 cm^{-1}. The lowest frequency can be assigned to ethylenic carbon-hydrogen spectrum following assignments in trans-stilbene. Without isotopic substitution studies assignment of other frequencies in the 3000-3100 cm^{-1} region are ambiguous. In the dihydrochloride aqueous solution spectrum two broad bands centered at 3270 cm^{-1} and 3400 cm^{-1} represent N-H symmetric stretching motion. The broadness of these lines is indicative of extensive hydrogen bonding with water. A line appearing at 3266 cm^{-1} in the polycrystalline t-BPE dihydrochloride Raman spectrum is probably the overtone 2X(C=C sym. str). In the deutrated salt the N-D symmetric stretch appears as a broad doublet with centers at 2400 cm^{-1} and 2510 cm^{-1}. The polycrystalline dideuterochloride Raman spectrum exhibits no bands in this region.

The absence of N-H, and N-D stretches in the polycrystalline Raman spectra of the salts along with the large shifts in frequency of modes coupling to N-H(D) deformations upon dissolution appears to indicate the relatively weak association of the proton (deuteron) for the nitrogen atom in the crystal lattice. This association is expected

to be influenced by the presence of the highly electronegative chloride ion nearby in the lattice.

The assignments in this chapter are central to an understanding of the Raman activities of t-1,2-bis(4-pyridyl)ethylene adsorbed at a polycrystalline silver electrode (Chapter 6).

CHAPTER VI

Raman Spectra of t-1,2-bis(4-pyridyl)ethylene adsorbed at a polycrystalline silver electrode.

Intense Raman scattering from trans-1,2-bis(4-pyridyl)ethylene adsorbed at a polycrystalline silver electrode has been observed in this study. The procedure for electrochemical pretreatment of the silver electrode is described in Chapter 4. Concentrations of t-BPE in initial studies were 2.5 mM in 0.1 M KCl, but concentrations as low as 250 nM t-BPE produced comparable Raman signals. Normal Raman signals from aqueous solutions of 2.5 mM t-BPE were too weak to be observed. Surface Raman spectra of t-BPE, in contrast, generally demonstrated signal intensity in the range 1×10^5 to 3×10^5 counts per second. Under similar electrochemical roughening procedures t-BPE molecules adsorbed to silver from bulk concentrations of 1 mM and above produced a brownish-black coating on the electrode surface while adsorption from bulk concentrations of 500 nM and less produced an electrode coating indistinguishable from that observed following electrochemical cycling in aqueous KCl solution alone. Thus studies of surface Raman spectra from t-BPE molecules adsorbed from bulk concentrations in excess of 1 mM are hereafter referred

to as "heavy coverage" spectra. Those spectra observed from t-BPE molecules adsorbed from bulk concentrations less than 500 nM are referred to as "light coverage" studies.

Heavy Coverage Raman Spectra of t-BPE under 5145 Å Excitation.

The Raman spectra of a heavy coverage of t-1,2-bis(4-pyridyl)ethylene adsorbed at a polycrystalline silver electrode under 5145 Å excitation are given in Table 3. Some important sections of the Raman spectra are shown in Figure 6. Compared in Table 3 and Figure 6 are the normal Raman spectrum of t-BPE (assigned in Chapter 5) and the surface Raman spectra of t-BPE recorded at -600 mV versus sce (i.e. relative to the saturated calomel electrode) immediately following the oxidation-reduction cycle, -50 mV versus sce and again at -600 mV versus sce (following recording of the spectrum at -50 mV). Symmetry assignments based on the molecular point group symmetry and possibly surface complex symmetries (C_2, C_s) are also included in Table 3.

In the Raman spectrum of t-BPE on silver recorded immediately after the oxidation reduction cycle (which appears just above the polycrystalline t-BPE Raman spectrum in Figure 7) some interesting differences and similarities to the normal Raman spectrum are observed. The most pronounced difference is the appearance of a new peak at 655 cm^{-1} in the surface spectrum. Assignment of this

Figure 7: Heavy Coverage Potential Dependence of the Surface Raman Spectrum of t-1,2-bis(4-pyridyl)ethylene on Silver. Compared are: the normal Raman spectrum of polycrystalline t-BPE (bottom spectrum); the surface Raman spectrum recorded at -600 mV immediately following the oxidation-reduction cycle (above polycrystalline spectrum); surface spectrum at -50 mV; and the surface spectrum recorded on returning to -600 mV (top spectrum). EXCITATION WAVELENGTH: 5145 Å (Ar^+).

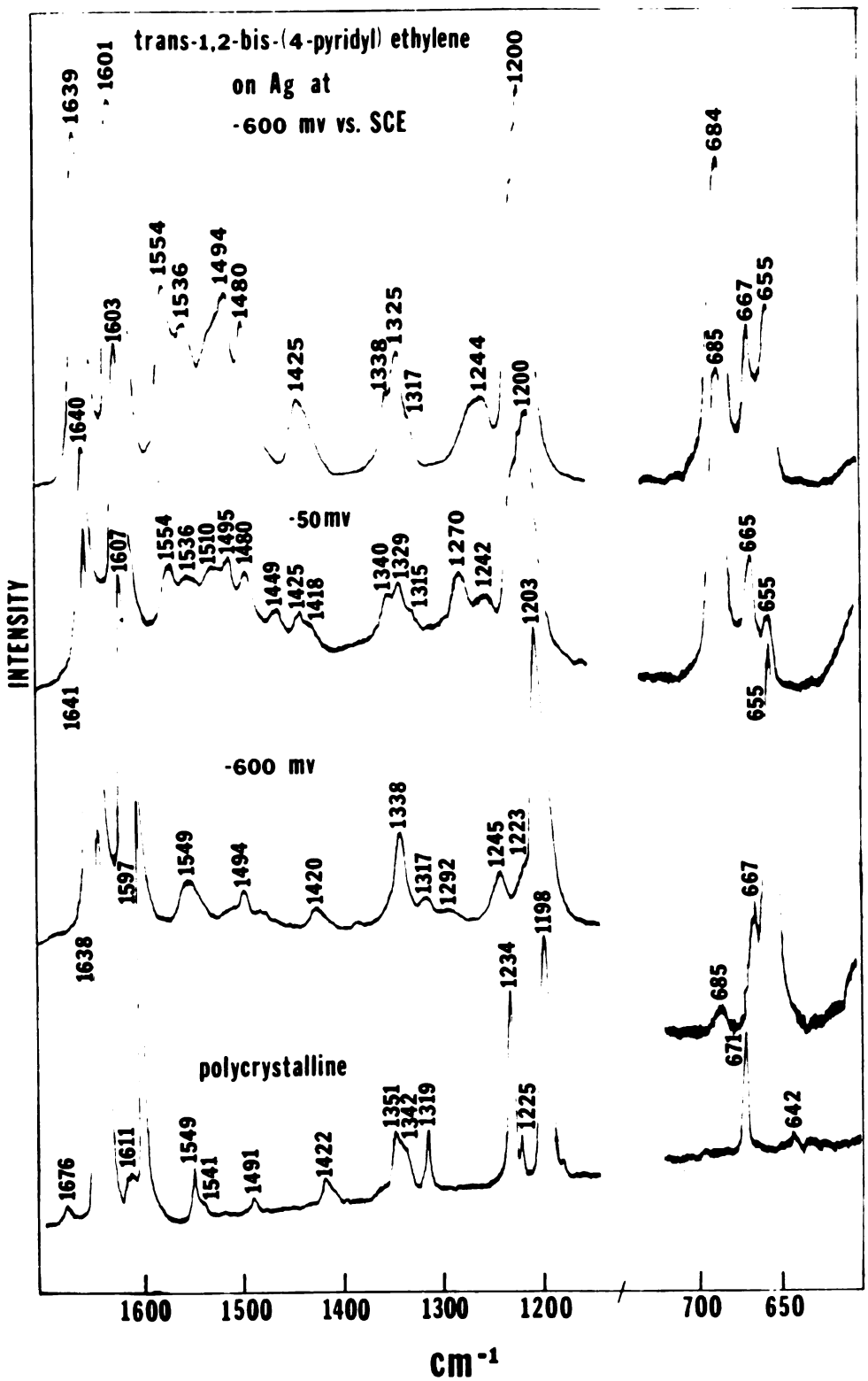
trans-1,2-bis-(4-pyridyl) ethylene
on Ag at
-600 mv vs. SCE
-50 mv
-600 mv
polycrystalline
INTENSITY
1639
1601
1200
684
1554
1536
1494
1480
1603
1425
1338
1325
1317
1244
1200
685
667
655
1640
1607
1554
1536
1510
1495
1480
1449
1425
1418
1340
1329
1315
1270
1242
1203
665
655
1641
655
1597
1549
1494
1420
1338
1317
1292
1245
1223
1198
667
1638
1234
685
671
1611
1549
1541
1491
1422
1351
1342
1319
1225
642
1676
1600
1500
1400
1300
1200
700
650
cm-1

TABLE 3: Raman Spectra of t-1,2-bis(4-pyridyl)ethylene adsorbed onto a polycrystalline silver electrode under 5145 Å excitation. Comparison made with polycrystalline t-1,2-bis(4-pyridyl)ethylene.

C_{2h} symmetry	Assignment Wilson #	Polycrystalline t-BPE	C_s	C_2	t-BPE on Ag at -600 mv*	t-BPE on Ag at -50 mv	t-BPE on Ag at -600 mv†
		43					
	Lattice	81					
	Vibrations	121			110br	110br	110br
		208					
	Ag-Cl str.				230	230	230
		240			230	230	230
					308	303	308
					350	350	350
					386	390	386
B_u	6a		A'	B		539 w	539 w
B_u	6b		A'	B	550 w		
B_g	11?				600	600	600
A_g	6a	642					
A_g	6b		A'	A	655	655	655
A_g	6b	671**	A'	A	667	665	665
A_g	11		A"	A	685 vw	685	684
A_g	4		A"	B	720 vw	720 vw	720 vw
A_u	4		A"	A	740 vw	740 vw	740 vw
	10a	excited state vibraton				834	

*Spectrum recorded immediately after the oxidation-reduction cycle.

†Spectrum recorded following recording spectrum at -50 mv.

**667 cm^{-1} in CH_2Cl_2 solution.

(TABLE 3 CONTINUES)

TABLE 3 CONTINUED.

C_{2h} symmetry	Assignment Wilson #	Polycrystalline t-BPE	C_s	C_2	t-BPE on Ag at -600 mv*	t-BPE on Ag at -50 mv	t-BPE on Ag at -600 mv†
A	ν_4 (eth)		A"	A	840 w	850	849
B_g	10a	878	A"	B	880	880	879
B_g	10b	887	A"	B			
B_g	17a	958	A"	B	958 vw		954 vw
B_g	5	976	A"	B	980	975 vw	972 vw
A_g	1	995	A'	A	1010	1008	1008
	excited state vibration					1040	
A_g	18a	1069	A'	A	1065	1060 vw	1057 vw
A_g	18b		A'	A	1094	1093 vw	1092 vw
	15				1118 vw		
A_g	C - ϕ str.	1198	A'	A	1203	1200	1200
A_g	9a	1225	A'	A	1223		
A_g	NH de , 9b	1234	A'	A	1245	1242	1244
	C_e - ϕ excited state vibration					1270	
B_u	C_e - H IP def		A"	B	1292 w		
A_g	3	1319	A'	A	1317	1315	1317 sh
A_g	C_e - H def		A"	B		1329	1325
A_g	2 × 6b	1342	A'	A			
A_g	14	1351	A'	A	1338	1340	1338
A_g	4 + 11	1411	A'	A	1412 sh		
B_u	19b					1418	1412

*Spectrum recorded immediately after the oxidation-reduction cycle.

†Spectrum recorded following recording spectrum at -50 mv.

(TABLE 3 CONTINUES)

TABLE 3 CONTINUED.

C_{2h} symmetry	Assignment Wilson #	Polycrystalline t-BPE	C_s	C_2	t-BPE on Ag at -600 mv*	t-BPE on Ag at -50 mv	t-BPE on Ag at -600 mv†
A_g	19b excited state vibration	1422	A'	A	1420	1425 1449	1425
A_g	2 × 4		A"	B		1480	1480
A_g	19a	1491	A'	A	1494	1495	1494
	19a		A'	B		1510	1508
A_g	2 × 4	1541	A'	A			
A_g	8b	1549	A'	A	1549	1536	1536
B_g	8b		A'	B		1554	1554
A_g	8a	1597	A'	A	1607	1603	1601
A_g	?	1611	A'	A			
A_g	C=C str.	1638	A'	A	1641	1640	1639
A_g	2 × ν_4 (eth)	1676	A'	A	1680	1678	1680

*Spectrum recorded immediately after the oxidation-reduction cycle.

†Spectrum recorded following recording spectrum at -50 mv.

Raman frequency is important to the discussion of molecular orientation at the surface and is reserved until other surface data are presented below.

Another distinct difference between the normal Raman spectrum and the surface Raman spectrum of t-BPE, observed in 0.1 M Cl^- electrolyte, is the appearance of an intense line at 230 cm^{-1}. Similar lines have appeared in the surface Raman investigations of pyridine[5] also and have been assigned to the Ag-Cl symmetric stretch because of its appearance in the surface Raman spectrum even in the absence of pyridine.[82] We concur with this assignment by noting that moving the electrode potential negative of the point of zero charge (p.z.c.), which occurs near -0.97 V for silver,[102a] the intensity of the 230 cm^{-1} line is attenuated to less than half its intensity at positive potentials and does not recover intensity upon return to positive potentials. The intensities of the other lines in the surface Raman spectrum of t-BPE do not show the same potential dependence. This indicates that, as expected, Cl^- ions leave the vicinity of the electrode surface at negative potentials and the vacant sites are filled by rearrangement of the molecules remaining at the surface. Thus, the number of Ag-Cl bonds decreases which accounts for the drop in intensity at 230 cm^{-1}. This is an important point: many researchers in efforts to locate a metal-nitrogen stretch in the surface Raman spectra of nitrogen-containing molecules have assigned the 230 cm^{-1} line to such a motion.

Other differences between the normal and surface Raman spectra of t-BPE include the appearance of new weak lines at 685 cm^{-1}, 600 cm^{-1}, 550 cm^{-1}, and a group of three vibrations in the 300-400 cm^{-1} region. The 685 cm^{-1} and 600 cm^{-1} lines can be assigned to the in-phase (A_u) and out-of-phase (B_g) components of vibration 11, respectively, following similar assigments in the vibrational spectra of trans-stilbene.[105] The 550 cm^{-1} line is assigned to the out-of-phase (B_u) component of vibration 6b by analogy to trans-stilbene spectra[105] and its appearance in the infrared spectrum of t-BPE.[100] The low frequency motions have not yet been assigned. A very weak line is also observed at 1118 cm^{-1} which could be the in-phase (A_g) component of vibration 15 which appears at 1148 cm^{-1} in pyridine[104] but is not observed in the infrared or Raman spectra of t-BPE. Another weak new line observed in the -600 mV surface spectrum occurs at 840 cm^{-1} which may be assigned to the in-phase (A_u) component of model ν_4 of ethylene which appears at 837 cm^{-1} in the infrared spectrum of t-BPE.[1]

Other than the differences mentioned above, the surface Raman spectrum of t-BPE observed at -600 mV under 5145 Å excitation after electrochemical cycling is very much like the normal Raman spectrum of t-BPE. Absence of Fermi resonance, intensity drops observed for vibrations ν_3 and ν_{9b} at 1317 and 1245 cm^{-1}, respectively, and the shift in

the frequency of ν_{6b} from 671 cm^{-1} in polycrystalline t-BPE to 667 cm^{-1} in the surface spectrum are all analogous to solution effects observed in the normal Raman spectrum of t-BPE (see Table 1). Most of the surface Raman lines are only slightly shifted from their counterparts in the polycrystalline spectrum.

Upon altering potential to -50 mV versus sce some extraordinary changes in the surface Raman spectrum of t-BPE are observed. The 655 cm^{-1} line becomes much less intense and the in-phase component of vibration 11 (A_u) at 685 cm^{-1} increases sharply in intensity. The very weak 550 cm^{-1} line disappears and a very weak line at 539 cm^{-1} appears which can be assigned to the out-of-phase motion 6a since it appears in the infrared spectrum.[109] The intensity of the Raman line at 880 cm^{-1} in the -600 mV spectrum drops, accompanied by an increase in intensity at 832 cm^{-1} in the -50 mV spectrum. The ethylenic ν_4 motion appears to shift to 850 cm^{-1} and increases in intensity on moving the potential to -50 mV. The ethylenic carbon to ring carbon symmetric stretch at 1200 cm^{-1} picks up some asymmetry on its high frequency side accompanied by the appearance of a new line at 1270 cm^{-1}. The in-phase (A_g) ethylenic hydrogen deformation appears at 1329 cm^{-1} and is assigned by analogy with the corresponding mode in the trans-stilbene vibrational spectra.[105]

A host of new vibrations appear in the 1400-1560 cm^{-1} range. Most of these lines can be assigned to the

out-of-phase (B_u) ring motions as shown in Table 3. The out-of-phase component of vibrational mode 8b is assigned to the new line at 1554 cm^{-1} by comparison to that observed in the infrared spectrum of t-BPE where 8b occurs at 1560 cm^{-1}. Similarly, the Raman line at 1510 cm^{-1} in the -50 mV surface spectrum can be assigned to the B_u component of vibration 19a which appears at 1504 cm^{-1} in the infrared spectrum. The Raman band at 1480 cm^{-1} has no counterpart in the infrared spectrum and is probably the totally symmetric overtone of vibration 4 (740 cm^{-1}) which is in Fermi resonance with the totally symmetric component of mode 19a at 1495 cm^{-1}. The line at 1418 cm^{-1} in the -50 mV spectrum can be assigned to the B_u component of mode 19b which appears in the infrared spectrum[1] also at 1418 cm^{-1}. A new line appears at 1449 cm^{-1} in the surface spectrum at this relatively positive potential which has not been assigned and will be discussed later in this section. The totally symmetric ethylenic carbon stretch at 1640 cm^{-1} is reduced to half the intensity of that line in the -600 mV spectrum. The increased height of the valley between the 1640 cm^{-1} line and the 1603 cm^{-1} line with decreased intensity at 1640 cm^{-1} indicates the possible presence of an isosbestic point accompanying a shift in the frequency of C=C to a frequency near 1600 cm^{-1}.

Upon returning to -600 mV the initial spectrum observed at this potential is not recovered. Instead, a spectrum is observed which maintains many of the features observed in

the -50 mV spectrum. The in-phase and out-of-phase components of the pyridine ring motions in the region 1400-1560 cm^{-1} increase in intensity and the intensity of the line at 684 cm^{-1} (ν_{11}, A_u component) is maintained. The intensity of the line at 655 cm^{-1} increases, but remains much weaker than that observed in the original spectrum recorded at -600 mV. The in-phase ethylenic hydrogen deformation at 1325 cm^{-1} increases in relative intensity. Interestingly, the vibrations at 1270 cm^{-1}, 1449 cm^{-1} and 832 cm^{-1} have disappeared from the spectrum upon moving the potential to -600 mV. The intensity of the C=C stretch at 1639 cm^{-1} has recovered at the more negative potential.

It must be noted that the spectroscopic changes observed above occur irreversibly. That is, the original spectrum observed at -600 mV is never recovered once the electrode potential has been shifted relatively positive. Also, and most importantly, these spectroscopic changes are observed only under laser excitation with wavelengths in the green or shorter. Excitation with low energy laser lines (e.g. 6471 Å, Kr^+) results in the observation of only the spectrum initially observed at -600 mV versus sce and the potential dependence of the surface Raman spectrum is completely reversible. Another requirement for the observation of irreversible potential dependent behavior is that the electrode must have a heavy coverage of t-BPE at the surface. In experiments with bulk t-BPE concentrations at 500 nM and less only reversible potential dependence

of the surface Raman spectrum is observed. These experimental data are addressed in the following sections. Molecular reorientation and surface complex formation are invoked to explain the anomalous potential-dependent behavior of the surface Raman spectrum.

Molecular Reorientation on Complexation of t-BPE at the Electrode Surface.

The experimental data presented in Figure 7 and itemized above can be understood by considering the formation of a surface complex between t-1,2-bis(4-pyridyl)ethylene and surface silver atoms. In the surface Raman spectrum of t-BPE observed at -600 mV immediately following the oxidation-reduction cycle the molecule can be considered to be bound to the silver surface through one of the nitrogen lone pairs, i.e. in an "end-on" configuration. This conclusion is reasonable in that the attachment of one point limits the amount of electrode density overlap between the metal and adsorbate. Thus, the surface Raman spectrum of t-BPE at -600 mV appears little different from the normal Raman spectrum. The major difference between the normal Raman spectrum and the surface spectrum is the appearance of an intense line at 655 cm^{-1}. The 655 cm^{-1} line can be assigned to vibration 6b occurring in the pyridine ring closest to the silver surface. When the nitrogen atom is attached to a substituent, vibration 6b always drops in frequency. In t-1,2-bis(4-pyridyl)ethylene

dihydrochloride and dideuterochloride 6b is observed at 651 cm^{-1} (see Table 1), in N-methyl pyridium[110] at 649 cm^{-1}, and in methyl viologen[106] at 657.5 cm^{-1}. The form of vibration 6b according to Long and Thomas[107] requires that the substituent have a component of motion in the same direction as the nitrogen atom and orthogonal to the nitrogen-substituent bond. Thus, some aplitude of silver motion is required in the vibration 6b when t-BPE is attached "end-on" to the surface. This silver motion is therefore available for vibronic coupling of metal electronic states with the incoming radiation and a resonance Raman mechanism becomes a plausible explanation of the observed large Raman intensities. In a resonance Raman enhancement mechanism only those modes are enhanced which most effectively couple to the electronic state in resonance. In the "end-on" configuration only one pyridine ring would show electron density overlap with the metal thus enhancing motions in that ring which are effective in vibronic coupling. Thus the 6b motion in the ring closest to the surface (655 cm^{-1}) appears with higher intensity than the same motion in the ring more remote to the surface (667 cm^{-1}). Motions which do not include motion of the nitrogen atom are expected to be absent from the surface spectrum of the "end-on" t-BPE. Thus, vibration 10b (888 cm^{-1}) cannot be found in the surface spectrum of t-BPE at -600 mV and mode 17a appears very weakly at 958 cm^{-1}. A pyridine vibration which is very similar to

motion 6b is mode 15. Vibrational mode 15 is not observed in the infrared or normal Raman spectrum of t-BPE but appears very weakly at 1118 cm^{-1} in the surface Raman spectrum of t-BPE in the "end-on" configuration. Most of the other modes observed in the surface Raman spectrum at -600 mV transform as the totally symmetric representation (C_{2h}) and may therefore be an indication of a Franck-Condon scattering mechanism (see Chapter 3).

On shifting the potential to -50 mV several ungerade modes appear, along with other changes. Ungerade modes appear exclusively in the infrared spectrum of t-BPE thus implicating a reduction in the symmetry of the system probed in the Raman experiment. The "surface selection rule", studied extensively by Hexter and Albrecht[91] does not provide an explanation for the appearance of infrared modes in the surface Raman spectrum of a centrosymmetric molecule such as t-BPE (see Figure 2). A reduction in symmetry upon complexation to surface silver atoms, in contrast, adequately accounts for the appearance of infrared modes.

The new line at 1270 cm^{-1} is assigned to the symmetric ehtylene-carbon-to-ring-carbon stretch in an excited π^* state of t-BPE. This conclusion is made on the basis of comparison with the excited state vibrational spectrum of trans-stilbene (observed experimentally by low-temperature, high-resolution crystal absorption spectroscopy of trans-stilbene in a dibenzyl matrix by Dyck and McClure[109]). In

trans-stilbene the C_{eth} - ϕ symmetric stretch is observed at 1191 cm^{-1} in the ground state (fluorescence spectrum) and at 1250 cm^{-1} in the excited state. A line at 1427 cm^{-1} in the excited state vibrations of trans-stilbene had no counterpart in the fluorescence spectrum and remained unassigned. A similar phenomenon occurs in the surface spectrum of t-BPE at -50 mV. A line at 1449 cm^{-1} apparently also has no counterpart in the ground state vibrations since it disappears along with other proposed π^* vibrations upon returning to -600 mV. The low-temperature, mixed crystal absorption spectrum of trans-stilbene exhibits a sequency of very strong lines separated by 1599 cm^{-1} which has been assigned[111] to the C=C symmetric stretch in the excited state. A similar shift in the C=C stretch in the t-BPE surface Raman spectrum at -50 mV is invoked here to explain the reduction in intensity at 1640 cm^{-1}. Such a shift would bring the frequency of the ethylene motion underneath the peak of vibration 8a occurring at 1603 cm^{-1}. The shift in the frequency of mode 10 from 880 cm^{-1} to 832 cm^{-1} on moving to relative positive potentials is analogous to a shift observed in going from the fluorescence spectrum to the absorption spectrum of trans-stilbene[111] where lines are observed at 866 cm^{-1} and 847 cm^{-1}, respectively. The potential dependence of the lines at 880 cm^{-1} and 832 cm^{-1} shown in Figure 8 is clear evidence that these Raman lines are associated with the same vibration, not different ones.

Figure 8: Potential Dependence of Mode 10 in the Surface Raman spectrum of t-BPE "flat" on the silver surface.
EXCITATION WAVELENGTH: 5145 Å (Ar^+).

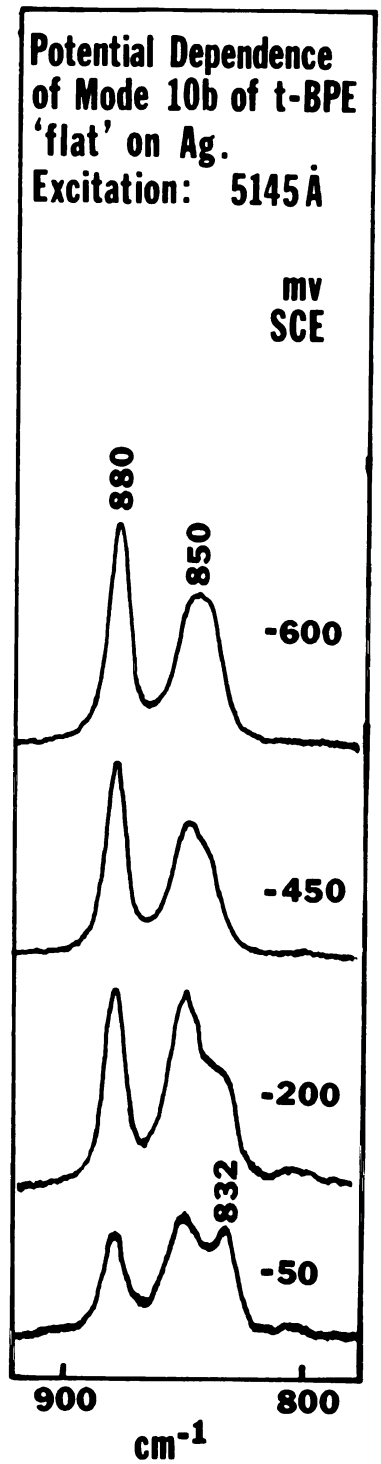
Potential Dependence
of Mode 10b of t-BPE
'flat' on Ag.
Excitation: 5145 Å
mv
SCE
880
850
-600
-450
-200
832
-50
900
800
cm-1

Thus it appears that vibrations from the π* state in t-BPE are observed in the surface Raman spectrum at -50 mV versus sce. There are two mechanisms which might reasonably account for the appearance of π* vibrations in the surface Raman spectrum. The first is the influence of saturation of the π* state by a high photon density excitation. If saturation occurred, normal Raman scattering from the excited state may be observed. However, these experiments were performed with laser powers of only 50 mW or less. A simple calculation of the number of photons per t-BPE molecule (assuming a minimal surface coverage and a beam waste of 0.5 nm radius) leads to conclusions that, for saturation to be a viable explanation for the appearance of excited state vibrations, the excited state lifetimes must be of the order of microseconds or larger, which is not likely.

The alternative explanation for the appearance of π* vibrations in the surface Raman spectrum of t-BPE is that the π* state becomes significantly stabilized in energy by electron density overlap with the metal. As discussed in Chapter 3, the pentaminebispyridylethylene ruthenium II complex[88] demonstrates considerable stabilization of the t-BPE π* state upon complexation such that the π* becomes an occupied state in the complex. In the "end-on" configuration at -600 mV there is little overlap of the molecular π system with metallic electron density and the charge on the silver atom is significantly diminished from the charge

on the ruthenium II atom. Hence no π* vibrations are observed at -600 mV. Even at -50 mV the charge on the surface silver atoms is still small and under red excitation π* vibrations are not observed. Therefore, in order to postulate that the appearance of π* in the surface Raman spectrum is a result of stabilization brought on by overlap of molecular and metal electron densities a reorientation of the molecule at positive potentials must occur. This reorientation must be intimately related to the requirement of 5145 Å (or shorter wavelength) radiation since reversible potential-dependent behavior is observed with red excitation.

Consider first the t-BPE molecule in the "end-on" configuration at -600 mV. In this configuration electronic eigenstates in the ring closest to the surface can be expected to be perturbed owing to electronic overlap with the metal (particularly those electronic states with non-zero electron density at the bonded nitrogen atom). Those parts of the molecule not experiencing overlap will be little perturbed. Thus of the two n states (i.e. two nitrogen lone pairs) one is expected to be significantly perturbed by interaction with the surface while the other remains fairly constant in energy. For t-BPE in solution the visible absorption spectrum shows a weak n-π* transition which peaks at 475 nm with a molar extinction coefficient of 1 M^{-1} cm^{-1} (Figure 9). This shoulder on the near UV π-π* transition[110] can be assigned to n-π* since in the dihydrochloride the intensity of the visible peak is

Figure 9: The Visible Absorption Spectra of
I. t-1,2-bis(4-pyridyl)ethylene and
II. t-1,2-bis(4-pyridyl)ethylene
dihydrochloride.

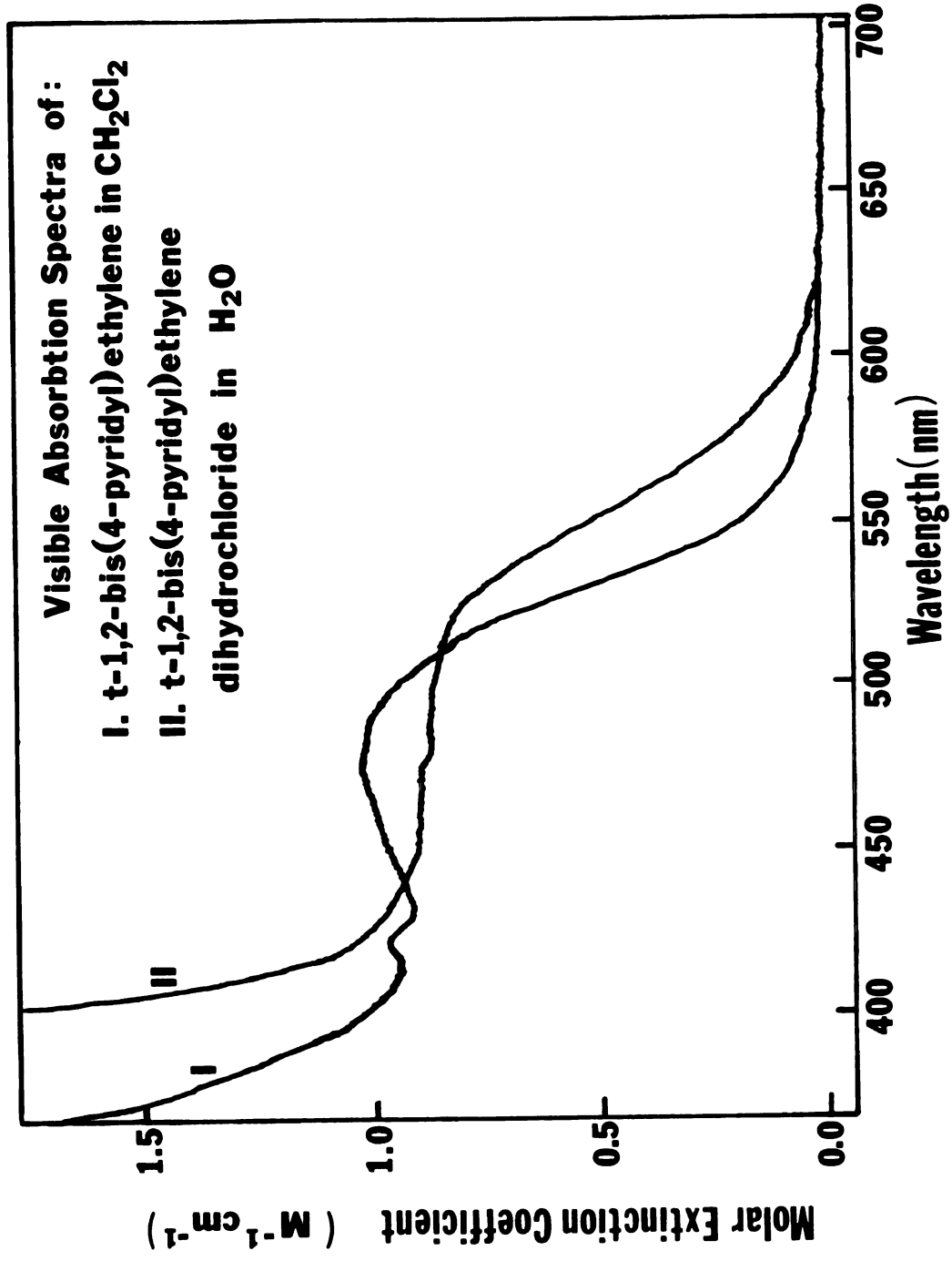
Visible Absorbtion Spectra of :
I. t-1,2-bis(4-pyridyl)ethylene in CH_2Cl_2
II. t-1,2-bis(4-pyridyl)ethylene dihydrochloride in H_2O
II
I
1.5
1.0
0.5
0.0
400
450
500
550
600
650
700
Wavelength(nm)
Molar Extinction Coefficient ($M^{-1}cm^{-1}$)

attenuated (typical of the behavior observed for n-π* transitions observed in other pyridine compounds upon acidification). The unbonded nitrogen lone pair of t-BPE in the "end-on" configuration at the surface is still available to undergo such an n-π* transition when excited with adequate energy. At 5145 Å excitation, as evident in Figure 9, the unbonded ring is slightly in resonance with the n-π* transition. The low symmetry of the surface complex may act to make the transition allowed and increase the actual molar absoptivity.

On moving to a relatively positive potential (-50 mV) an electron excited from the unbound nitrogen lone pair into the ethylenic π* orbital would be expected to experience a force of attraction to the positively polarized electrode surface. The coulombic attraction of the π* electron for the positively charged metal surface may cause the molecule to shift its nuclear equilibrium configuration in the excited state. The coordinate along which the shift occurs is that coordinate connecting the π* orbital with the positively charged electrode surface. In general, this coordinate will include contributions from all normal coordinates of the t-BPE molecule with components of motion of the ethylene carbons out of the plane of the molecule. Thus, an electron excited out of the unbound n state to a π* state experiences a force which shifts the equilibrium configuration of the excited state relative to the ground state along the coordinate connecting the

π^* orbital with the surface. The motion of the unbound part of the molecule out of the molecular plane closer to the electrode surface can be expected to lead to further electron density overlap with the metal. The increased overlap afforded by the molecule "lying down" on the surface can act to stabilize significantly the π^* state to within the occupied eigenstates of the silver-t-BPE complex. Thus, the π^* state appears as a ground state in the surface Raman spectrum of t-BPE at -50 mV potential under 5145 Å excitation.

The absence of similar molecular orientation at -600 mV (observed initially following anodization) is accounted for by remembering that at -600 mV the positive charge at the electrode surface is reduced (relative to that at -50 mV). The reduced electrode polarization diminishes the force experienced by an electron in the π^* state. Reemission occurs from an excited state only slightly shifted along the coordinate connecting the π^* orbital with the metal surface. Thus reorientation is not affected.

With t-BPE molecules now "flat" on the surface, and extensive electron density overlap of all sections of the molecule with the metal, more vibrations are expected to couple effectively to electronic transitions between eigenstates of the surface complex electronic manifold. Therefore, more modes appear, with greater intensity, in the surface Raman spectrum of t-BPE by virtue of a resonance Raman enhancement mechanism. Accordingly, the

ring motions in the region 1400-1560 cm^{-1} increase in intensity since the rings are now flat on the surface. Observation of the in-phase ethylenic hydrogen deformation at 1329 cm^{-1} is further indication that other sections of the molecule experience electron density overlap with the metal at -50 mV.

The irreversibility in the potential dependence of the surface Raman spectrum of t-BPE, evidenced by the different spectrum observed on return to -600 mV, is a manifestation of the extensive molecule-metal overlap in the "flat" configuration. The stabilization afforded by the overlap makes the "flat" configuration thermodynamically favored over the "end-on". The disappearance of the π^* vibrations on returning to the -600 mV potential implies that only at relatively positive potentials is the π^* state sufficiently stabilized to enter the manifold of occupied states. Evidence in the excitation profile of t-BPE at different potentials corroborates the stabilization of energy states on going to positive potentials (see the following section).

Not all t-BPE molecules have changed orientation at the surface, as evidenced by the lack of complete attenuation at 1640 cm^{-1}, 1200 cm^{-1}, and 880 cm^{-1} as well as the increase in intensity at 655 cm^{-1} after returning to -600 mV. Regardless of the number of times the potential is shifted positive (-50 mV), the intensity of the 655 cm^{-1} line is never completely attenuated. This indicates that

the surface can only accomodate a limited number of molecules in the "flat" configuration with "end-on" molecules filling the gaps.

The enhancement mechanism being proposed in this discussion is one of a resonance Raman enhancement brought about by the increased density of electronic states upon complexation to the silver surface. Evidence that electronic energy distribution in the complex differs from that of the molecule itself can be obtained from the excitation profile of t-BPE on silver. This is discussed in the next section.

Excitation Profile of t-BPE on Silver.

The variation in the intensity of lines in the surface Raman spectrum of t-BPE with excitation frequency is reported in Figure 10. The excitation frequency profile was recorded in the rhodamine 6G range from 15350 cm^{-1} to 17350 cm^{-1}. The internal standard to which all intensities were normalized was the 935 cm^{-1} line of the perchlorate ion (ClO_4^-) which was added to the supporting electrolyte at a concentration of 0.5 M. The focusing used was point focus and the intensity of the 935 cm^{-1} could be regulated by positioning the electrode surface at different depths in the electrolyte. The intensities of the t-BPE surface Raman lines are corrected for the fourth power dependence of the scattered frequency (ω_s) in equation (1) of Chapter 3. Normalization to intensities at one excitation frequency was not carried out since doing so would effectively double

Figure 10: Excitation Profile at t-1,2-bis(4-pyridyl)ethylene on silver at -600 mV sce in the end-on configuration (Rhodamine 6G excitation frequency range). Data points are normalized to the 935 cm^{-1} line of the perchlorate internal standard and corrected for the $\bar{\nu}^4$ dependence of the normal Raman cross section.

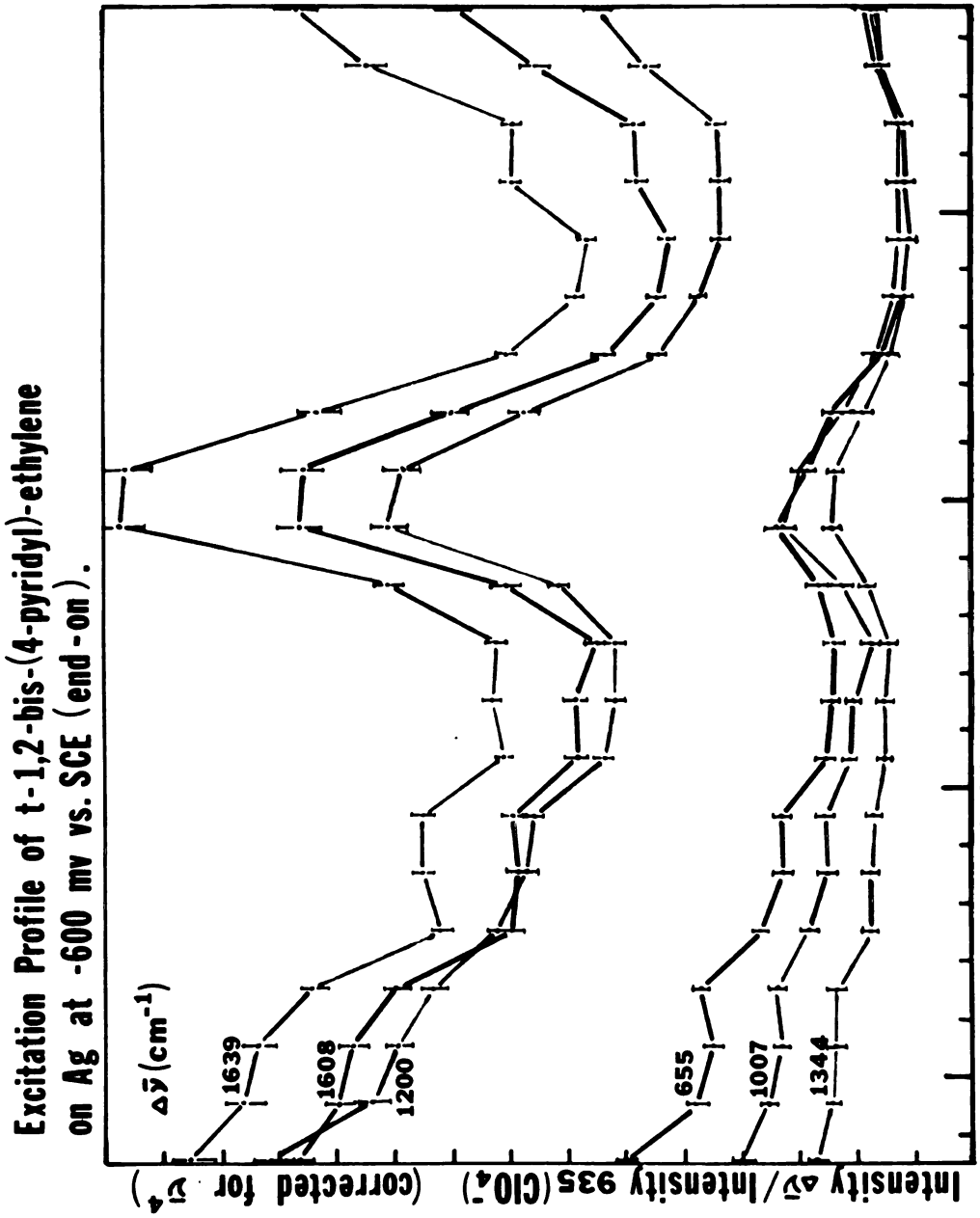
Excitation Profile of t-1,2-bis-(4-pyridyl)-ethylene
on Ag at -600 mv vs. SCE (end-on).
Δν̄(cm⁻¹)
1639
1608
1200
655
1007
1344
Intensity Δν̄/Intensity 935(ClO4⁻) (corrected for ν̄⁴)
15500
16000
16500
17000
cm⁻¹

the absolute random error. Therefore the most intense points in the excitation profile arise from the most intense line in the surface Raman spectrum. The excitation profile was examined for a heavy coverage of t-BPE molecules on silver in the "end-on" configuration observed at -600 mV versus sce. Owing to intensity fluctuations with movement of the laser beam to different points on the silver surface precautions were taken to assure excitation of the surface spectrum at the same point on the surface for each excitation frequency. The experimental arrangement is discussed in Chapter 4. The values plotted in Figure 10 and listed in Table 4 were obtained for each Raman line at each excitation frequency by the equation:

$$F = \frac{I_{\nu'}}{I_{935}} (\bar{\nu}_s^{\,4})^{-1} (1 \times 10^{18}) \qquad (12)$$

where F is the value plotted, $I_{\nu'}$ is the intensity of the vibrational Raman line at a particular exciation frequency, I_{935} is the intensity of the internal standard (ClO_4^-) line at 935 cm^{-1} and $\bar{\nu}_s$ is the scattered frequency in wavenumbers. The absolute random error in the points (F) was calculated from

$$\Delta F = \frac{(\Delta I_{\nu'})(\bar{\nu}_s^{\,4})^{-1}(1 \times 10^{18})}{I_{935}} + \frac{(\Delta I_{935}) I_{\nu'} (\bar{\nu}_s^{\,4})(1 \times 10^{18})}{I_{935}^2}$$

$$+ \frac{(\Delta \bar{\nu}_s) 4 I_{\nu'} (1 \times 10^{18})}{I_{935} \bar{\nu}^{\,5}} . \qquad (13)$$

TABLE 4: Excitation Profile of t-1,2-bis(4-pyridyl)ethylene on silver at -600 mV versus sce (corrected for ω^4).†

#	Excitation Frequency*	Vibrational Frequency (cm^{-1}) 655	1007	1200	1242	1344	1608	1640
1.	15351.7	60.32	40.49	121.46	39.65	27.09	116.11	135.39
2.	15451.6	48.03	35.66	103.98	30.66	24.58	109.63	126.19
3.	15552.1	44.89	33.02	99.77	29.68	23.99	107.27	123.69
4.	15652.5	47.08	34.10	93.48	28.19	23.62	99.03	114.18
5.	15751.5	37.04	28.41	82.42	22.79	17.90	79.02	92.23
6.	15851.8	32.76	25.19	77.32	21.31	17.75	78.78	95.20
7.	15950.7	33.34	25.50	75.88	21.36	17.06	79.61	95.37
8.	16048.7	25.35	21.19	63.80	18.51	15.23	68.40	81.20
9.	16150.0	24.42	20.68	61.81	17.10	15.56	68.82	83.23
10.	16249.4	23.87	16.89	61.93	16.62	14.70	65.07	82.64
11.	16350.3	26.60	22.39	71.58	20.35	18.06	80.86	101.12
12.	16450.5	33.82	33.31	101.19	27.22	24.59	116.76	148.04
13.	16549.8	28.63	29.54	98.45	26.38	24.19	115.88	146.88
14.	16649.4	24.36	22.51	77.34	19.80	19.28	90.04	113.65
15.	16750.3	15.82	16.45	54.13	14.08	14.09	63.73	80.88
16.	16851.5	12.02	13.73	47.11	12.63	11.97	54.49	68.78
17.	16950.2	10.86	12.80	43.88	11.20	10.88	52.51	66.84
18.	17046.5	11.83	12.05	43.83	11.17	12.01	58.15	79.77
19.	17149.6	11.36	12.72	44.25	11.36	11.84	58.43	79.54
20.	17250.0	15.63	15.96	56.65	15.51	16.20	75.48	104.79
21.	17344.1	15.47	18.38	64.51	15.69	17.76	89.55	116.89

†Absolute random errors do not exceed 5%.

*Excitation frequency is in cm^{-1}.

The magnitude of the Δ quantities in eqn. (13) were $\Delta I_{\nu'} = \pm 1$ cm, $I_{935} = \pm 1$ cm and $\Delta \bar{\nu}_s = \pm 2$ cm^{-1}. Thus, the absolute error in each point in Figure 10 is less than 5%.

The excitation profile shows the increased intensity enhancement in going toward red excitation wavelengths as observed in the surface Raman studies of pyridine and other molecules at silver as discussed in Chapter 2. More importantly, however, is that the excitation profile exhibits a peak at 16500 cm^{-1} which does not correspond to the frequency of any absorption in the visible absorption spectrum of t-BPE (Figure 9). The extinction coefficient of the t-BPE visible absorption spectrum at 16500 cm^{-1} (606 cm^{-1}) is near zero. The peak indicates a 0-0 transition from the ground state to an excited state, i.e. from the state of zero vibrational quantum number in the ground state to that in the excited state. This is indicated by the demonstration of a peak at 16500 cm^{-1} in the profile of each vibrational mode intensity. If the transition between vibrational states of the ground and excited state of vibrational quantum number greater than zero the peak in the profile would be shifted for each vibrational frequency. There is some evidence in the profile of a 0-1 transition also (i.e. a transition from the zeroth vibrational level of the ground state to the first vibronic component of the excited state). This evidence is the appearance of a crossover of intensities of the 1200 cm^{-1} line and the

1608 cm^{-1} line at 15750 cm^{-1}. This may be the 0-1 component of the transition which peaks (0-0) in the red not shown in this profile range. If this does indicate a 0-1 transition then the 0-0 is expected at 14550 cm^{-1} (687 cm^{-1}) which is near maxima observed in other surface Raman excitation profiles (Chapter 2). If indeed the crossover at 15750 cm^{-1} implicates a 0-1 transition, then the 1608 cm^{-1} line is expected to show some relative intensity increase approximately 400 cm^{-1} further to the blue. At 16150 cm^{-1} the 1608 cm^{-1} profile appears to increase slightly compared to the 1200 cm^{-1} line which supports assignment of the 0-1 transition.

The appearance of a 0-0 transition at 16500 cm^{-1} indicates the presence of an excited state not normally accessible to excitation in the molecule itself. The state however may be a complex state generated by electron density overlap between t-BPE and the silver surface. The appearance of an intense 0-0 component and a weak or non-existent 0-1 component indicates that the excited state position along all normal coordinates is little shifted from the equilibrium configuration in the ground state. Generally, to observe Franck-Condon scattering in a resonance Raman spectrum the excited state is required to be shifted along a nuclear coordinate such that upon excitation to the excited state a force is experienced. For Franck-Condon scattering a 0-1 transition or transition to higher vibrational quanta is expected to be observed

with considerable intensity in the excitation profile. Herzberg-Teller resonance Raman scattering requires no such shift in the excited state to contribute to the scattered intensity. Thus, a 0-0 transition is expected to be the strongest peak in the excitation profile of a Herzberg-Teller scatterer. It can therefore be suggested that the intense 0-0 transition in the excitation profile of t-BPE on the silver surface is a result of Herzberg-Teller coupling of excited states of the surface complex.

The appearance of an intense absorption at 16500 cm^{-1} fortifies the hypothesis presented in this thesis that the distribution of states of the molecule at the surface is significantly altered and increased in density upon formation of a surface complex. The complex formed in the "end-on" configuration can be expected to alter the electronic state distribution of states which demonstrate electron density at the bound nitrogen atom.

The peak in the excitation profile observed at -600 mV is observed to be potential-dependent as shown in Figure 11. In this figure the excitation profiles of the 655 cm^{-1} line in the t-BPE surface Raman spectrum are compared at -400 mV and at -600 mV. The actual intensities (normalized to I_{935} and $\bar{\nu}_s$[4]) are listed in Table 5. The 655 cm^{-1} mode is the most characteristic line of the "end-on" configuration of t-BPE on silver. It is observed in Figure 11 that the intensity of the t-BPE spectrum at -400 mV relative to the internal standard is reduced compared to that observed at

Figure 11: Potential Dependence of the Excitation Profile of the 655 cm^{-1} (ν_{6b}) Line in the Surface Raman Spectrum of t-BPE on Silver.

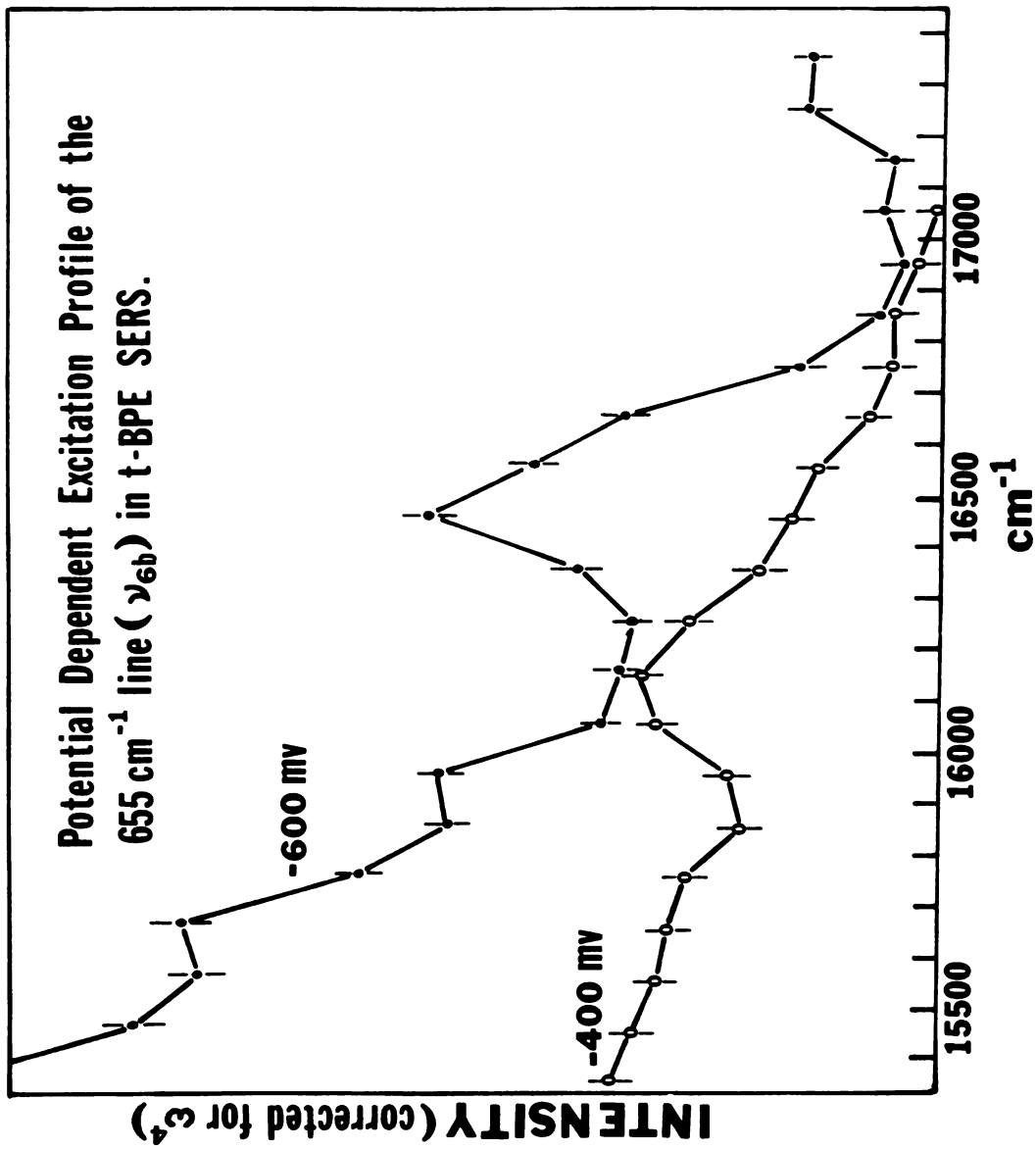
Potential Dependent Excitation Profile of the
655 cm-1 line (ν6b) in t-BPE SERS.
-600 mv
-400 mv
INTENSITY (corrected for ν4)
15500
16000
16500
17000
cm-1

TABLE 5: Potential Dependent Excitation Profile of the 655 cm^{-1} line (ν_{6b}) in the Raman spectrum of t-1,2-bis(4-pyridyl)ethylene on silver at -600 and -400 mV versus sce.†

	-600 mV (sce)		-400 mV versus sce	
#	Excitation Frequency*	Intensity (655 cm^{-1})	Excitation Frequency	Intensity (655 cm^{-1})
1.			15225.2	27.57
2.	15351.7	60.32	15354.0	25.86
3.	15451.6	48.03	15452.0	24.99
4.	15550.0	44.89	15555.0	23.75
5.	15652.5	47.08	15654.7	23.26
6.	15751.5	37.04	15755.0	22.41
7.	15851.8	32.76	15854.8	19.62
8.	15950.7	33.34	15951.2	20.26
9.	16048.7	25.35	16048.0	23.86
10.	16150.0	24.42	16151.5	24.34
11.	16249.4	23.87	16247.7	22.19
12.	16350.3	26.60	16350.2	18.74
13.	16450.5	33.82	16450.3	18.96
14.	16549.8	28.63	16554.2	17.17
15.	16649.4	24.36	16650.2	15.97
16.	16750.3	15.82	16749.5	15.74
17.	16851.5	12.02	16850.8	13.50
18.	16950.2	10.86	16950.3	12.39
19.	17046.5	11.83	17051.0	12.39
20.	17149.6	11.36	17153.8	11.13
21.	17250.0	15.63	17250.0	10.23
22.	17344.1	15.47	17349.2	9.28

†Absolute random errors do not exceed 5%.

*Frequency in cm^{-1}.

-600 mV. This is a manifestation of the combined increase in concentration of ClO_4^- ion near the more positive surface at -400 mV with the decrease in the number of adsorbed t-BPE molecules on moving to positive potentials.

The important point to be taken from the potential dependence of the excitation profile is that the peak shifts to lower energy with the corresponding shift to more positive potentials. The peak in the profile at -400 mV occurs at 16150 cm^{-1} relative to the 16500 cm^{-1} peak in the -600 mV profile. The shift to lower energy at positive potentials is consistent with the appearance of the π^* state in the -50 mV spectrum of t-BPE on silver (Figure 7) and its disappearance on returning to -600 mV. That is, stabilization is sufficient at positive potentials for π^* to become an occupied state but not at more negative potentials.

Frequently in SERS studies researchers have reported potential dependence of surface Raman intensities and drawn conclusions about surface coverage and other information essential to analysis of the enhancement mechanism. The potential dependence of the excitation profile of t-BPE at a silver electrode demonstrates that such conclusions can be premature and misleading without knowledge of the shifts in intensity expected by excitation profile arguments. The excitation profiles reported here were determined by continuous variation of excitation frequency with spectra recorded every 100 cm^{-1} ($\sim$ 4.1 nm). In other excitation

profiles reported in the literature (see Chapter 2 for references) spectra have been reported in intervals of 500-1500 cm^{-1}. The full width at half height (FWHH) of the peak observed in the excitation profile of t-BPE on silver is approximately 300 cm^{-1}. Therefore, early profiles reported may actually have missed important structure in the excitation profiles and consequently the density of states for adsorbates at a metal surface has not previously been recognized as large. Most researchers have concentrated on explanation of the increased enhancement to the red which can be easily understood if the density of states is high.

Light Coverage Studies and the Raman Spectrum of an Ag (t-BPE) Complex.

Another requirement for the observation of the irreversible potential-dependent behavior observed for the t-BPE surface Raman spectra in Figure 7 is that the adsorbate coverage must be heavy. As mentioned earlier, when the bulk concentration of t-BPE prior to the oxidation-reduction cycle does not exceed 500 nM the adsorbate coverage of the electrode is light and only reversible potential dependence of the SERS spectra is observed. Some insight into the effect of light coverage can be gained by analysis of the potential dependence of the light coverage spectrum of t-BPE as shown in Figure 12. The spectra shown were excited with 6578 Å radiation (Rhodamine 6G emission) although any

Figure 12: Potential Dependence of the Surface Raman Spectrum of a Light Coverage of t-BPE on Silver.
EXCITATION WAVELENGTH: 6578 Å (Dye Laser Emission).

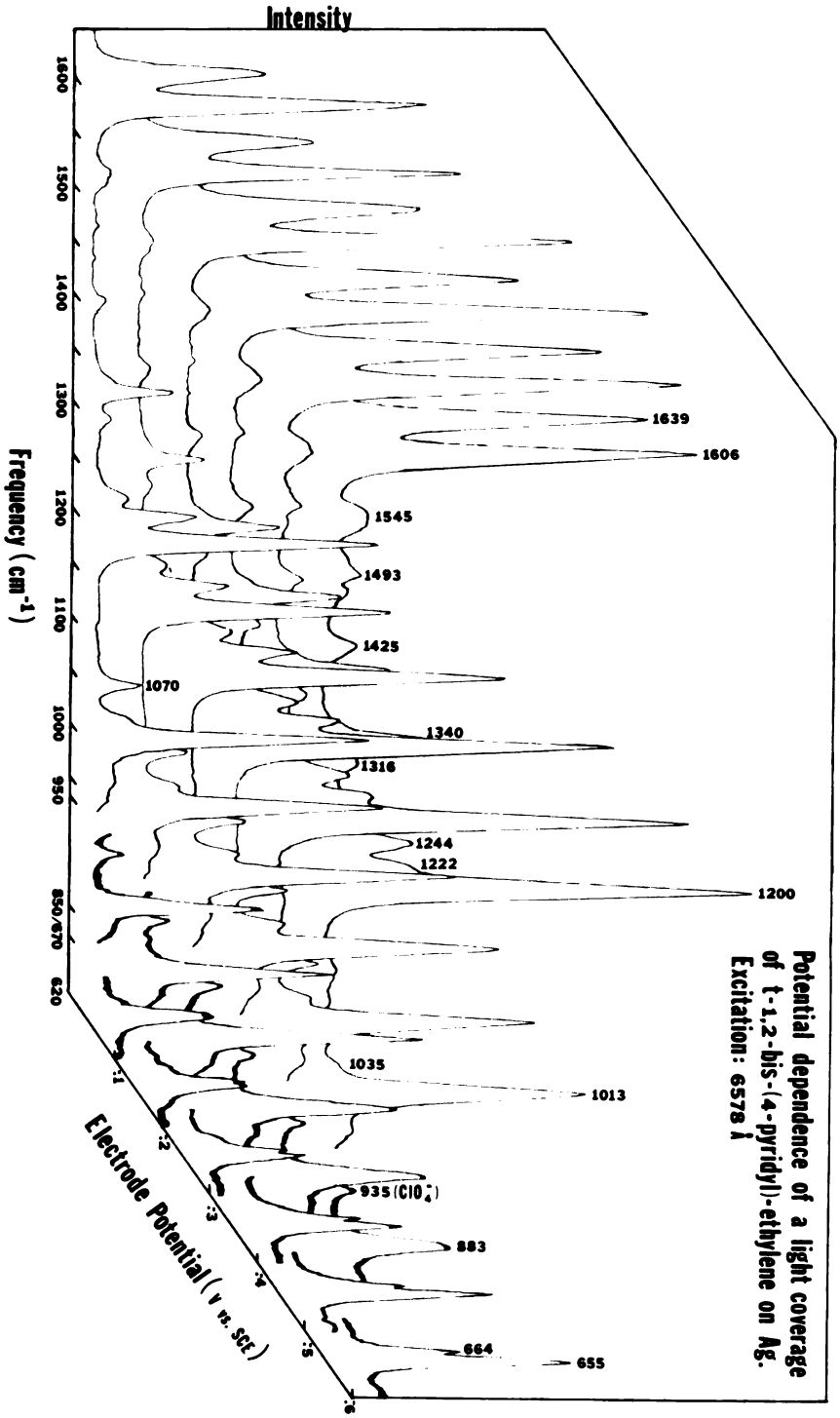
Intensity
Frequency (cm⁻¹)
1600
1500
1400
1300
1200
1100
1000
950
850/870
620
1639
1606
1545
1493
1425
1070
1340
1316
1244
1222
1200
1035
1013
935 (ClO₄⁻)
883
664
655
Electrode Potential (V vs. SCE)
-.1
-.2
-.3
-.4
-.5
-.6
Potential dependence of a light coverage of t-1,2-bis-(4-pyridyl)-ethylene on Ag.
Excitation: 6578 Å

wavelength excitation of light coverages produces only reversible potential dependence of the observed surface spectrum. An interesting feature of the potential dependence shown in Fig. 12 is the dynamics of the 655 cm^{-1} line. On moving to positive potentials the 655 cm^{-1} line decreases in intensity and shifts to higher frequency, coalescing with the 664 cm^{-1} line (ν_{6b}). This strengthens the previous assignment of the 655 cm^{-1} line to motion 6b in the ring attached to the silver surface as discussed in an earlier section of this chapter. A similar b-type mode, 9b, observed at 1244 cm^{-1} in the surface spectrum exhibits similar potential-dependent behavior, decreasing sharply in intensity on going to positive potentials.

This and other changes in the surface Raman spectrum of a low coverage of t-BPE can best be understood by comparison with the normal Raman spectrum of a polycrystalline silver complex of t-BPE shown in Fig. 13. The stoichiometry of the complex has not yet been determined but some conclusions can still be drawn in the comparison. In the polycrystalline silver complex spectrum the 1201 cm^{-1} line (C_{eth} - ϕ symmetric stretch) appears at the same intensity as the ν_1 mode at 1025 cm^{-1}. Similarly in the surface spectrum of t-BPE at -100 mV versus sce the two vibrations appear with similar intensity. Two lines appearing at 1037 cm^{-1} and 1040 cm^{-1}, probably split by site symmetry in the crystalline matrix, in the polycrystalline complex spectrum can be assigned to the pyridine ring vibration ν_{12}

Figure 13: Normal Raman Spectrum of a Polycrystalline Silver Complex at t-BPE ($Ag_n(t\text{-}BPE)_m$). EXCITATION WAVELENGTH: 6471 Å (Kr^+).

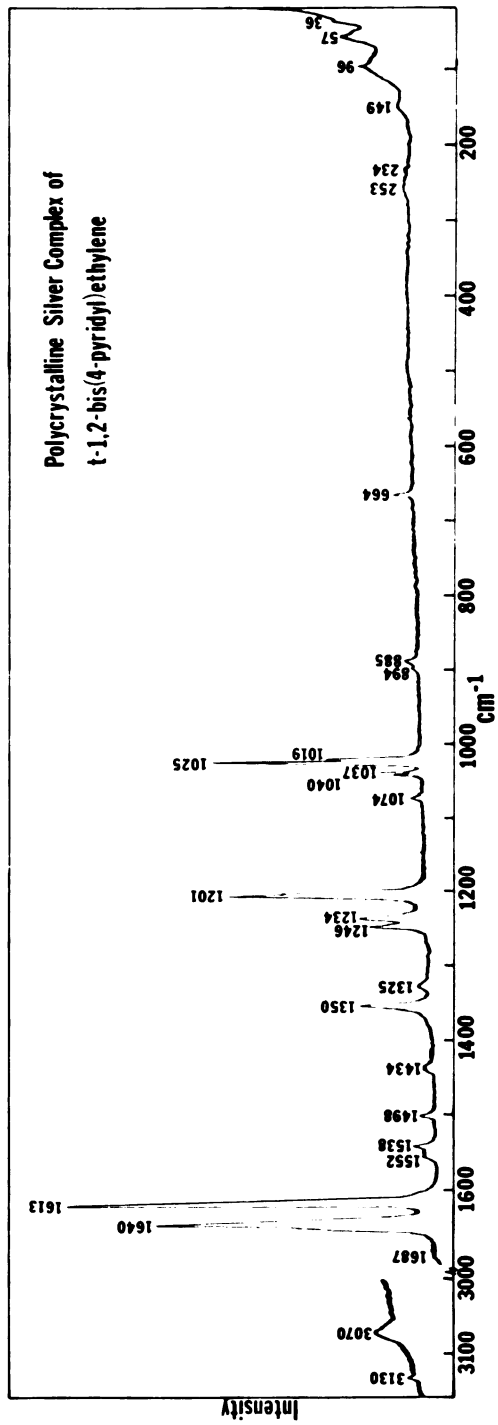
Polycrystalline Silver Complex of
t-1,2-bis(4-pyridyl)ethylene
Intensity
cm-1
3100
3000
1600
1400
1200
1000
800
600
400
200
3130
3070
1687
1640
1613
1552
1538
1498
1434
1350
1325
1246
1234
1201
1074
1040
1037
1025
1019
894
885
664
253
234
149
96
57
36

TABLE 6: Raman Spectrum of a polycrystalline silver complex of t-1,2-bis(4-pyridyl)-ethylene and comparisons to the Raman Spectrum of t-1,2-bis(4-pyridyl)ethylene on silver (light coverage*) at -400 mV sce† and to the polycrystalline t-BPE Raman Spectrum.

Assignment Wilson#	Polycrystalline Agn(t-BPE)m	t-BPE on Silver at -400 mV (sce)	Polycrystalline t-BPE
	36		43
Lattice	57		
Modes	96		
	149	110br	121
Ag-Cl str.		230	
skeletal vibr.	234	230	240
Ag-N str.	253		
6b		655	
	664	663	671
10a	885	883	878
10b	894		887
1	1019	1013	995
	1025		
12	1037	1034	
	1040		
18a	1074	1065	1069
C_e - ϕ str.	1201	1197	1198
9a	1234	1223	1225‡
9b	1246	1239	1234
3	1325	1313	1319
14	1350	1338	1351

*The light coverage spectra are recorded in Figure 12 .

†Point of local maximum in the current-potential plot of t-1,2-bis(4-pyridyl)ethylene on silver, Figure .

‡Vibration occurs at 1220 in CH_2Cl_2 solution. (TABLE 4 CONTINUES).

TABLE 6 CONTINUED.

Assignment Wilson #	Polycrystalline Agn(t-BPE)m	t-BPE on Silver at -400 mV (sce)	Polycrystalline t-BPE
19b	1434	1421	1422
19a	1498	1491	1491
8b	1538	1538	1549
10a + 4	1552		
8a	1613	1602	1597
C=C str.	1640	1634	1638
C-H	3070		3013
stretch	3130		3024
			3038
			3054

which occurs in the Raman spectrum of pyridine at 1037 cm^{-1} and is the most intense line in the spectrum. Vibration 12 is conspicuously absent from the heavy coverage spectrum but appears weakly at 1035 cm^{-1} in the light coverage spectrum, reaching maximum intensity at the -400 mV potential. The appearance of ν_{12} in the light coverage surface Raman spectrum of t-BPE and its appearance in the Raman spectrum of the polycrystalline silver complex strengthens the hypothesis of the existence of a surface complex. The C=C symmetric stretch at 1639 cm^{-1} attenuates in intensity going to positive potentials and us currently not completely understood. It seems that most of the scattering observed in the light coverage originates in the part of the molecule closest to the surface. Thus, the C_{eth} - ϕ symmetric stretch (1200 cm^{-1}) and the C=C symmetric stretch are attenuated at positive potentials and the ν_1 vibrations (1013 cm^{-1}) appears to narrow. The reason for more intensity arising from the closer part of the molecule can only be decided when the state in which the excitation wavelength is in resonance (assuming a resonance Raman enhancement mechanism) becomes known. There are several electronic excited states which, by using typical building up principles, exhibit electron density, only at the rings and not in the ethylene bridge. Resonance Raman excitation to such a state would be expected to result in increased intensity for the bound ring only. The attenuations of the above mentioned line intensities may

not be observed in the heavy coverage because of intense scattering from multilayers.

Although some of the features of the light coverage surface Raman spectra are not completely understood other features can be utilized to understand the requirement of heavy coverage for the observation of the "flat" configuration. At positive potentials the silver surface atoms have developed nearly a unit positive charge per silver atom. The silver atom in the polycrystalline silver complex is, of course, formally in the +1 oxidation state, experiencing a full positive charge. With a light coverage of t-BPE molecules at the surface, chloride and perchlorate ions are expected to occupy more surface sites. The increased concentration of anions at the positively polarized surface acts to screen the positive charge seen by the neutral t-BPE molecule at the surface. The screening effect is invoked to account for differences between the light coverage spectrum and that observed for heavy coverages and for the polycrystalline silver complex.

Modes with components of motion orthogonal to the direction of the attraction force at the surface (i.e. those modes in the end-on configuration which are orthogonal to the surface normal) and are not expected to be influenced by charge fluctuations at the surface. However, modes with components of motion along the direction of the attractive force <u>are</u> expected to be influenced by charge fluctuation

at the surface. Modes which involve asymmetric stretch along the surface normal (end-on configuration) demonstrate the largest sensitivity to surface coverage. Examples of this are now discussed. Vibration 9a, which appears at 1234 cm^{-1} in the polycrystalline silver complex Raman spectrum demonstrates asymmetric stretching along the surface normal. This vibration appears at 1233 cm^{-1} in the heavy coverage surface Raman spectrum of t-BPE at -100 mV but at 1225 cm^{-1} in the light coverage spectrum. Similarly, vibration 19a appears at 1498 cm^{-1} in the polycrystalline silver complex spectrum and at 1497 cm^{-1} in the heavy coverage spectrum of t-BPE on silver at -100 mV. The motion 19a appears at 1493 cm^{-1} in the light coverage spectrum shown in Figure 12. These observed shifts and the shifts of other a-type modes in the light coverage spectrum relative to the heavy coverage and complex spectra are therefore understood by considering the reduced positive charge seen by the light coverage of t-BPE molecules owing to anion screening.

This screening is undoubtedly responsible for the lack of reorientation of the t-BPE molecule in a light coverage under 5145 Å irradiation. As discussed in the previous section, reorientation of the t-BPE molecule occurs through excitation into a π^* orbital which, owing to the proximity of the positively charged surface, experiences a force along the coordinate connecting the π^* orbital with the silver surface. With the positive charge on the electrode screened

by the presence of large numbers of anions in the light coverage situation the force exerted on the π^* electron is reduced. The reduction in the force is apparently sufficiently large enough such that reorientation cannot be affected. Thus, under light coverage conditions, the "flat" configuration never materializes (at any excitation wavelength) and completely reversible potential-dependent behavior of the surface spectrum is observed.

The effect of exciton splitting of an excited state of one t-BPE molecule relative to the excited state of its neighbor on the surface may also account for the observed coverage-dependent phenomena. However, physical evidence for both the exciton model and the screening model are currently lacking and further study is needed.

Negative Potential Results and the Reduction Product of t-BPE.

Interesting potential-dependent spectroscopic phenomena are also observed on moving to potentials negative of -600 mV. As shown in Figure 14, the surface Raman spectra of t-BPE develops features characteristic of the "flat" configuration. This is observed by comparing the "end-on" spectrum at -400 mV with spectra observed on moving to -1.0 V versus sce. In the spectrum observed at -800 mV intensity has developed at the 681 cm^{-1} line (ν_{11}, Au) with decreasing intensity at 655 cm^{-1}. This indicates that the "end-on" configuration is diminishing in

Figure 14: Potential Dependence of the Surface Raman Spectra of t-BPE Potentials -400 mV, -600 mV, -800 mV and -1.0 V versus sce.
EXCITATION WAVELENGTH: 5145 Å (Ar^+).

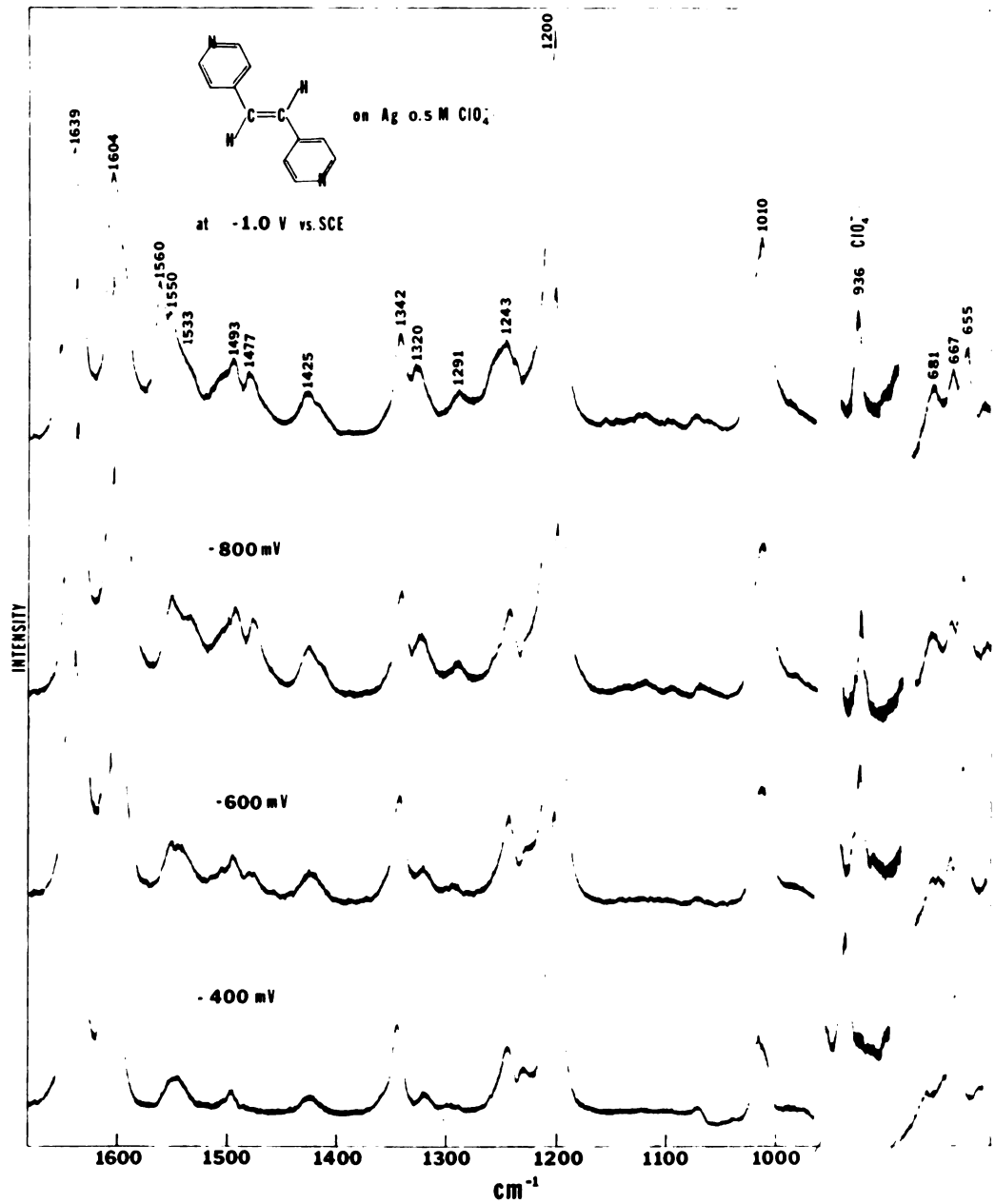
on Ag o.s M ClO4
at -1.0 V vs.SCE
-1639
1604
1560
1550
1533
1493
1477
1425
1342
1320
1291
1243
1200
1010
936 ClO4
681
667
655
-800 mV
-600 mV
-400 mV
INTENSITY
1600
1500
1400
1300
1200
1100
1000
cm-1

prominence and the "flat" configuration takes its place. The increase in intensity of the vibrational lines in the region 1400-1560 cm^{-1} is further indication that the rings are beginning to lie down on the surface and experience electron density overlap with the metal. The increased intensity at 1320 cm^{-1} (C_{eth} - H in-place, in-phase, deformation) is consistent with that observed in going to the flat configuration. By comparing the relative intensities of the C=C symmetric stretching vibration at 1639 cm^{-1} and the intensity at 1200 cm^{-1}, it is apparent that the 1639 cm^{-1} band becomes attenuated relative to the C_{eth} - ϕ stretch at 1200 cm^{-1}. This may be indicated of the electronic state from which the Raman signal is originating from.

At potentials near the p.z.c. (point of zero charge) of silver (i.e. near -900 mV sce in 0.1 M Cl^-) it might be expected that electronic excited states would become occupied by transfer of electron density from the metal to the adsorbate. The lowest such excited state for t-BPE can be determined by using known electron density distributions for the two rings and the ethylene bridge[111] and applying building-up principles. The most probable lowest excited state is one of Bg symmetry which therefore can contain a contribution from the ethylenic π^* orbital which transforms as Bg symmetry in the molecular C_{2h} point group. In this state there is no electron density at the ring carbon involved in bridging to the ethylene carbon. Thus,

no overlap will exist between the π* orbital and the ring carbon at the 4-position. The force constant of the C_{eth} - φ bond is therefore not expected to be different from that in the ground state. Accordingly, the C_{eth} - φ symmetric stretch at 1200 cm^{-1} is not attenuated by a shift to another frequency even though the system is in a π* state. The C=C symmetric stretch, however, is expected to be attenuated since the force constant of the bond between the ethylene carbons will change and move under the symmetric ring stretch near 1600 cm^{-1}.

A new peak appears in the negative potential surface Raman spectra of t-BPE at 1291 cm^{-1}. This mode can be assigned to the ethylenic hydrogen out-of-phase, in-plane deformation (Bu) because of its appearnace at 1289 cm^{-1} in the infrared spectrum of t-BPE as observed by Katsumoto.[1] Interestingly this mode does not appear in the spectrum of the "flat" configuration at -600 mV as shown in Figure 7. This may indicate that the state bound in the "flat" configuration is a state which contains only in-phase electron structure (i.e. is of A type symmetry) while the state observed on sweeping to negative potentials is probably an out-of-phase state as denoted by the Bg symmetry assigned above.

The reasons for the molecular reorientation at negative potentials are similar to those for reorientation under 5145 Å irradiation at -50 mV (Fig. 7). With the occupation of a π* orbital at negative potentials reorientation may

occur in order that better adsorbate-metal overlap be affected. The force experienced by the π^* electron in the vicinity of the still relatively weakly positive electrode surface is undoubtedly small and accounts for the minimal amount of reorientation observed spectroscopically. Reorientation of the end-on molecules is further facilitated by decrease in surface concentration of anions from the supporting electrolyte. The surface sites vacated by anions at negative potentials can be filled by molecular reorientation of the neutral t-BPE molecule at the surface.

At potentials negative of the p.z.c. (i.e. -1.0 V versus sce) anomalous spectroscopic changes are observed which further indicate electron transfer from the metal to the adsorbate. The totally symmetric ring motion (8a) at 1604 cm^{-1} becomes attenuated in intensity accompanied by appearance of a new line at 1560 cm^{-1}. The high frequency side of the C=C symmetric stretch at 1639 cm^{-1} develops a shoulder in the surface Raman spectrum of t-BPE at -1.0 V. Some distortion in the 1240 cm^{-1} range is also observed. These changes can be best understood by continuing to alter potential in the negative direction. At -1.2 V versus sce an obviously distinct surface Raman spectrum of t-BPE is observed (Figure 15).

In Figure 15, the 1561 cm^{-1} peak, which was developing in the spectrum at -1.0 V, has become the most intense line in the spectrum. This line is assigned to the totally symmetric pyridine ring motion 8a in the "new" molecule by

Figure 15: Surface Raman Spectrum of the Two-Electron Reduction Product of t-BPE on Silver at -1.2 V versus sce.
EXCITATION WAVELENGTH: 5145 Å (Ar^+).

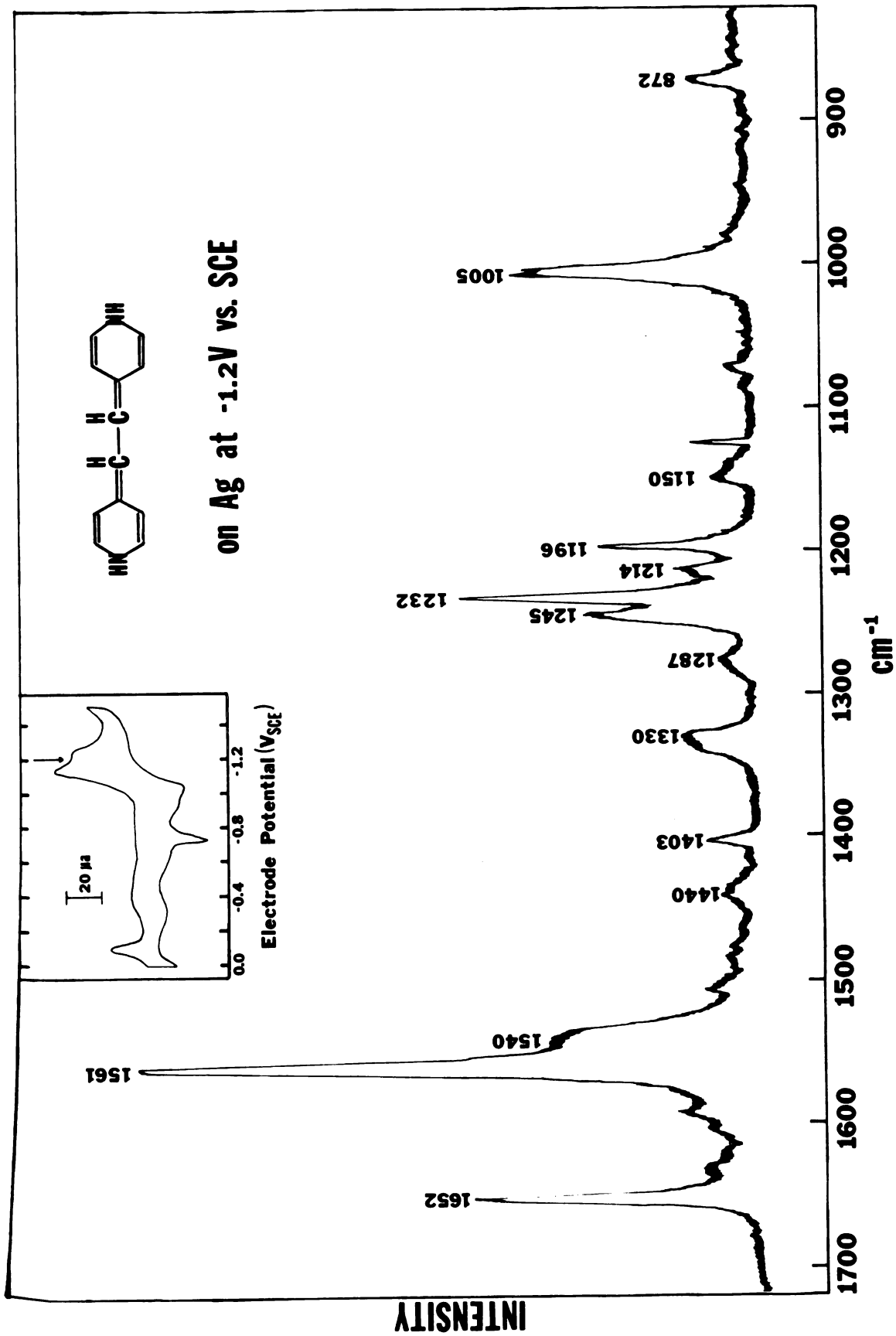
on Ag at -1.2V vs. SCE
INTENSITY
cm-1
1700
1600
1500
1400
1300
1200
1100
1000
900
1652
1561
1540
1440
1403
1330
1287
1245
1232
1214
1196
1150
1005
872
20 μa
0.0
-0.4
-0.8
-1.2
Electrode Potential (VSCE)

TABLE 7: Raman Spectrum of the two-electron reduction product of t-1,2-bis(4-pyridyl)ethylene on silver at -1.2 v versus sce. Excitation: 5145 Å.

Vibrational Frequency (cm^{-1})	Suggested Assignment (Wilson #)
641	(6b) in-plane ring deformation
871	10a out-of-plane CH deformation
1005	(1) symmetric ring stretch
1071	(18a) in-plane C-H deformation
1085	(18b) in-plane C-H deformation
1150	(15) in-plane C-H deformation
1196	(9a) in-plane C-H deformation
1214	?
1232	? central carbon symmetric stretch
1245	(9b) in-plane N-H deformation
1287	out-of-phase C_e-H deformation
1330	14 ring stretch
1403	19b ring motion
1440	?
1507	(19a) ring stretch
1540	(8b) ring stretch
1561	(8a) symmetric ring stretch
1593	? unreduced t-BPE vibration
1630	? unreduced t-BPE vibration
1652	C_e-C_ϕ stretch

reason of the attentuation of the 1604 cm^{-1} line at -1.0 V accompanying the growth at 1560 cm^{-1}. It is clear that the very intense C_{eth} - ϕ symmetric stretch occurring at 1200 cm^{-1} in the -1.0 V spectrum is absent from the 1200 region in the surface spectrum at -1.2 volts. The shoulder observed on the high frequency side of the ethylenic C=C stretch in the -1.0 V spectrum has developed into a sharp line at 1652 cm^{-1} in the -1.2 V spectrum and the 1639 cm^{-1} line is essentially completely attenuated. The high frequency motion at 1652 cm^{-1} is clearly a C=C stretch. These changes and others observed in the -1.2 V surface Raman spectrum of t-BPE on silver can be understood by first examining the current-potential profile of t-BPE which is inset in Figure 15. At approximately 1.1 V versus sce the bis pyridyl ethylene molecule undergoes a two-electron reduction. This reduction was examined by Volke and Holubek[110] in 1962. They found that in solutions of neutral pH the yellow reduction product of t-1,2-bis(4-pyridyl)ethylene was unstable and quite different from the ethane reduction products of less symmetrical isomers than the 4-substituted bipyridyl ethylene. The difference was manifested by reoxidation of the yellow reduction product and the reappearance of the original reduction after electrolysis which indicated a reversible electrode process. The ethane reduction product of t-1,2-bis(4-pyridyl)ethylene was only obtained by reduction in acidic solutions. Volke and Holubek suggested the structure of the reduction product

to be that shown in Figure 15. The suggestion was that the two electron reduction involved protonation at the nitrogens in the pyridine rings rather than at the central ethylene carbons. The 1962 reference,[110] however, offered no experimental evidence of the proposed structure of the reduction product. The surface Raman spectrum of the reduction product shown in Figure 15 is the first physical evidence to support the suggested structure. The 1652 cm^{-1} line can be assigned with confidence to the C=C symmetric stretch between the ethylene carbon and the 4-position ring carbon. The increased force constant relative to the ethylenic C=C symmetric stretch (1639 cm^{-1}) is consistent with the large C=C force constant in substituted ethylenes ($R_2C{=}CH_2$) in which one end of the double bond has a carbon which is bonded only to carbon atoms. The symmetric C=C stretch occurs in the range 1658-1644 cm^{-1} in such compounds.[103] Therefore, the absence of the single bond C_{eth} - ϕ stretch at 1200 cm^{-1} is also accounted for.

Other assignments in the surface Raman spectrum of the t-BPE reduction product can be made. The sharp line at 1196 cm^{-1} is probably vibration 9a in the rings of the reduction product. Vibration 9a appears to move consistently to lower frequency in going to negative potentials as observed in Figure 14. There 9a appears at 1224 cm^{-1} in the end-on spectrum at -400 mV but shifts under the C_{eth} - ϕ stretch at 1200 cm^{-1} in the -1.0 V spectrum. The sharp line at 1232 cm^{-1} is assigned to the symmetric

stretch of the central carbon single bond in the reduction product for lack of a better assignment for the relatively intense line. Other modes in the reduction product do not appear significantly shifted from their positions in the unreduced t-BPE surface Raman spectrum. For example, the intense line at 1005 cm^{-1} can certainly be assigned to the totally symmetric ring motion ν_1 in the reduction product. The appearance of a weak line at 1440 cm^{-1} is interesting in comparison to the spectrum observed at -50 mV which contained π^* vibrations. In that spectrum, a line was observed at 1449 cm^{-1} which eluded assignment. The 1449 cm^{-1} was characteristic of the π^* state in that it disappeared upon returning to -600 mV. The reduction product of t-BPE is related to the occupation of π^* orbitals at positive potentials. The reduction product is, of course, the result of addition of electrons to the t-BPE molecule which necessarily occupy π^* orbitals in the unreduced molecule. Thus the 1440 cm^{-1} mode in the spectrum of the reduction product and the 1449 cm^{-1} mode in the -50 mV spectrum of t-BPE are probably the same normal coordinate and assignment as such fortifies the hypothesis of presence of π^* states in the surface Raman spectrum of t-BPE at -50 mV under 5145 Å irradiation. Suggested assignments of many of the observed lines in the t-BPE reduction product spectrum are listed in Table 6.

Monoprotonated t-BPE on Silver.

In Figure 16 the surface Raman spectrum of t-BPE was recorded in an electrolyte of pH 5.6. The top spectrum in the figure was recorded under 5145 Å excitation and demonstrates some significant differences from the usual spectrum of t-BPE on silver at -50 mV. These results were observed for low coverages of t-BPE on silver and therefore at -50 mV only the end-on configuration is evident.

The differences between the pH 5.6 spectrum (top, Figure 16) and the neutral pH spectrum are consistent with spectroscopic changes observed in comparison of the normal Raman spectra of t-BPE and its dihydrochloride. For example, in the solution spectra of t-BPE (Figure 6) and its dihydrochloride the symmetric C_{eth} - ϕ stretch is observed at 1195 cm^{-1} and 1210 cm^{-1}, respectively. In the surface Raman spectrum of t-BPE at pH 5.6 (5145 Å excitation) the 1200 cm^{-1} line (C_{eth} - ϕ stretch) appears markedly attenuated and the neighboring 1222 cm^{-1} line appears to have gained intensity. The shift in the C_{eth} - ϕ symmetric stretch to higher frequency on formation of the hydrochloride can account for these intensity variations. A new line in the SERS spectrum of t-BPE at pH 5.6 occurs at 1582 cm^{-1} at -50 mV. This line can be assigned to motion 8b in the protonated ring by virtue of the shift to higher frequency of mode 8b in the normal Raman spectrum of t-BPE upon formation of the hydrochloride. In t-BPE mode 8b appears at 1549 cm^{-1} in the normal Raman spectrum and at

Figure 16: Excitation Wavelength Dependence of the Surface Raman Spectrum of Monoprotonated t-BPE on Silver at -50 mV (sce). ELECTROLYTE pH: 5.6.

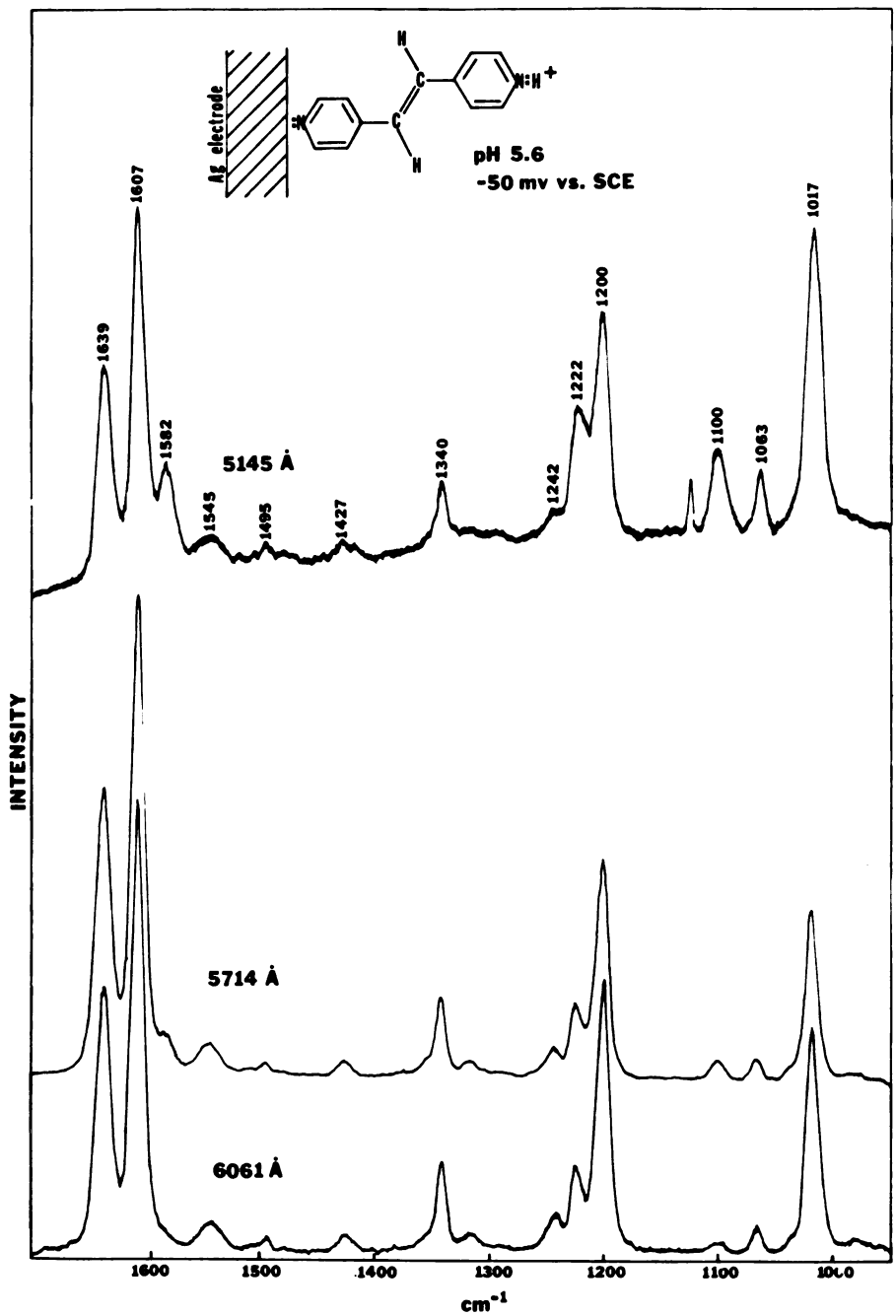
Ag electrode
pH 5.6
-50 mv vs. SCE
5145 Å
5714 Å
6061 Å
INTENSITY
1639
1607
1582
1545
1495
1427
1340
1242
1222
1200
1100
1063
1017
1600
1500
1400
1300
1200
1100
cm-1

TABLE 8: Raman Spectrum of Monoprotonated t-1,2-bis(4-pyridyl)ethylene on silver at -50 mV and -600 mV at pH 5.6 and at -600 mV after base (OH^-) is added. Excitation: 5145 Å. Region: 1000-1700 cm^{-1}.

Assignment Wilson #	Monoprotonated t-BPE on Ag		Base (OH^-) Added
	-50	-600 mV	-600 mV
1	1017	1006	1012
18a	1063	1056	
18b	1100	1095	
C_e-ϕ sym. str.	1200	1199	1201
9a	1222		
9b (NH def)	1242	1243	1246
C_e - H def. (out-of phase)		1287	1286
3		1316	1322
14	1340	1338	1338
4 + 11	1414	1409	
19b	1427	1424	1422
19a	1495	1490	1491
8b	1545	1538	1543
8b (out-of-phase)		1555	
8b (protonated ring)	1582	1574	
8a	1607	1603	1606
C_e=C_e sym. str.	1639	1637	1639

1605 cm^{-1} in the dihydrochloride. The increased intensity of mode 18b at 1100 cm^{-1} in the surface Raman spectrum of t-BPE at pH 5.6 can be understood in that 18b is expected to couple to N-H deformation. Thus it appears that the t-BPE molecule on the electrode surface is monoprotonated at pH 5.6.

This conclusion is not unreasonable. In the end-on configuration the t-BPE molecule has one nitrogen lone pair extending into the electrolyte solution. Lavalee and Fleischer[88] report values of 5.92 and 4.49 for the pK_2 and pK_1 values (negative logarithm of the acid dissociation constants), respectively, of t-BPE. Though the acid dissociation of the complex (t-BPE at the silver surface) is expected to be somewhat different from the dissociation constants in the ligand, the difference is probably small owing to several factors. In the pentaminebispyridylethylene ruthenium II complex the pK_a is observed to be 5.0 ± 0.1.[88] For t-BPE on silver the charge built up on the silver atom is significantly lower than that on the ruthenium atom in the +2 oxidation state. Also, as discussed earlier the increased concentrations of electrolyte anions at the surface are expected to screen the full positive charge on the electrode surface. Thus it is expected that the pK_a of the t-BPE molecule-silver surface complex will not be significantly lower than the pK_2 of the t-BPE ligand alone. Future surface titration experiments should clarify this point.

Some further evidence that the surface spectrum observed at pH 5.6 is that of the monoprotonated t-BPE molecule is presented in Figure 17. There the potential dependence of the pH 5.6 surface spectrum and the spectrum observed after addition of base (KOH) are shown. The appearance of the characteristic lines of the protonated ligand (i.e. 1574 cm^{-1}, 1095 cm^{-1} and other changes) at -600 mV as well as at -50 mV shows the insensitivity of the pK_a value on the true polarization at the electrode surface. The disappearance of the lines, characteristic of the monoprotonated t-BPE-silver complex, upon addition of base is very convincing evidence for the protonation phenomenon at the silver surface.

Returning to Figure 16 briefly, some interesting excitation frequency dependence for the monoprotonated spectrum is discovered. The lines characteristic of the monoprotonated species are absent under red excitation but grow in intensity with increasing frequency of the exciting line. This is consistent with the notion that for light surface coverage at positive potentials most of the light scattering intensity originates in the parts of the t-BPE molecule which are closest to the silver surface. The intensity from the ring more remote to the silver surface increases only as a consequence of coming into resonance with a weak $n \rightarrow \pi^*$ transition in the visible absorption spectrum of both t-BPE and its dihydrochloride (see Figure 9). This evidence also corroborates the hypothesis that the $n \rightarrow \pi^*$ transition from

Figure 17: Surface Raman Spectrum of Monoprotonated t-BPE on Silver at -50 mV (sce), -600 mV (sce), and at -600 mV (sce) after Addition of Base (OH^-).
EXCITATION WAVELENGTH: 5145 Å (Ar^+).

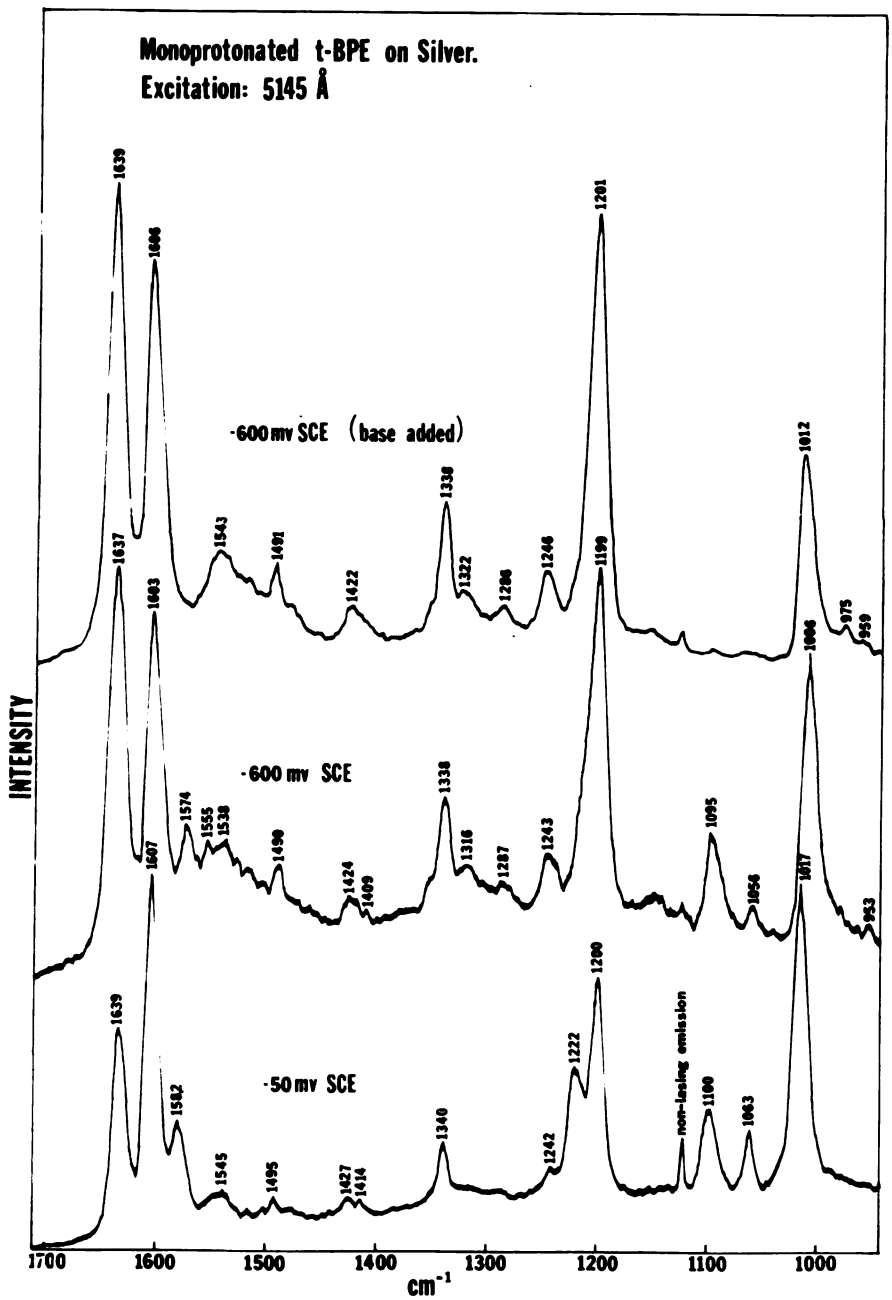
Monoprotonated t-BPE on Silver.
Excitation: 5145 Å
-600 mv SCE (base added)
-600 mv SCE
-50 mv SCE
INTENSITY
1639
1606
1543
1491
1422
1338
1322
1206
1244
1201
1190
1012
975
959
1637
1603
1574
1555
1538
1490
1424
1409
1338
1316
1287
1243
1095
1056
1007
953
1639
1582
1545
1495
1427
1414
1340
1242
1222
1200
non-lasing emission
1180
1063
1700
1600
1500
1400
1300
1200
1100
1000
cm-1

the outside ring can still occur though the distribution of electronic states in the ring closer to the silver surface is significantly perturbed from the distribution of states in the molecule in solution. That the electronic states of the section of the t-BPE molecule not experiencing electron density overlap with the silver surface in the end-on configuration, are not significantly perturbed is a requirement for the reorientation mechanism proposed in earlier sections of this chapter. The lines which have been interpreted as characteristic of the monoprotonated t-BPE molecule on the surface also appear in the heavy coverage spectrum observed at -50 mV under 5145 Å excitation i.e. the spectrum of the flat molecule containing π^* vibrations. This spectrum is shown in Figure 18. An interesting experimental fact observed in the studies of the monoprotonated surface spectrum of t-BPE on silver is that upon addition of sufficient acid all surface Raman signals, identifiable as originating from t-BPE molecules, disappear. It is not difficult to understand this fact. A doubly-protonated t-BPE molecule is quite positively charged and is not likely to approach the positively polarized electrode. Also protonating both nitrogens eliminates the possibility of end-on complexation to the metal surface.

Influence of ClO_4^- on the Surface Spectrum of t-BPE.

The addition of 0.5 M perchlorate for purposes of use as an internal standard in excitation profile experiments

Figure 18: Surface Raman Spectrum of Monoprotonated t-BPE on Silver at -50 mV (sce) in the "flat" Configuration.
EXCITATION WAVELENGTH: 5145 Å (Ar^+)

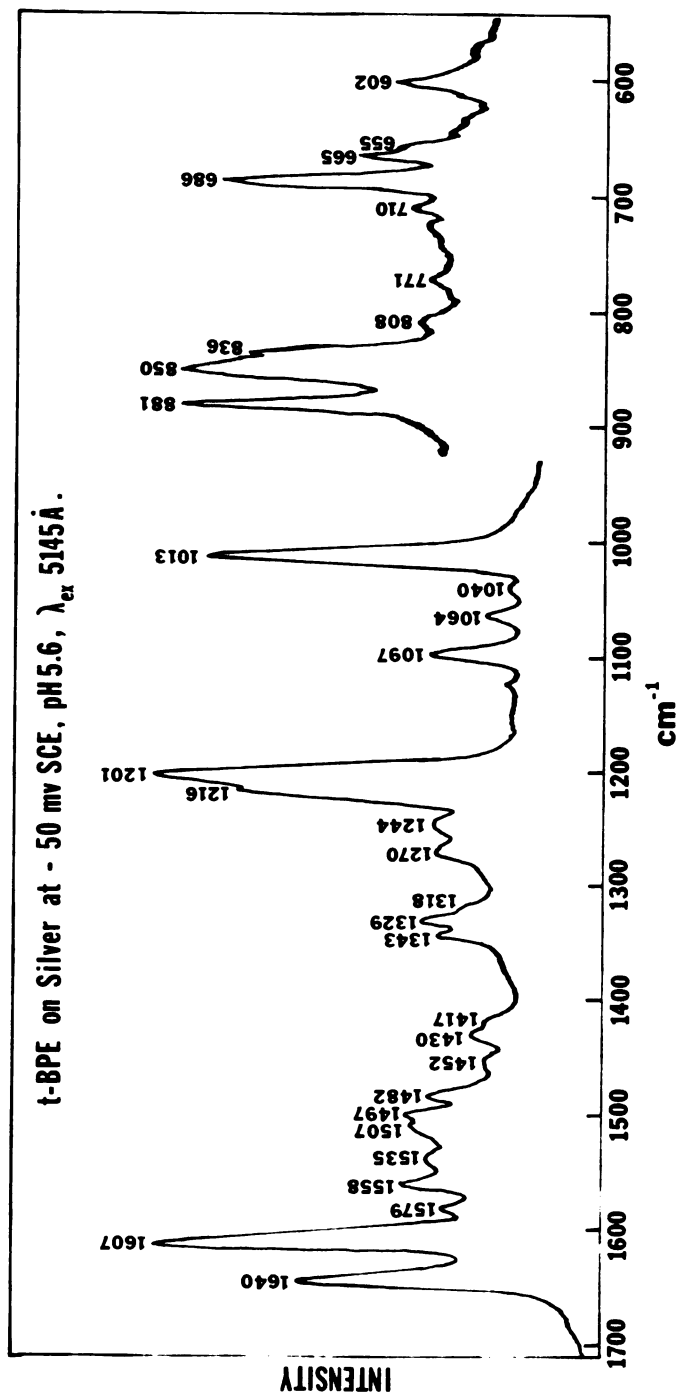
t-BPE on Silver at - 50 mv SCE, pH5.6, λ_{ex} 5145Å.
INTENSITY
cm^{-1}
602
655
665
686
710
771
808
836
850
881
1013
1040
1064
1097
1201
1216
1244
1270
1318
1329
1343
1417
1430
1452
1482
1497
1507
1535
1558
1579
1607
1640
600
700
800
900
1000
1100
1200
1300
1400
1500
1600
1700

has some important influences in the Raman spectrum observed for t-BPE on silver. In general, the screening of the positive charge developed at the silver electrode surface is invoked as responsible for the effects produced by the presence of ClO_4^-. For the potential dependence of the t-BPE surface spectrum in the negative potential range effects observed in simple 0.1 M chloride electrolytes are exaggerated with 0.5 M ClO_4^- present. That is, on going to negative potentials t-BPE molecules in the end-on position "lie down" at more positive potentials with half molar perchlorate ions present than in their absence. In both 0.5 M ClO_4^-/0.1 M Cl^- and 0.1 M Cl^- alone electrolyte solutions when altering potential in the positive direction the surface Raman signal is attenuated owing to the displacement of adsorbed t-BPE molecules by anions at the metal-solution interface. This reduction in surface Raman intensity at positive potentials is understandably augmented by the presence of 0.5 M ClO_4^-.

In the spectrum of t-BPE "flat" on the silver surface some very interesting influences of the 0.5 M ClO_4^- presence are observed. After initiating the molecule reorientation of t-BPE molecules from the end-on configuration to the "flat" configuration at -50 mV under 5145 Å excitation the potential was moved to -600 mV and the spectra shown in Figure 19 were observed. In 0.1 M Cl^- only the spectrum at -600 mV typifies what has been assigned to the "flat" spectrum in earlier sections of this chapter. Relative

Figure 19: Influence of 0.5 M ClO_4^- on the Observed Surface Raman Spectrum of t-BPE "flat" on the Silver Surface at -600 mV (sce). EXCITATION WAVELENGTH: 5145 Å (Ar^+).

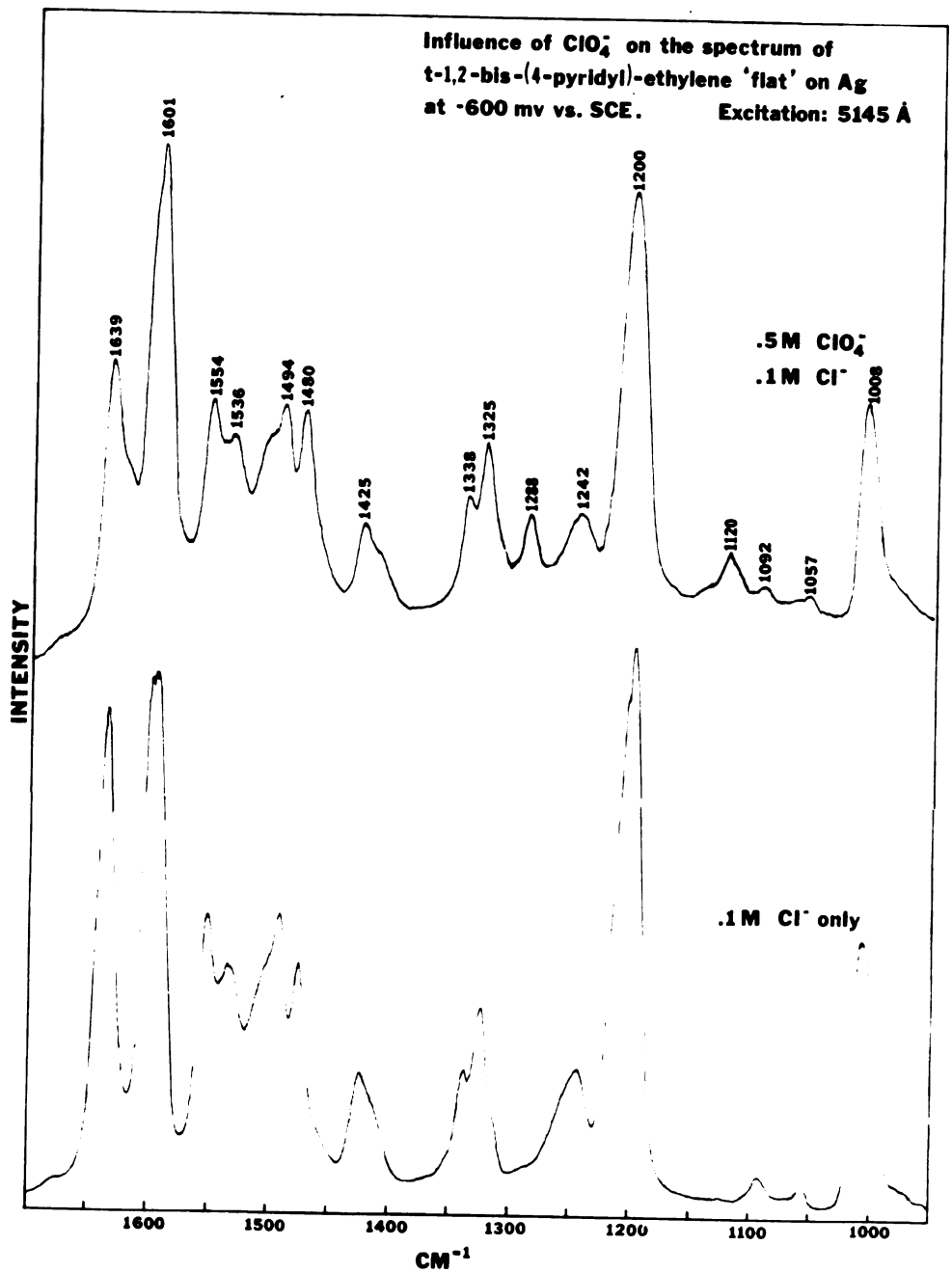
Influence of ClO_4^- on the spectrum of
t-1,2-bis-(4-pyridyl)-ethylene 'flat' on Ag
at -600 mv vs. SCE.
Excitation: 5145 Å
.5 M ClO_4^-
.1 M Cl^-
.1 M Cl^- only
INTENSITY
1639
1601
1554
1536
1494
1480
1425
1338
1325
1288
1242
1200
1120
1092
1057
1008
1600
1500
1400
1300
1200
1100
1000
CM^{-1}

to that spectrum, in the spectrum observed at the same potential with 0.5 M ClO_4^- also present some distinct differences are evident. The intensity of the ethylenic C=C symmetric stretch at 1639 cm^{-1} remains attenuated in the -600 mV spectrum in 0.5 M ClO_4^-/0.1 M Cl^- while regaining intensity in 0.1 M Cl^- alone. Also, noticed in the perchlorate spectrum is the appearance of a line at 1288 cm^{-1} which also appears when the t-BPE molecules lie down at negative potentials (earlier section) and which has been assigned to the out-of-phase component of an in-phase ethylenic hydrogen deformation. The weak line at 1120 cm^{-1} is probably the pyridine ring motion ν_{15}. The reason for these differences could rest in the idea that the state that is observed is the highest occupied molecular orbital (HOMO). The HOMO in the case with 0.5 M ClO_4^- present may be different from that when only 0.1 M Cl^- present as a result of screening. The high concentration of anions diminishes the effective charge at the surface and thus stabilization of different states may result. The state observed in the 0.5 M ClO_4^-/0.1 M Cl^- solution is probably the same state that begins to appear at negative potentials with the t-BPE molecules in the end-on configuration. That is, a π^* state which involves no overlap of electron density between the π^* orbital and the closest pyridine carbon atom which consequently causes no shift in the C_{eth} - ϕ stretch (1200 cm^{-1}) but shifts the C=C stretch to lower frequency, attenuating the line at

1639 cm^{-1}. The spectrum observed at -600 mV with only 0.1 M Cl^- present may involve electron density mixing with an unexcited π state since neither of the lines at 1639 cm^{-1} and 1200 cm^{-1} are shifted or attenuated in intensity.

Photodegradation of t-BPE Multilayers on Silver.

In the observation of the excitation profile of t-BPE on silver some anomalous frequency dependence is observed. Figure 20 demonstrates this anomalous behavior. The intensity of pyridine ring vibration ν_{11} appears to increase in intensity with increasing excitation wavelength. Initially this phenomenon was attributed to the distinction of the red state appearing in the excitation profile. That is, it was thought that ν_{11} was effective in vibronic coupling to the red excited state but not to other higher energy excited states. However, further investigation proved these assumptions erroneous. The 683 cm^{-1} line (ν_{11}) is absent from the surface Raman spectrum of a light coverage of t-BPE molecules at the electrode-electrolyte interface. The spectra recorded in Figure 20 were obtained with a heavy coverage of t-BPE molecues on the surface. Also, as shown in Figure 21 the intensity of the ν_{11} vibration is photosensitive to red excitation. In Figure 21 a series of consecutive spectra were recorded in the 625-700 cm^{-1} region. The only variable changing in this experiment was the time the sample was irradiated. It

Figure 20: Excitation Wavelength Dependence of the ν_{11} (683 cm^{-1}) Vibration t-BPE on Silver at -400 mV versus sce.

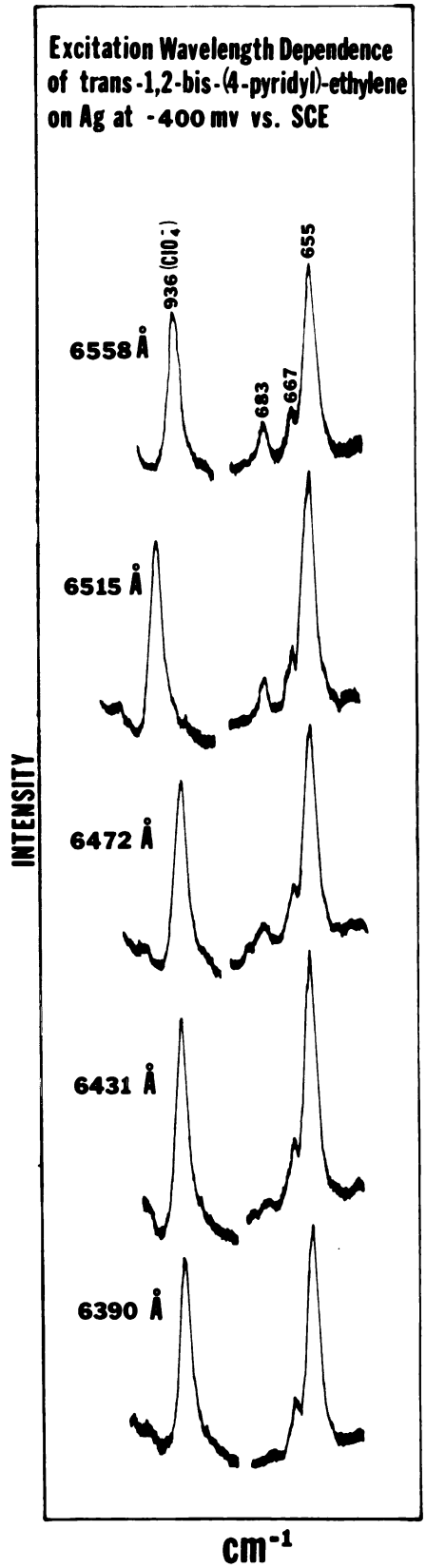
Excitation Wavelength Dependence
of trans-1,2-bis-(4-pyridyl)-ethylene
on Ag at -400 mv vs. SCE
936 (ClO_4^-)
655
683
667
6558 Å
6515 Å
6472 Å
6431 Å
6390 Å
INTENSITY
cm^{-1}

Figure 21: Photodegradation of Multilayers of t-1,2-bis(4-pyridyl)ethylene on Silver: Loss of Intensity at 684 cm^{-1}.

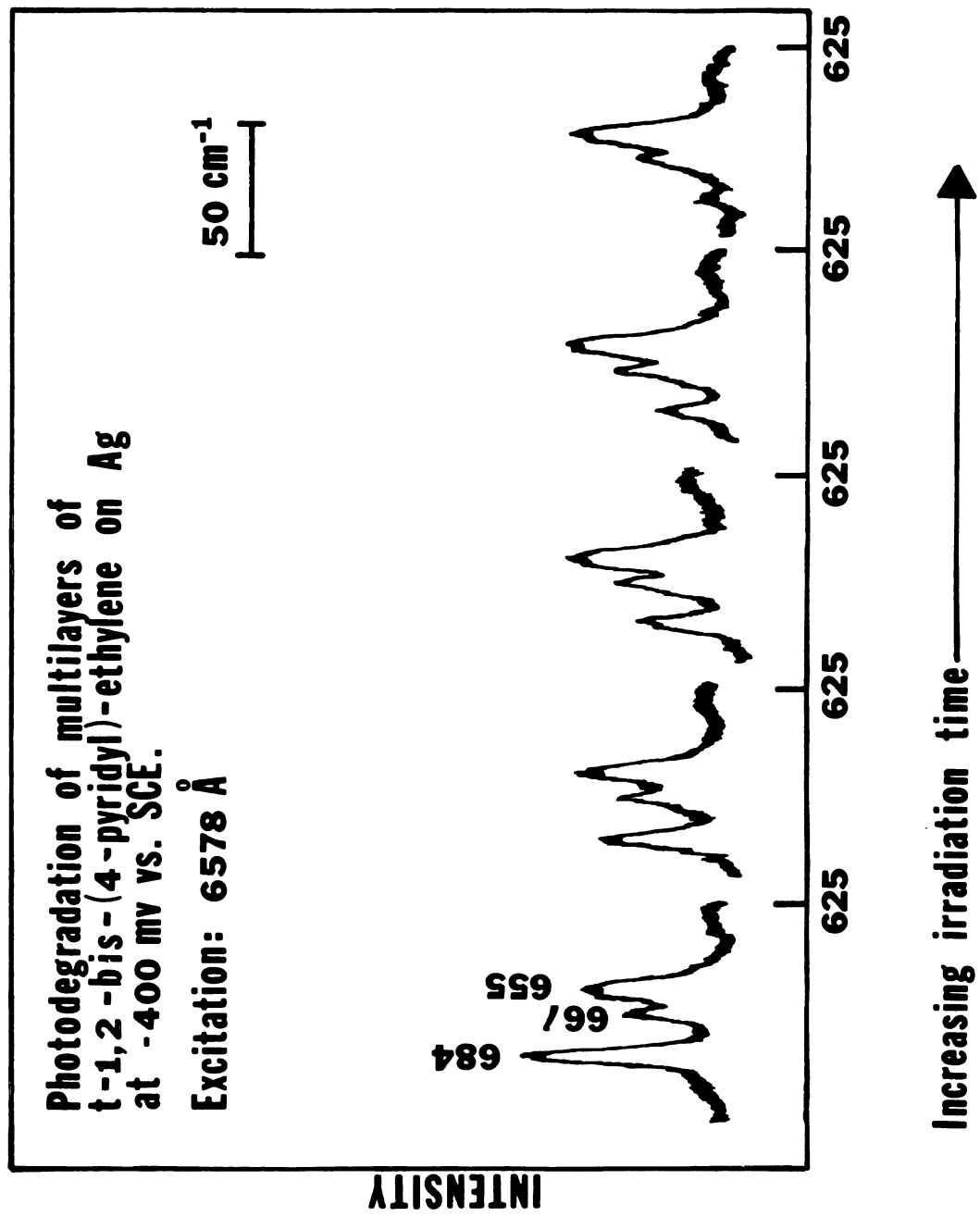
Photodegradation of multilayers of
t-1,2-bis-(4-pyridyl)-ethylene on Ag
at -400 mv vs. SCE.
Excitation: 6578 Å
50 cm-1
684
661
655
625
625
625
625
INTENSITY
Increasing irradiation time

is clear from the figure that the 684 cm^{-1} line is attenuated in intensity with increasing irradiation time. However, the neighboring vibrations 6b at 667 cm^{-1} and 655 cm^{-1} retain full intensity throughout the time of the experiment. The phenomenon pictured in Figure 21 occurred over a time range of 30 minutes at an incident laser power of 50 mW. Obviously, there is evidence of photodegradation but the signal from the molecules at the surface is not degraded. The degradation must occur in the multilayers of t-BPE molecules at the surface. This can be deduced from the absence of the 684 cm^{-1} line in the light coverage spectrum and the absence of degradation of the characteristic surface mode at 655 cm^{-1}. The photodegradation must necessarily be accompanied by a visible absorption. Since the 684 cm^{-1} line increases in intensity in the red so too must the absorption be in the red. But the t-BPE molecule has no visible absorption spectrum above approximately 600 nm. However, in the multilayers the rapid adsorption of t-BPE molecules to the electrode surface probably produced a very low site symmetry seen by each t-BPE molecule. The site symmetry in the multilayers is expected to be C_1. Therefore, just as the symmetry of the one-sided attachment of t-BPE molecules to the silver surface is liable to make forbidden transitions allowed so also will the low symmetry in the multilayers. The actual transition could also be an intermolecular one which for stacked flat molecules is likely to occur along the stacking direction.

An out-of-plane mode, such as pyridine vibration ν_{11}, has nuclear coordinate components only in the stacking direction and may therefore be expected to couple effectively to intermolecular transitions.

The visible sign of photodegradation in the multilayers is the appearance of a burn hole in the surface coating where the laser beam has been focused. The absence of attenuation in the Raman signals from the molecules directly associated with the silver surface (denoted by the characteristic 655 cm^{-1} line) is probably a consequence of the ability of the metal substrate to serve as a heat sink, offering an alternative excited state decay pathway to decomposition.

The appearance of surface Raman signals from the multilayers should be treated as a caution signal in interpretations. Rowe et al[58] and other researchers have reported surface enhanced Raman signals from multilayers. The possible influence of site symmetry lowering of the molecular symmetry on the absorption of incident radiation was not addressed. The observation of surface enhanced Raman signals from absorbed molecules not in direct contact with the metal surface is inconsistent with the proposed enhancement mechanism of surface complex resonance Raman scattering offered in this thesis.

CHAPTER VII

Surface Enhanced Raman Spectra of Amino Acids and Future Studies.

Surface enhanced Raman scattering has been shown to be a versatile probe of dynamics at a metal-dielectric interface. For t-1,2-bis(4-pyridyl)ethylene adsorbed at a polycrystalline silver electrode nearly every vibrational mode of the molecule, both infrared and Raman active modes, has been observed in the SERS spectrum. Molecular orientation at the surface could be interpreted from irreversible potential-dependent behavior of the surface Raman spectrum. The structure of the reduction product was determined with confidence. Similar studies can be applied to other molecules.

The new researcher-controlled experimental parameter of continuous electrode potential variations has direct application to systems incorporating electron transfer. The importance of electron transfer in biological systems makes those systems logical candidates for study by surface Raman techniques. Generally, Raman studies of large biologically important molecules have been concentrated in resonance Raman investigations of the chromophore. These studies are very effective in determining contributions to UV/vis absorption spectra by different chromophores and distinction

of similar chromophores in regard to substituents which may couple to the electronic transitions. The influence of the protein substructure on energy transfer is often invoked to describe dynamics observed in the chromophoric resonance Raman spectrum. The actual structure of many proteins has eluded determination owing to the inability to crystallize many of the large molecular weight molecules. The dynamics of protein structure change during oxidation and reduction at the redox center is essentially unknown.

Because of the intense light scattering observed from molecules adjacent to the metal electrode surface in the SERS experiment it is reasonable to assume that the outer amino acid residues of an adsorbed protein should exhibit intense SERS signals. Thus, the SERS experiment may be applicable to analysis of structure, amino acid sequence, and energy transfer at the outer sections of a large protein molecule. The combination of potential dependent spectroscopic phenomena and structure and orientation interpretations with excitation wavelength dependence of an adsorbed protein promises to make deep inroads into the mechanisms of energy transfer in biologically important molecules. Of course, distinction of amino acid residues and their orientation at the electrode surface are pre-requisites to any interpretation of outer protein structure. In this chapter the surface enhanced Raman spectrum of two small amino acids, L-glycine ($NH_2CH_2COO^-$) and L-leucine

[$(CH_3)_2CHCHNH_2COO^-$] are presented and interpreted in terms of orientation at the electrode surface. It is hoped that distinctions in the surface enhanced Raman spectrum of these and other amino acids may be extrapolated to assignments in surface spectra of adsorbed protein molecules in the future.

The intensity of the surface enhanced Raman signals from the adsrobed amino acids are significantly reduced from the signals observed from t-1,2-bis(4-pyridyl)ethylene on silver. The signals observed from the amino acids on silver generally were in the range 3×10^3 counts per second, or less, whereas the signals obtained from t-BPE on silver ranged from 1×10^5 to 3×10^5 counts per second. The reasons for the sharp drop in intensity are consistent with the ligating ability of t-BPE, over that of the amino acids, in conjunction with a resonance Raman enhancement mechanism involving a silver complex. The normal Raman scattering cross section of the highly conjugated t-BPE molecule over that of the saturated amino acids examined here may also account for the remarkable intensity of t-BPE surface Raman signals. As mentioned previously, the hydrophobic character of t-BPE undoubtedly assists in the facile adsorptions of the bipyridine to the silver surface. The amino acids are polar molecules and are therefore hydrophilic.

Notwithstanding the low intensity of the surface Raman signals from glycine and leucine some interpretations of

molecular orientation at the electrode surface can still be made. The Raman spectra of L-leucine and L-glycine on silver at -600 mV under 5145 Å excitation are shown in Figure 22 and the frequencies and assignments are listed in Table 9. These spectra were recorded in a bulk pH of 11.0. Since at this pH both amino acids are above their respective isoelectric points the molecules carry a negative charge associated with the carboxylate group. No surface Raman spectrum was observable from amino acids at the silver electrode when the pH of the bulk solution was below the isoelectric point of the amino acids. Therefore, it can be assumed that the negatively charged amino acids adsorb more strongly to the positively polarized electrode than do the neutral compounds in agreement with the t-BPE results.

The pH adjustment from neutral solution was accomplished by addition of KOH. The formation of silver oxide (Ag_2O) and silver hydroxide (AgOH) was possible in the hydroxide media. In order to determine the presence of the oxides at the surface and their influence on the surface Raman spectrum observed for the amino acid system the normal Raman spectra of the two polycrystalline oxides was obtained. Both Ag_2O and AgOH are black opaque solids which required a back scattering geometry for observation of the normal Raman spectra. These spectra are shown in Figure 23 and the frequencies listed in Table 10. The normal Raman spectra of these two silver oxides have not been previously

Figure 22: Surface Raman Spectra of L-leucine and L-glycine on Silver at -600 mV (sce). EXCITATION WAVELENGTH: 5145 Å (Ar^+).

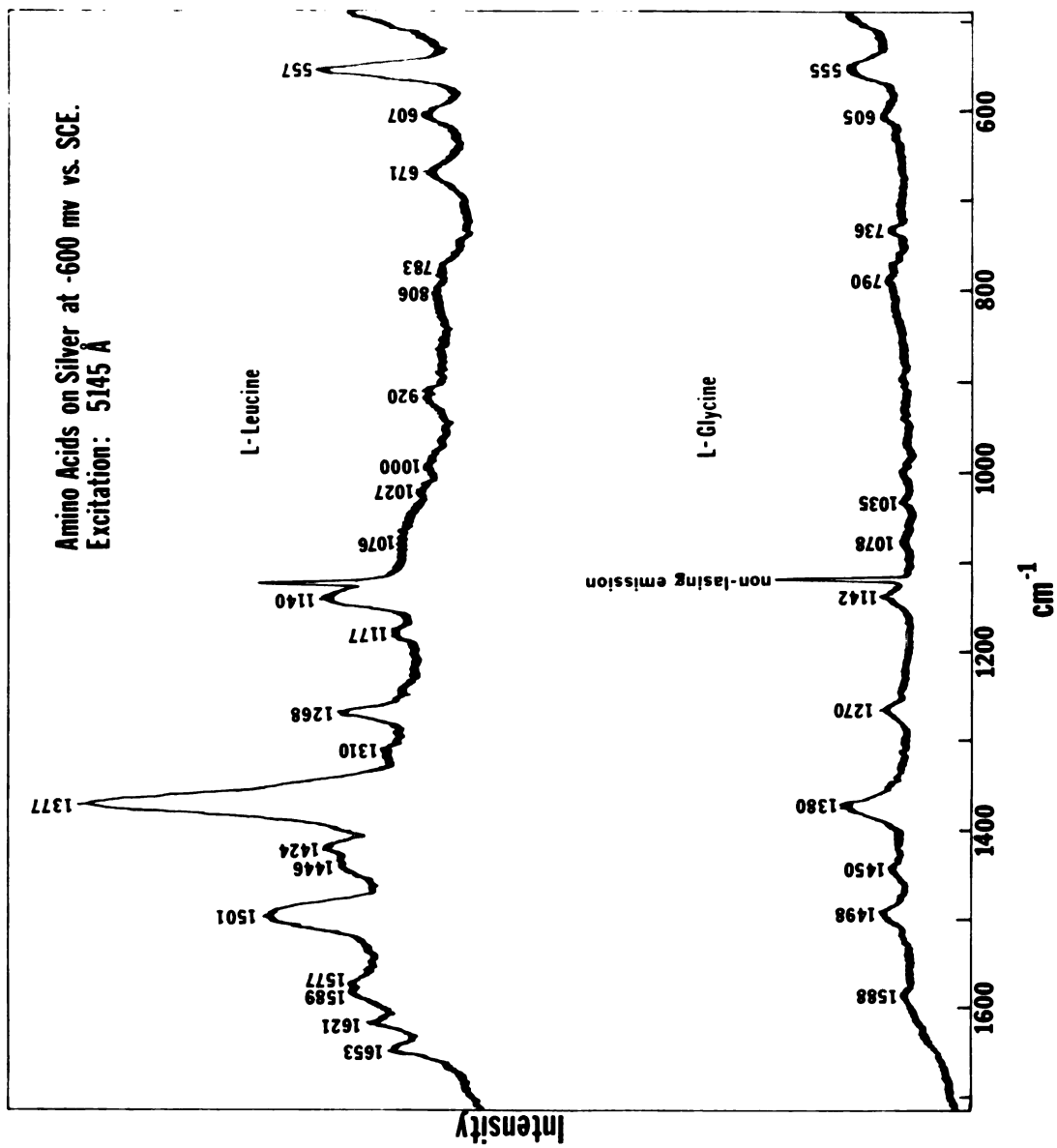
Amino Acids on Silver at -600 mv vs. SCE.
Excitation: 5145 Å
L-Leucine
L-Glycine
non-lasing emission
Intensity
cm-1
557
607
671
783
806
920
1000
1027
1076
1140
1177
1268
1310
1377
1424
1446
1501
1577
1589
1621
1653
555
605
736
790
1035
1078
1142
1270
1380
1450
1498
1588
600
800
1000
1200
1400
1600

TABLE 9: Raman Spectra of L-Glycine and L-Leucine adsorbed onto a polycrystalline silver electrode at -600 mV sce, in the frequency region 550-1700 cm^{-1}. Excitation: 5145 Å.

Assignment	L-glycine	L-leucine
NH_2 torsion	555	557
COO^- wag	605	607
COO^- bend		671
teflon?	736	
	790	783
		806
CH_2 rock		920
CH_3 rock		1000
CCN asymmetry stretch	1035 w	1027 w
	1078	1076
NH_2 rock	1142	1140
stretch of $CH-(CH_3)_2$		1177
CH_2 twist	1270	1268
CH_2 wag		1310
COO^- symmetry stretch	1380	1377
methyl group motion?		1424
CH_2 bend	1450	1446
NH_2 symmetry deformation	1498	1501
		1577
COO^- asymmetric stretch	1588	1589
NH_2 degenerate deformation		1621
		1653

Figure 23: Normal Raman Spectra of Polycrystalline Ag_2O and AgOH Utilizing a Back-scattering Geometry.
EXCITATION WAVELENGTHS: 5145 Å (Ar^+) AgOH
6471 Å (Kr^+) Ag_2O

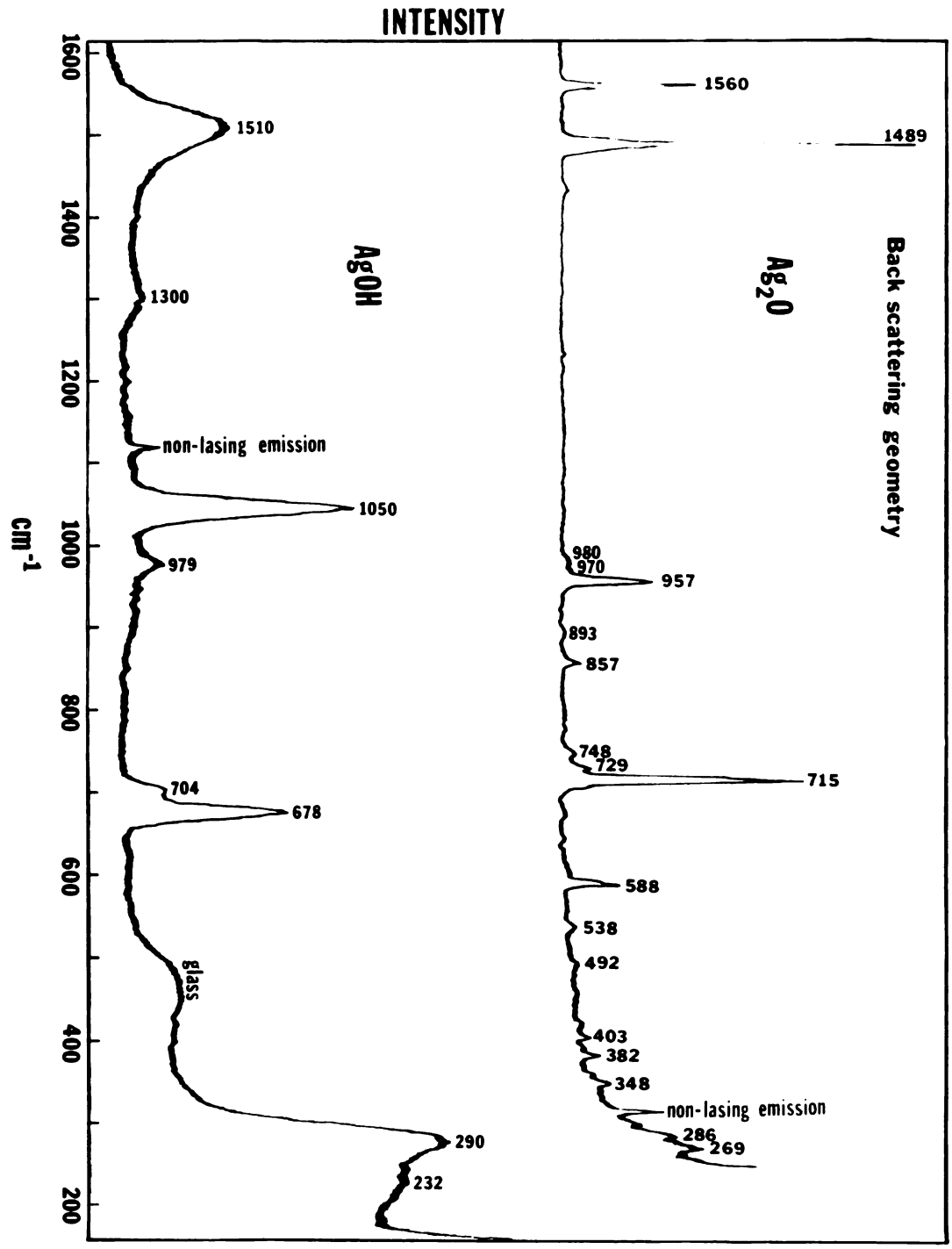
INTENSITY
1600
1400
1200
1000
800
600
400
200
cm-1
AgOH
1510
1300
non-lasing emission
1050
979
704
678
glass
290
232
Ag2O
Back scattering geometry
1560
1489
980
970
957
893
857
748
729
715
588
538
492
403
382
348
non-lasing emission
286
269

TABLE 10: Raman Spectra of Polycrystalline AgOH and Ag_2O in the region 200-1600 cm^{-1} using a back scattering geometry.

Polycrystalline AgOH	Polycrystalline Ag_2O*
232	269
290	286
	348
	382
	403
	492
	538
	588
678	715
704	729
	748
	857
	957
	970
979	980
1050	1489
1300	1560
1510	

reported in the literature though the infrared spectrum of Ag_2O has been reported.[112,113] No attempt at assignment of observed frequencies is made. Further study is required for such assignment. Qualitatively, the effect of hydrogen bonding in the back scattering spectrum of AgOH is manifested in the broadening of all Raman lines in comparison to those observed in the spectrum of Ag_2O. The spectra of the two silver compounds were obtained mainly to examine their interference in the surface Raman spectrum of the amino acids. No interference was observed, however, and it can be concluded that either the silver oxides are not present or that the intensity of their surface signal is too weak to be observed.

Returning now to the surface Raman spectra of the amino acids shown in Figure 22 some interesting anomalies are observed. Assignments of the observed surface Raman spectra for L-leucine and L-glycine are made by comparison to other vibrational spectroscopic studies of amino acids.[114-120] The suggested assignments are listed in Table 9. The most important and distinct difference between the surface spectra of L-leucine and that of L-glycine is the appearance of a line at 671 cm^{-1} in the leucine spectrum which is absent from the glycine. This mode has been assigned to the $-COO^-$ bend in leucine and is expected to occur in the same region of the glycine surface spectrum. The $-COO^-$ bending vibration occurs at 690 cm^{-1} in the infrared spectrum of glycine and at 694 in the Raman spectrum

of polycrystalline γ-glycine.[117] The most intense line in both surface spectra appears at 1377 cm^{-1} in L-leucine and 1380 cm^{-1} in L-glycine and is probably the symmetric stretching motion of the $-COO^-$ group. The line at 1424 cm^{-1} in the surface spectrum of L-leucine has no counterpart in the spectrum of L-glycine and is accordingly assigned to motion in the methyl substituents in leucine. The COO^- asymmetric stretch appears as a doublet at 1589 cm^{-1} and 1577 cm^{-1} in the surface spectrum of L-leucine, but as a singlet at 1588 cm^{-1} in the spectrum of L-glycine. The appearance of splitting in the asymmetric stretching motion of the COO^- group in the leucine spectrum may be a consequence of bonding of one oxygen atom at the surface while the other remains free. This explanation is also invoked to account for the appearance of a COO^- bend in the leucine spectrum and not in glycine. In glycine if both oxygen atoms are bound to the surface the bending vibration would be significantly dampled and probably shifted in frequency. The $-NH_2$ deformations above 1600 cm^{-1} in the surface Raman spectrum of L-leucine appear more intense relative to the same vibrations in the glycine spectrum. This may also be a manifestation of the way in which glycine is attached to the surface. If the glycine molecule is attached through both carboxylate oxygens it may be forced into a configuration which keeps the $-NH_2$ group from coming in contact with the surface. With only one oxygen attached in the leucine situation the molecules

maintain flexibility on the surface and allow the amine group to contact the surface. The clear distinction between the surface Raman spectra of L-leucine and L-glycine on silver may be extrapolated to distinguish the same amino acid residues in a protein adsorbed at an electrode surface.

Future Surface Raman Studies.

The analysis of experimentally observed surface Raman spectra presented in this thesis can be applied to nearly any molecule. Molecules which have demonstrated ability as ligands in metal complexes undoubtedly will exhibit intense surface Raman scattering. Those molecules which are of particular interest to the verification of the surface dynamics of t-1,2-bis(4-pyridyl)ethylene on silver are the isomers to the highly symmetrical 4,4'-bipyridylethylene (i.e. the isomers with nitrogens in positions other than the 4 position). The very low frequency region (0-100 cm^{-1}) of the surface Raman spectrum of t-BPE should demonstrate significant spectroscopic changes accompanying the molecular reorientation from the end-on to the flat configuration. Gerack et al.[121] attributed potential dependent dynamics of the low frequency surface spectrum of pyridine to reorientation of the molecule to the "standing up" position at less negative potentials. Determination of surface coverage is particularly important to the designation of an enhancement factor. The

monoprotonated t-BPE molecule generates a surface Raman spectrum distinct from the unprotonated molecule and may therefore be exploited in accurate determination of surface coverage through titration. The titration technique has some obvious advantages over electrochemical techniques which require sweeping of electrode potential. Also the surface Raman spectrum of monoprotonated t-BPE is observed even at very light coverages (250 n$\underline{M}$ bulk concentrations). Electrochemical measurements are generally insensitive or irreproducible at such low coverages.

Excitation profiles in regions of the visible spectrum other than the rhodamine 6G region are necessary to analyze the energy distribution of eigenstates in t-BPE and other adsorbates. Profiles should also be obtained at other potentials, as shown to be important in the discussion of potential-dependent surface Raman intensities. The use of teflon as an internal standard should be exploited in the preparation of the excitation profiles in that ClO_4^- demonstrates its own potential dependent behavior at the electrode surface.

The application of SERS to biological molecules should be accelerated. The advantages of observation of these molecules at the electrode surface include flourescence quenching by the metal surface, absence of photodecomposition problems owing to the behavior of the metal as a heat sink, and the ability to vary continuously

potential while observing the effect of electron transfer on the surface Raman spectrum.

Further experimentation and theoretical investigation on the influence of the multiple enhancement mechanisms, proposed to account for the anomalous surface Raman intensities, are necessary, but at this time applications of the SERS technique are more generally worthwhile.

The most important conclusion which can be drawn from this thesis is that any discussion of origination of Raman intensities from surface adsorbates must include mention of surface complex formation and the resonance Raman intensity enhancement expected from the perturbation of molecular electronic state distributions.

APPENDIX A

The form of the normal coordinates of some pyridine vibrational modes, as determined by Long and Thomas,[107] are depicted in this appendix. Discussion of the form of the normal coordinates was central to the assignment of lines in the normal Raman spectrum of t-1,2-bis(4-pyridyl)ethylene (see Chapter 5).

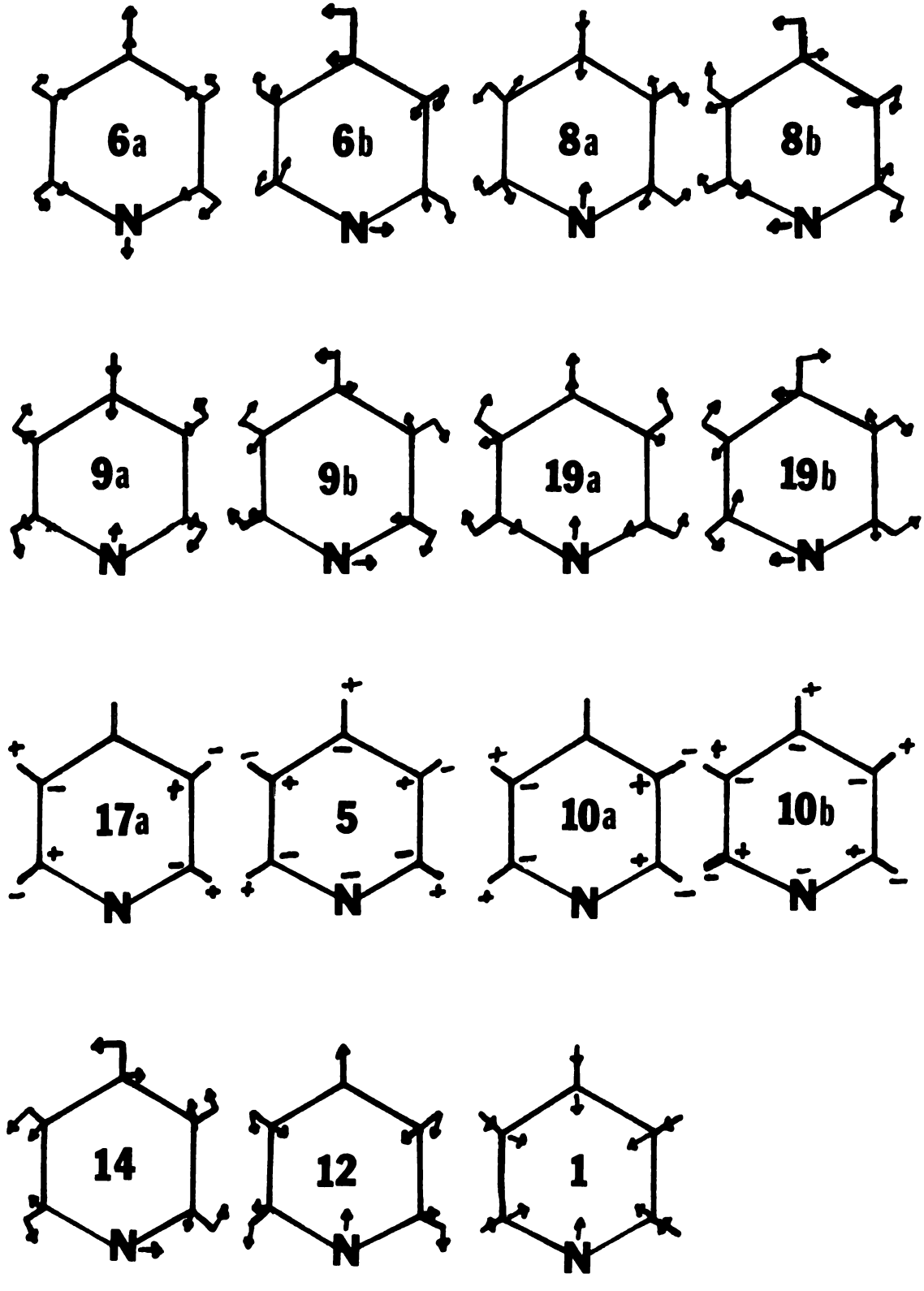
6a
6b
8a
8b
9a
9b
19a
19b
17a
5
10a
10b
14
12
1
N

List of References

REFERENCES

1. T. Katsumoto; Bull. Chem. Soc. Japan 33, 1376 (1960).

2. M. Fleischmann, P.J. Hendra, A.J. McQuillan; Chem. Phys. Lett. 26(2), 163 (1974).

3. R.L. Paul, A.J. McQuillan, P.J. Hendra, M. Fleischmann; J. Electroanal. Chem. 66, 245 (1975).

4. A.J. McQuillan, P.J. Hendra, M. Fleischmann; J. Electroanal. Chem. 65, 933 (1975).

5. D.L. Jeanmaire, R.P. van Duyne; J. Electroanal. Chem. 84, 1 (1977).

6. D.L. Jeanmaire, R.P. van Duyne; J. Electroanal. Chem. 66, 235 (1975).

7. J.A. Creighton, M.G. Albrecht, R.E. Hester, J.A.D. Matthew; Chem. Phys. Lett. 55, 55 (1978).

8. B. Pettinger, U. Wenning, D.M. Kolb; Ber. Bunsenges. Phys. Chem. 82, 1326 (1978).

9. J.A. Creighton, C.G. Blatchford, M.G. Albrecht; J. Chem. Soc. Faraday II 75, 790 (1979).

10. M. Moskovits; J. Chem. Phys. 69, 4159 (1978).

11. M. Moskovits; Solid State Comm. 32, 59 (1979).

12. J.A. Creighton, C.G. Blotchford, J.R. Campbell; Proc. of the VIIth Int. Conf. on Raman Spectroscopy, 398-399 (1980) (W.G. Murphy, ed.).

13. J.I. Gersten; J. Chem. Phys. 72(10), 5779 (1980).

14. F. King, G.C. Schatz, and R.P. van Duyne; J. Chem. Phys. 69, 4472 (1979).

15. G.C. Schatz, R.P. van Duyne; Surface Sci. 101, 425 (1980).

16. C.S. Allen, G.C. Schatz, R.P. van Duyne; Chem. Phys. Lett. 75(2), 2101 (1980).

17. S. Efrima, H. Metiu; Chem. Phys. Lett. 60(1), 59 (1978).

18. S. Efrima, H. Metiu; J. Chem. Phys. 70(4), 1602 (1979).

19. S. Efrima, H. Metiu; J. Chem. Phys. 70(5), 2297 (1979).

20. S. Efrima, H. Metiu; J. Chem. Phys. 70(4), 1939 (1979).

21. S. Efrima, H. Metiu; Israel Journal of Chem. 18, 17 (1979).

22. G. Karzeniewski, T. Maniv, H. Metiu; Chem. Phys. Lett. 74(2), 301 (1980).

23. P.K. Avavind, H. Metiu; Chem. Phys. Lett. 74(2), 301 (1980).

24. M.R. Philpott, J. Chem. Phys. 62(5), 1812 (1975).

25. E.N. Economon, K.L. Ngai; Adv. Chem. Phys. 27, 265 (1974).

26. Y.Y. Teng, E.A. Stein; Phys. Rev. Lett. 19, 511 (1967).

27. D. Beaglehole; Phys. Rev. Lett. 22, 708 (1969).

28. I. Pockrand; J. Phys. D9, 2423 (1976).

29. H. Raether, Nuovo Cimento 39B, 817 (1977).

30. H. Raether, Phys. Thin Films 9, 145 (1977).

31. A. Girlando, M.R. Philpott, D. Heitmann, J.D. Swalm, R. Santo, J. Chem. Phys. 72(9), 5187 (1980).

32. A. Girlando, J.G. Gordon II, D. Heitmann, M.R. Philpott, H. Seki, J.D. Swolen; Surf. Sci. 101, 417 (1980).

33. A. Otto; Z. Phyzik 241, 398 (1968).

34. E. Kretschmann; Z. Phyzik 241, 313 (1971).

35. R.M. Hexter, M.G. Albrecht; Spectrochim. Acta 35A, 233 (1979).

36. A. Brillante, I. Pockrand, M.R. Philpott, J.D. Swalen; Chem. Phys. Lett. 57(3) 395 (1978).

37. W. Carius, O. Schröter; Experimentelle Technik der Physik 28(1), 35 (1980).

38. B. Pettinger, A. Tachjeddime, D.M. Kolb; Chem. Phys. Lett. 66(3), 544 (1979).

39. W.P. Chen, J.M. Chen; Surf. Sci. 91, 601 (1980).

40. B. Pettinger, U. Wenning, H. Wetzel; Surf. Sci. 101, 490 (1980).

41. R. Donnhaus, R.E. Benner, R.K. Chang, I. Chabay; Surf. Sci. 101, 367 (1980).

42. A. Otto; Surf. Sci. 101, 99 (1980).

43. I. Pockrand, A. Brillante, D. Mobins; Chem. Phys. Lett. 69(3), 499 (1980).

44. J.G. Gordon II, S. Ernest; Surf. Sci. 101, 499 (1980).

45. A. Regis, J. Corset; Chem. Phys. Lett. 70(2) 305 (1980).

46. A. Regis, J. Corset; Extended Abstracts, 81-1 Spring Meeting of the Electrochemical Society, 921 (1981).

47. M.W. Howard, R.P. Cooney, A.J. McQuillan; J. Raman Spec. 9(4), 273 (1980).

48. R.P. Cooney, A.J. McQuillan, M.W. Howard; Proc. of the VIIth Int. Conf. on Raman Spectroscopy, 400 (1980) (W.G. Murphy, ed.).

49. J.C. Tsang, J.E. Demuth, P.N. Sanda, J.R. Kirtzey; Chem. Phys. Lett. 76(1) 54 (1980).

50. G.W. Robinson; Chem. Phys. Lett. 76(2), 191 (1980).

51. E. Burstein, Y.J. Chen, C.Y. Chen, S. Lundquist, E. Tosatti; Solid State Comm. 29, 567 (1979).

52. C.Y. Chen, E. Burstein, S. Lundquist; Solid State Comm. 32, 63 (1979).

53. R.R. Smardzewski, R.J. Colton, J.S. Murday; Chem. Phys. Lett. 68(1), 53 (1979).

54. S.R. Kelemen, A. Kaldor; Chem. Phys. Lett. 73(2), 205 (1980).

55. J.E. Demuth, K. Christmann, P.N. Sanda; Chem. Phys. Lett. 76(2), 201 (1980).

56. R.R. Chance, A. Prock, R. Silbey; Adv. Chem. Phys. 37, 1 (1978).

57. D.A. Zwemer, C.V. Shank, J.E. Rowe; Chem. Phys. Lett. 73,(2), 201 (1980).

58. J.E. Rowe, C.V. Shank, D.A. Zwemer, C.A. Murray; Phys. Rev. Lett. 44(26), 1770 (1980).

59. H. Seki, M.R. Philpott; J. Chem. Phys. 73(10), 5376 (1980).

60. C.Y. Chen, I. Davoli, G. Ritchie, E. Burstein; Surf. Sci. 101, 363 (1980).

61. J.P. Heritage, J.G. Bergman, A. Pinczuk, J.M. Worlock; Chem. Phys. Lett. 67(2,3), 229 (1979).

62. R. Dornhaus, M.B. Long, R.E. Benner, R.K. Chang, Surf. Sci. 93, 240 (1980).

63. G.R. Erdheim, R.L. Birke, J.R. Lombardi; Chem. Phys. Lett. 69(3), 495 (1980).

64. W. Krasser, H. Ervens, A. Fadini, A.J. Renouprez; J. Raman Spec. 9(2) 80 (1980).

65. M. Moskovits, D.P. Dilello; J. Chem. Phys. 73(12), 6068 (1980).

66. T.M. Cotton, S.G. Schultz, R.P. van Duyne; J. Am. Chem. Soc. 102, 7960 (1980).

67. M.E. Lippitsch; Chem. Phys. Lett. 79(2), 224 (1981).

68. E. Koglin, J.M. Sequaris, P. Valenta; J. Mol. Str. 60, 421 (1980).

69. M. Moskovits, D.P. DiLella; Chem. Phys. Lett. 73(3), 500 (1980).

70. M.R. Philpott, J.G. Gordon II, B. Pettinger, Extended Abstracts, 81-1 Spring Meeting of the Electrochemical Society, 896 (1981).

71. T.H. Wood, M.V. Klein; J. Vac. Sci. & Tech. 16, 459 (1979).

72. M. Moskovits, D. DiLella, P. McBreen, R. Lipson, A. Gohin; Proc. of the VIIth Int. Conf. on Raman Spectroscopy, 394 (1980) (W.G. Murphy, ed.).

73. H. Wetzel, B. Pettinger, U. Wenning; Chem. Phys. Lett. 74(1), 173 (1980).

74. E. Burstein, C.Y. Chen, S. Lundquist; Proc. of the Joint US-USSR Symposium on Theory of Light Scattering in Condensed Matter, (Plenum Press, New YOrk, 1979).

75. R.P. van Duyne; Chemical and Biochemical Applications of Lasers, Vol. 4, (C.B. Moore, ed), (Academic Press, New York, 1978).

76. T.E. Furtak, Solid State Comm. 28, 903 (1978).

77. T.E. Furtak, G. Trott, B.H. Loo; Surf. Sci. 101, 374 (1980).

78. W.A. Goddard III, T.C. McGill; J. Vac. Sci. Technol. 16(5) 1308 (1979).

79. A. Otto, J. Timper, J. Billman, G. Kovacs, I. Pockrand; Surf. Sci. 92, L55-L57 (1980).

80. A. Otto; Surf. Sci. 92, 145 (1980).

81. J.I. Gersten; J. Chem.Phys. 72(10), 5779 (1980).

82. H. Wetzel, H. Gerischer, B. Pettinger; Chem. Phys. Lett. 78(2), 392 (1981).

83. J.R. Lombardi, E.A. Shields Knight, R.L. Birke; Chem. Phys. Lett. 79(2), 214 (1981).

84. J. Billmann, A. Otto, I. Pockrand, J. Timper; Proc. of the VIIth Int. Conf. on Raman Spectroscopy, 424 (1980) (W.G. Murphy, ed.).

85. B. Pettinger, H. Wetzel; Chem. Phys. Lett. 78(2), 398 (1981).

86. J.R. Lombardi, R.L. Birke; Extended Abstracts 81-1 Spring Meeting of the Electrochemical Society, 894 (1981).

87. D.L. Rosseau, J.M. Friedmann, P.F. Williams, in: Topics in Current Physics, Vol. 2 Raman Spectroscopy of Gases and Liquids, (A. Weber, ed.), chapter 6.

88. D.K. Lavalee, E.B. Fleischer; J. Am. Chem. Soc. 94(8), 2583 (1972).

89. H.B. Gray, C.J. Ballhausen; J. Am. Chem. Soc. 85, 260 (1963).

90. H.A. Pearce and N. Sheppard; Surf. Sci. 59, 205 (1976).

91. R.M. Hexter, M.G. Albrecht, Spectrochim. Acta 35A, 233 (1979).

92. A.C. Albrecht, J. Chem. Phys. 34(5), 1476 (1961).

93. J. Tang, A.C. Albrecht, in Raman Spectroscopy, Theory and Practice, Vol. 2, pp. 33-68 (1970) (H.A. Szymanski, ed.).

94. R.J.H. Clark, B. Stewart; Structure and Bonding 36, 1 (1979).

95. S.L. Ross; Introduction to Ordinary Differential Equations (Xerox College Publishing, MA) (1966) Chapter 5, pp. 152-160.

96. B. Pettinger, U. Wenning, H. Wetzel; Chem. Phys. Lett. 67(1), 192 (1979).

97. U. Wenning, B. Pettinger, H. Wetzel; Chem. Phys. Lett. 70(1), 49 (1980).

98. D.P. Shoemaker, C.W. Garland, J.I. Steinfeld; Experiments in Physical Chemistry, 3rd ed. (1974) pp. 455-457.

99. Chemical Rubber Co; Handbook of Chemistry and Physics, 52nd ed. p. B232.

100. H.H. Perkampus, E. Baumgarten; Spectrochim. Acta 20, 359 (1964).

101. E.B. Wilson; Phys. Rev. 45, 706 (1934).

102. E. Spinner; J. Chem. Soc., 3870 (1963).

102a. G. Valette, A. Hamelin; J. Electroanal. Chem. 45, 301 (1973).

103. G. Herzberg; Molecular Spectra and Molecular Structure II Infrared and Raman Spectra of Polyatomic Molecules, (Van Nostrand Reinhold Co.) (1945), 247-249.

104. F.R. Dallish, W.G. Fateley, F.F. Bentley; Characteristic Raman Frequencies of Organic Compounds (Wiley-Interscience) (1974) pp. 263-272.

105. Z. Meic, H. Gusten; Spectrochim. Acta 34A, 101 (1978).

106. A. Regis, J. Corset; Extended Abstracts 81-1, Spring Meeting of the Electrochemical Society, 921 (1981).

107. D.A. Long, E.L. Thomas; Trans. Faraday Soc. 59, 783 (1963).

108. E. Spinner; Aust. J. Chem. 20, 1805 (1967).

109. R.H. Dyck, D.S. McClure; J. Chem. Phys. 36(9), 2326 (1962).

110. J. Volke, J. Holubek; Coll. Czech. Chem. Commun. 27, 1777 (1962).

111. W.L. Jorgensen, L. Salem; The Organic Chemists Book of Orbitals (Academic Press, NY) (1973).

112. E.F. Gross, F.I. Kreingold; Optics and Spectroscopy 10, 211 (1961).

113. V.M. Kirillova, E.N. Lotkova; Optics and Spectroscopy 20, 181 (1966).

114. M. Tsuboi, T. Onishi, I. Nakagawa, T. Shimanouchi, S. Migushima; Spectrochim. Acta 12, 253 (1958).

115. R.K. Khanna, P.J. Miller; Spectrochim. Acta 26A, 1667 (1970).

116. R.K. Khanna, M. Horak, E.R. Lippincott; Spectrochim. Acta 22, 1759 (1966).

117. M.A. Salimov, V.A. Pchelin, A.V. Kerimbekov; Russ. J. Phys. Chem. 37(10), 1231 (1963).

118. M. Tsuboi, T. Takenishi, A. Nakamura; Spectrochim. Acta 19, 271 (1963).

119. K. Machida, A. Kagayama, Y. Saito, Y. Kuroda, Y. Uno; Spectrochim. Acta 33A, 569 (1977).

120. R.S. Krishnan, V.N. Sankaranarayanan, K. Krishnan; J. Ind. Inst. Sci. 55(2), 66 (1973).

121. A.Z. Genack, D.A. Wertz, T.J. Gramila; Surf. Sci. 101, 381 (1980).